

OPTIMIZATION OF COMPACT ELECTROMAGNETIC ENERGY  
HARVESTERS FOR WIRELESS SENSOR APPLICATIONS

A THESIS SUBMITTED TO  
THE GRADUATE SCHOOL OF NATURAL AND APPLIED SCIENCES  
OF MIDDLE EAST TECHNICAL UNIVERSITY

BY

OĞUZ YAŞAR

IN PARTIAL FULFILLMENT OF THE REQUIREMENTS  
FOR  
THE DEGREE OF MASTER OF SCIENCE  
IN  
ELECTRICAL AND ELECTRONICS ENGINEERING

JUNE 2017



Approval of the thesis:

**OPTIMIZATION OF COMPACT ELECTROMAGNETIC ENERGY  
HARVESTERS FOR WIRELESS SENSOR APPLICATIONS**

Submitted by **OĞUZ YAŞAR** in partial fulfillment of the requirements for the degree  
of **Master of Science in Electrical and Electronics Engineering Department,**  
**Middle East Technical University** by,

Prof. Dr. Gülbin Dural Ünver

Dean, Graduate School of **Natural and Applied Sciences**

Prof. Dr. Vqri c'Ykq nw

Head of Department, **Electrical and Electronics Engineering**

Prof. Dr. Haluk Külâh

Supervisor, **Electrical and Electronics Eng. Dept., METU**

**Examining Committee Members:**

Prof. Dr. Tayfun Akın

Electrical and Electronics Engineering Department, METU

Prof. Dr. Haluk Külâh

Electrical and Electronics Engineering Department, METU

Asskuv Prof. Dr. Serdar Kocaman

Electrical and Electronics Engineering Department, METU

Assoc. Prof. Dr. Kıvanç Azgın

Mechanical Engineering Department, METU

Prof. Dr. Feza Arıkan

Electrical and Electronics Engineering Department, Hacettepe University

**Date:**

15.06.2017

**I hereby declare that all information in this document has been obtained and presented in accordance with academic rules and ethical conduct. I also declare that, as required by these rules and conduct, I have fully cited and referenced all material and results that are not original to this work.**

Name, Last Name: Oğuz Yaşar

Signature:

## **ABSTRACT**

# **OPTIMIZATION OF COMPACT ELECTROMAGNETIC ENERGY HARVESTERS FOR WIRELESS SENSOR APPLICATIONS**

Yaşar, Oğuz

M.Sc., Department of Electrical and Electronics Engineering

Supervisor: Prof. Dr. Haluk Kùlah

May 2017, 106 pages

The developments in wireless sensor systems force researchers to analyze how to satisfy power requirements of these systems. Batteries can be the main candidate to be used as power source; however, they affect negatively the continuity of the wireless systems due to their limited lifetime. In order to provide continuous power source, energy harvester modules are proposed. With the advancements on IC technology, it is possible to convert extracted energies to power sources for the sensors operating in wireless environments. Therefore, the optimized design of the harvester to generate desired power for wireless sensor nodes is essential.

The aim of this thesis study is to design, optimize, fabricate and test the electromagnetic (EM) energy harvesters to be used as power source for wireless systems. Since most of the vibrations in nature exist in low frequency levels ( $< 10$  Hz), the proposed harvester should be capable of operating at low frequency and low amplitude vibrations. Additionally, the design should be compact enough in size; hence, device volume is limited with  $8 \text{ cm}^3$ .

This thesis study presents an optimization study for decreasing the operation frequency and increasing the output power of a miniature EM energy harvester. Incorporating a non-magnetic inertial mass (tungsten) along with the axially oriented moving magnets is the main strategy to reach optimum results. Dimensions of the magnets are optimized according to the harvester dimensions and magnetic flux gradients. Additionally, coil length, width, resistance and position have been optimized through finite element analysis (FEA) and experimentally validated.

Simulation results show that using a single-magnet structure is not sufficient for increasing the output power of the system. Also, test results reveal that multi-magnet structures yield to higher output voltages and smaller resonance frequencies. Effects of the improvements on the moving structure are analyzed in detail and experimentally validated. The operation frequency of the harvester decreases with axially oriented moving magnets, while the output power increases due to greater magnetic flux contributions provided by repulsive forces. Compared to the single-magnet structure, a modified design with a similar size yields to a decrease in the resonance frequency (from 15 Hz to 7.2 Hz) and an increase in the output power. The optimized harvester has a volume of 7 cm<sup>3</sup> and generates 0.53 V<sub>RMS</sub>, 266 μW<sub>RMS</sub> output power (@7.2 Hz and 0.5g peak acceleration).

Keywords: Energy Harvesting, Vibration-Based Energy Harvesting, Electromagnetic Energy Harvester, Optimized Energy Harvester, Energy Harvester Modeling.

## ÖZ

# KOMPAKT ELEKTROMANYETİK ENERJİ ÜRETEÇLERİNİN KABLOSUZ ALGILAYICI UYGULAMALARI İÇİN ENİYİLEMESİ

Yaşar, Oğuz

Yüksek Lisans, Elektrik ve Elektronik Mühendisliği Bölümü

Tez Yöneticisi: Prof. Dr. Haluk Külah

Mayıs 2017, 106 sayfa

Kablosuz algılayıcı sistemlerindeki son gelişmeler, araştırmacıları bu sistemlerin güç gereksinimlerini nasıl karşılayacaklarını analiz etmeye zorlamaktadır. Piller güç kaynağı olarak kullanılabilir ana aday olabilir, bununla birlikte, sınırlı ömürleri nedeniyle kablosuz sistemlerin sürekliliğini olumsuz etkilemektedirler. Sürekli güç kaynağı sağlamak için enerji üretici modülleri önerilmektedir. IC teknolojisindeki ilerlemelerle, üretilen enerjileri, kablosuz ortamlarda çalışan sensörler için güç kaynaklarına dönüştürmek mümkündür. Bu nedenle, kablosuz sensör düğümlerine istenen gücü üretmek için, optimize edilmiş üreteç tasarımı çok önemlidir.

Bu tez çalışmasının amacı, kablosuz sistemler için güç kaynağı olarak kullanılmak üzere elektromanyetik (EM) enerji üretici tasarlamak, optimize etmek, imal etmek ve test etmektir. Doğadaki titreşimlerin çoğu alçak frekans seviyelerinde (<10 Hz) mevcut olduğundan, önerilen üreteç düşük frekanslı ve düşük genlikli titreşimlerle çalışabilir olmalıdır. Ayrıca tasarım yeterince kompakt olmalı, bu nedenle cihaz hacmi 8 cm<sup>3</sup> ile sınırlandırılmıştır.

Bu tez çalışması, minyatür EM enerji üreticinin çalışma frekansını azaltmak ve çıkış gücünü artırmak için bir optimizasyon çalışması sunmaktadır. Eksenel olarak yönlendirilmiş hareketli mıknatıslarla birlikte manyetik olmayan bir atalet kütesinin

(tungsten) bir araya getirilmesi, eniyilenmiş sonuçlara ulaşmanın ana stratejisidir. Mıknatısların boyutları üreteç boyutlarına ve manyetik akı gradyanlarına göre optimize edilmiştir. Buna ek olarak bobin uzunluğu, genişliği, direnci ve konumu simülasyon analizi (FEA) ile eniyilenmiş ve deneysel olarak onaylanmıştır. Simülasyon sonuçları, tek mıknatıslı bir yapının kullanılmasının sistemin çıkış gücünün artırılması için yeterli olmadığını göstermektedir. Ayrıca, test sonuçları, çok mıknatıslı yapıların daha yüksek çıkış gerilimlerine ve daha küçük rezonans frekanslarına neden olduğunu ortaya koymaktadır. Hareketli yapı üzerindeki iyileştirmelerin etkileri detaylı olarak analiz edilmiş ve deneysel olarak onaylanmıştır. Üretecin çalışma frekansı aksel olarak yönlendirilmiş hareketli mıknatıslarla azalırken, çıkış gücü, itici kuvvetler tarafından sağlanan daha fazla manyetik akı katkısı nedeniyle artar. Tek mıknatıslı yapıya kıyasla, benzer boyuta sahip modifiye edilmiş bir tasarım, rezonans frekansında (15 Hz'den 7.2 Hz'ye) bir azalışa ve çıktı gücünde (161  $\mu$ W'dan 266  $\mu$ W'a) bir artışa neden olur. Optimize edilmiş üretecin hacmi 7 cm<sup>3</sup>'tür ve 0,53 V<sub>RMS</sub>, 266  $\mu$ W<sub>RMS</sub> çıkış gücü üretir (@ 7.2 Hz ve 0,5 g tepe ivme).

Anahtar Kelimeler: Enerji Üretimi, Titreşime Dayalı Enerji Üretimi, Elektromanyetik Enerji Üretici, Eniyilenmiş Enerji Üretici, Enerji Üretici Modellemesi.

*To my parents*

*and*

*my fellows*



## ACKNOWLEDGEMENT

This work is in part supported by Ministry of Science, Industry and Technology (SAN-TEZ) Project No: 1375, Turkey. This work is in part of the Chist-ERA E-CROPS project, funded by grant no. 112E175 of the Scientific & Tech. Research Council of Turkey (TUBITAK).

Hereby, I would like to give my best thanks to my thesis supervisor, Prof. Dr. Haluk Klah for all his support, guidance and valuable comments during this thesis study. Without his help, this work would never have come into life.

I would like to give my special thanks to Dr. zge Zorlu, who had a great help from the beginning to the end of this thesis. With his encourage and support, this work become more valuable.

I would also like to thank Dr. zlem Őardan Sukas for her kind help and invaluable instructions in the preparation of publications and this thesis study.

My sincere thanks are for my friends in BioMEMS research group who helped me a lot with their valuable discussions and cordial friendships. I would especially thank to Hasan UluŐan for his great help during this thesis study.

In the end, I am grateful to my lovely parents for their invaluable love and patience. With their emotional support, I was always motivated to conduct my research projects.



## TABLE OF CONTENTS

ABSTRACT.....	vii
ÖZ .....	ix
ACKNOWLEDGEMENT .....	xiii
TABLE OF CONTENTS.....	xv
LIST OF TABLES .....	xix
LIST OF FIGURES .....	xxi
CHAPTERS .....	1
INTRODUCTION .....	1
1.1. Batteries as an Energy Sources .....	2
1.2. Ambient Energy Sources and Energy Harvesters .....	3
1.3. Vibration Based Energy Harvesting .....	6
1.3.1. Electrostatic (Capacitive) Energy Scavengers.....	6
1.3.2. Piezoelectric Energy Scavengers .....	8
1.3.3. Electromagnetic (Inductive) Energy Harvesters.....	9
1.4. Review of Electromagnetic Energy Harvesters .....	12
1.5. Objective of the Thesis Study .....	20
1.6. Outline of the Thesis .....	21

DESIGN MODELLING AND SIMULATION.....	23
2.1. Properties of Magnetic Levitation System.....	24
2.1.1. Linear & Non-linear EM Energy Harvesters.....	24
2.1.2. Preference of Non-linear Systems.....	26
2.2. Modeling of Magnetic Levitation System.....	27
2.2.1. Mathematical Representation of the System.....	27
2.2.2. Effect of System Parameter on Output Power.....	29
2.3. Analysis and Simulation Results of Proposed System.....	30
2.4. Conclusion.....	42
MATLAB SIMULATOR.....	43
3.1. Operation Principle of the Simulator.....	43
3.2. Discrete Time Analysis.....	46
3.2.1. Determination of Initial Conditions.....	47
3.2.2. Magnetic Force Definition of the System.....	49
3.2.3. Deficiencies of the model.....	51
3.3. Continuous Time Analysis.....	54
3.3.1. Determination of Initial Conditions.....	55
3.3.2. Sampling Process and Magnetic Force Definition.....	56
3.3.2.1. Sampling Process.....	56
3.3.2.2. Magnetic Force Definition.....	58
3.3.3. Flowchart of the Model.....	60
3.4. Simulation Results of MATLAB Simulator.....	61
3.5. Conclusion.....	65
FABRICATION AND EXPERIMENTAL TEST RESULTS.....	67
4.1. Fabrication and Test Setup.....	67
4.2. Testing of Proposed 8 cm <sup>3</sup> Energy Harvester.....	70

4.3.	Tests of Proposed AA Battery Sized EM Energy Harvesters .....	74
4.3.1.	1 <sup>st</sup> Generation AA Battery Sized EM Harvester .....	75
4.3.2.	2 <sup>nd</sup> Generation AA Battery Sized EM Harvester .....	78
4.3.3.	3 <sup>rd</sup> Generation AA Battery Sized EM Harvester .....	81
4.3.4.	4 <sup>th</sup> Generation AA Battery Sized EM Harvester .....	84
4.3.5.	5 <sup>th</sup> Generation AA Battery Sized EM Harvester .....	87
4.4.	Comparison of Test Results with Simulation Results.....	91
4.5.	Actual and Estimated Resonance Frequencies of the Designs .....	94
4.6.	Conclusion .....	95
	CONCLUSION AND FUTURE WORK .....	97
	REFERENCES .....	103



## LIST OF TABLES

### TABLES

Table 1.1: Comparison of energy scavenging sources in terms of transduction mechanism and power density.....	4
Table 1.2: Comparison of electromagnetic and piezoelectric systems in terms of their operation specifications [22].....	12
Table 1.3: Ambient vibration sources with acceleration amplitude and excitation frequencies.....	19
Table 2.1: Comparison of magnet and coil parameters according to their effect on output voltage .....	38
Table 2.2: Design specifications of the moving magnet for low frequency and low excitation amplitudes .....	39
Table 4.1: System specifications of the proposed EM energy harvester.....	74
Table 4.2: The performance comparison of the 1 <sup>st</sup> generation AA battery sized and 8 cm <sup>3</sup> volume designs. ....	77
Table 4.3: Comparison of the proposed 1 <sup>st</sup> generation AA battery sized design with 2 <sup>nd</sup> generation AA battery sized design. ....	80
Table 4.4: The performance comparison of the 2 <sup>nd</sup> generation AA battery sized and 3 <sup>rd</sup> generation AA battery sized design.....	83
Table 4.5: Comparison of the proposed 3 <sup>rd</sup> generation AA battery sized design with 4 <sup>th</sup> generation AA battery sized design.....	87
Table 4.6: Comparison of the proposed 4 <sup>th</sup> generation AA battery sized design with 5 <sup>th</sup> generation AA battery sized design.....	90

Table 4.7: Comparison of the proposed 8 cm<sup>3</sup> square prism volume energy harvester with 5<sup>th</sup> generation AA battery sized design. ....92

Table 4.8: Comparison all of the proposed designs with each other in tabular form. ....92

Table 4.9: Comparison of the predicted and actual values of the resonance frequencies for the proposed EM harvester designs. ....94

## LIST OF FIGURES

### FIGURES

Figure 1.1: Ideal lifetime of a wireless sensor systems [6].....	2
Figure 1.2: An eletret based electrostatic energy harvester with top and side views [17].....	7
Figure 1.3: A piezoelectric cantilever energy and its response to the excitation [19].	9
Figure 1.4: Schematic diagram of the proposed electromagnetic energy harvester. .	11
Figure 1.5: Picture and drawing of the prototype design [25].	13
Figure 1.6: Single cylindrical and double-concentric hallbach array of D-cell sized design. [26].	14
Figure 1.7: FEA model of the design proposed by Munaz with magnetic flux lines [27].....	15
Figure 1.8: Non-resonant EM energy harvester design with top and side views [28]. .....	16
Figure 1.9: Schematic description of the EM harvester design proposed by Fondevilla [29].....	16
Figure 1.10: The EM energy harvester design to be attached on the wheels and operation principle [30].	17
Figure 1.11: Acceleration vs frequency characteristics of vibration sources, found in various applications, and types of energy harvesters designed for these sources [23]. .....	18

Figure 2.1: Frequency response curves of the relative velocity for the non-linear and a linear oscillator for several excitation amplitudes, (a) 0.1m/s <sup>2</sup> (b) 2m/s <sup>2</sup> and (c) 4 m/s <sup>2</sup> [6, 38].	25
Figure 2.2: (a) Schematic diagram of electromagnetic energy harvester. (b) Model of the resonant electromagnetic energy generator.	27
Figure 2.3: Schematic models of analyzed magnetic structures: (a) single-magnet, (b) magnet with inertial mass, inertial mass between (c) axial & (d) oppositely faced magnets.	33
Figure 2.4: (a) 3D view of the finite element model, showing magnetic flux density norm of stationary magnet (Ø: 2.5 mm h: 3 mm) at z=0. (b) Variation of magnetic flux density norm on the coil surface with magnet displacement.	34
Figure 2.5: (a) Magnetic flux density norm change on the coil surface. (b) Variation of the magnetic flux density norm on the coil surface with the increasing magnet height.	35
Figure 2.6: Variation of the magnetic flux density norm on the coil surface with the change in the magnet radius.	37
Figure 2.7: Calculated output power for various coil lengths at low frequency (8 Hz) vibrations.	39
Figure 2.8: Finite element analysis results showing flux lines for (a) single-magnet, (b) inertial mass placed on top of magnet, inertial mass placed between (c) axial & (d) oppositely faced magnets.	40
Figure 2.9: Plot of the magnetic flux density norm along the radial component of the coil surface.	41
Figure 3.1: Flowchart of the operation introduced to MATLAB model for detection of the resonance frequency.	45
Figure 3.2: Rest position determination of magnet placed below (a) and above (b) of equilibrium position.	48
Figure 3.3: Exponential data fit to magnetic force versus displacement data extracted from COMSOL.	49

Figure 3.4: Sampling operation of sine wave for (a) smaller and (b) larger sampling frequencies.....	51
Figure 3.5: Displacement characteristics of the moving magnet under 1 m 10 Hz sinusoidal excitation for several sampling frequencies (a) 2 kHz, (b) 1 kHz, (c) 500 Hz and (d) 250 Hz.....	53
Figure 3.6: Comparison of original and calculated sine waves when number of data taken in one period of time is $10^5$ .....	57
Figure 3.7: Definition of magnetic force acting on suspended part. ....	59
Figure 3.8: Flowchart of continuous time analysis.....	60
Figure 3.9: Frequency response plot of displacement for 8 cm <sup>3</sup> cube design. ....	62
Figure 3.10: Frequency response plot of displacement for 1 <sup>st</sup> generation AA battery design.....	62
Figure 3.11: Frequency response plot of displacement for 2 <sup>nd</sup> generation AA battery design.....	63
Figure 3.12: Frequency response plot of displacement for 3 <sup>rd</sup> generation AA battery design.....	63
Figure 3.13: Frequency response plot of displacement for 4 <sup>th</sup> generation AA battery design.....	64
Figure 3.14: Frequency response plot of displacement for 5 <sup>th</sup> generation AA battery design.....	64
Figure 4.1: Fabricated EM harvester prototypes (a) h:19 mm, Ø:20 mm, 6 cm <sup>3</sup> , N:1500 (b) h:46 mm, Ø:14 mm, 7 cm <sup>3</sup> , N:1200.....	68
Figure 4.2: Block diagram (a) and schematic representation (b) of the test setup. ...	69
Figure 4.3: (a) Structure of the EM energy harvester and (b) the fabricated prototype where the inertial mass is composed of Ø: 10 mm, h: 3 mm, 1.7 gram NdFeB magnet and Ø: 10 mm, h: 5 mm, 6.8 gram tungsten-copper mass. (S3 on Figure 4.1. (a)).....	70

Figure 4.4: Simulation and test results of the harvester output for different coil position. (8 Hz, 3 mm peak-to-peak vibration with 0.4 g peak acceleration).....	71
Figure 4.5: Frequency response of EM harvester prototypes (S1-S6) at 0.5 g peak vibration acceleration. S3, where the coil is placed 5 mm above the bottom of the harvester, gives the maximum output. ....	72
Figure 4.6: Frequency response of S3 at 0.7 g peak vibration acceleration for different inertial masses, where the maximum output voltage is obtained with 1.7 gram magnet and 6.8 gram tungsten-copper mass (Mag1.7-WCu6.8).....	73
Figure 4.7: Harvested AC voltage from S3 with 1.7 gram magnet and 6.8 gram tungsten-copper inertial mass at 15 Hz and 0.7 g peak acceleration (Oscilloscope screen).....	73
Figure 4.8: System specifications of the 1 <sup>st</sup> generation AA battery sized energy harvester.....	75
Figure 4.9: Test results of the harvester output for different coil position. (10 Hz, 2.5 mm peak-to-peak vibration with 0.5 g peak acceleration).....	76
Figure 4.10: Frequency response of EM harvester prototypes (P1-P9) at 0.5 g peak vibration acceleration. P3, where the coil is placed 15.5 mm above the bottom of the harvester, yields the maximum output. ....	77
Figure 4.11: System specifications of the 2 <sup>nd</sup> generation AA battery sized energy harvester.....	78
Figure 4.12: Test results of the harvester output for different coil position. (8.6 Hz, 1.7 mm peak-to-peak vibration with 0.5 g peak acceleration).....	79
Figure 4.13: Frequency response of EM harvester prototypes (P1-P9) at 0.5 g peak vibration acceleration. P3, where the coil is placed 15.5 mm above the bottom of the harvester, yields the maximum output. ....	80
Figure 4.14: System specifications of the 3 <sup>rd</sup> generation AA battery sized energy harvester.....	81
Figure 4.15: Test results of the harvester output for different coil position. (9 Hz, 2.5 mm peak-to-peak vibration with 0.5 g peak acceleration).....	82

Figure 4.16: Frequency response of EM harvester prototypes (P1-P9) at 0.5 g peak vibration acceleration. P8, where the coil is placed 20.5 mm above the bottom of the harvester, yields the maximum output.....	83
Figure 4.17: System specifications of the 4 <sup>th</sup> generation AA battery sized energy harvester.....	85
Figure 4.18: Simulation and test results of the harvester output for different coil position. (10 Hz, 1.2 mm peak-to-peak vibration with 0.5 g peak acceleration).....	86
Figure 4.19: Frequency response of EM harvester prototypes (P1-P9) at 0.5 g peak vibration acceleration. P3, where the coil is placed 15.5 mm above the bottom of the harvester, yields the maximum output.....	86
Figure 4.20: System specifications of the 5 <sup>th</sup> generation AA battery sized energy harvester.....	88
Figure 4.21: Simulation and test results of the harvester output for different coil position. (10 Hz, 2.5 mm peak-to-peak vibration with 0.5 g peak acceleration).....	89
Figure 4.22: Frequency response of EM harvester prototypes (P1-P9) at 0.5 g peak vibration acceleration. P3, where the coil is placed 15.5 mm above the bottom of the harvester, yields the maximum output.....	89
Figure 4.23: Frequency response of the EM energy harvester designs to 0.5 g sinusoidal excitation. ....	91
Figure 4.24: Harvested AC voltage from P3 at 7 Hz and 0.5 g peak acceleration (Oscilloscope screen).....	93



# CHAPTER 1

## INTRODUCTION

Recent developments in wireless systems became remarkable under the influence of emerging technology. To give example, advances in Micro Electromechanical Systems (MEMS) and compact semi-conductor technologies established a suitable environment for the research of low-power wireless sensors and actuators. Typical application areas of these devices in our daily life contain domestic, commercial, military, health, environmental and industrial sectors. As an example, stability of critical structures can be monitored and any fatigue or aging can be detected using [1]. While such systems are providing effective solutions to our daily problems, their wireless nature reveals a concern: How to supply energy to these systems? Batteries have been utilized as the main power source of such electronic systems. However, batteries are bulky and their lifetime is limited. Advances in small, lightweight and low-cost network elements have decreased the power requirement of these devices down to microwatts. Since the power requirement of small wireless devices is low, self-powered wireless sensor networks can be obtained by powering them up with the energy extracted from the environment [2, 3]. Environmental sources mainly appear as solar, thermal, RF and vibration in nature [4, 5]. Solar cells have long lifetime and provide high power density. Nevertheless, their performance highly depends on the environmental variations. Thermoelectric generators help to recover waste heat by converting it to electrical power, but this type of generators have low energy

conversion efficiency and limited applications. RF power is a good candidate to generate power for low power wireless and portable applications. However, the harvested energy highly depends on the distance from the main RF power source. Among these sources, vibration is a promising energy harvesting solution for low power wireless network applications due to its abundance in nature and clean profile.

### 1.1. Batteries as an Energy Sources

A battery is a device that stores energy in chemical form and converts that energy into electricity. Due to its ease of use and efficiency, batteries surpass other power sources and are extensively used from laser-pointers to laptops. However, longevity of this energy source is the main problem especially for today's advanced technology. Autonomous wireless sensor systems is an example of emerging technology, which operates continuously. The batteries as an energy source affect these systems negatively and disturb continuity due to their poor lifetime. Figure 1.1 illustrates the lifetime of the wireless sensor systems when batteries are used as a power source [6].

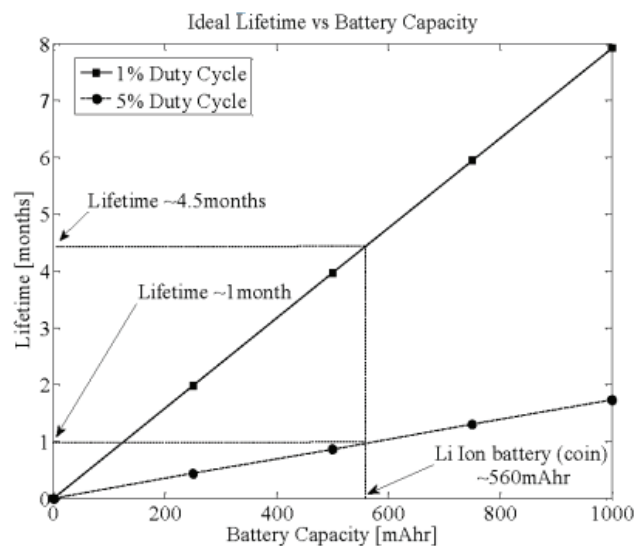


Figure 1.1: Ideal lifetime of a wireless sensor systems [6].

Comparing improvements on battery industry and advancing technology, it is clear that improvements on technology is much greater than that of the battery industry. That means, power requirements of the electronics industry continue to reduce compared to advancements in battery technology. As the technological gap between these technologies increases, compensation of energy requirement of electronic devices becomes a big challenge. Wireless sensor systems are good examples to the advanced technology, where energy requirement of these systems is still supplied by the batteries. However, according to Figure 1.1, batteries could not satisfy power expectations of such systems in the face of advanced improvements. As duty cycle of the systems increases, lifetime of the batteries decreases. Therefore, the capacitive power source dependence of wireless systems makes them unfavorable. With conventional batteries and battery variations, lifetime of wireless systems is limited, since continuous operation becomes impossible. [7] Also, battery industry is not capable to keep up with the rapid changes in electronic industry. For this reason, the customers use several batteries for electronic devices during their lifetime. Thus, power requirement of these systems should be fulfilled by continuous and effective power generation methods. A promising alternative is the replacement of batteries with environmental energy sources, which will be investigated in detail in the following sections.

## **1.2. Ambient Energy Sources and Energy Harvesters**

Most well-known ambient energy sources include solar and wind energies which are used in diverse applications. Over the past decade, researchers' major effort has been powering up autonomous sensors using various energy sources. Thomas et al. [8], reported an extensive study on powering small electric unmanned systems. Based on this study, energy for powering autonomous systems is categorized into five: radiant, mechanical, thermal, magnetic and biochemical. The most important concept on the choice of the ambient energy source depends on the energy density,

necessary for autonomous systems. Table 1.1 shows the power densities and transduction mechanisms of various types of energy sources [9-11]. The power density values for different energy sources are presented for 1-year and 10-year lifetime, separately. According to this comparison, it is clear that power density of ambient energy sources remains constant owing to their abundance in nature. However, for capacitive energy sources, significant decrease on power density is observed in long-term operation. Additionally, relatively low power density, need for replacement and dirt are their other disadvantages. As a result, for portable and wireless systems, ambient energy sources are more suitable compared to capacitive sources using electrochemical transduction.

Table 1.1: Comparison of energy scavenging sources in terms of transduction mechanism and power density.

Energy Source	Transduction Mechanism	Power Density	Power Density
		( $\mu\text{W}/\text{cm}^3$ ) 1-year lifetime	( $\mu\text{W}/\text{cm}^3$ ) 10-year lifetime
Solar	Photovoltaic	15.000 sunny	15.000 sunny
		150 cloudy	150 cloudy
Vibration	Piezoelectric		
	Electrostatic	4-800	4-800
	Electromagnetic		
Temperature Gradient	Thermoelectric	60 @ 5°C gradient	60 @ 5°C gradient
Radio Frequency @2.4 GHz [35]	Electromagnetic	400 @ 1 m	400 @ 1 m
	Induction	15.8 @ 5 m	15.8 @ 5 m

Fluid Flow	Wind, Wave	air: 200-800 water: 500 - mW/cm <sup>3</sup>	
Batteries (Lithium) (non-rechargeable)	Electrochemical	89	7
Batteries (Lithium) (rechargeable)	Electrochemical	13.7	0
Fuel (methanol)	Cells Electrochemical	560	56

In terms of power density and long lifetime photovoltaic cells are good candidates for wireless systems compared to other ambient energy sources. However, sunlight dependency is the main drawback of this energy source. Geographical locations and weather conditions have a great influence on the daylight intensity. Additionally, photovoltaic cells are not applicable to indoor applications. The operation principle and description of ambient energy sources are clarified in [4, 12]. Among these energy sources, vibration becomes prominent due to its abundance in nature, cleanness and relatively high power density. Vehicle and machine motions, human movements and any moving environmental sources are some examples of vibration sources. Most of the vibrations in nature occur at low frequencies (<10 Hz), hence efficient design for high power output is the main challenge of vibration based systems.

### **1.3. Vibration Based Energy Harvesting**

In vibration based energy harvesting, electrical energy is generated by the relative displacement of a moving structure with respect to stationary coil surface or capacitance plate. This is possible through three techniques; electrostatic (capacitive), piezoelectric and electromagnetic (inductive) energy harvesting. Various types of micro systems powered by using vibration based energy harvesting are reported in literature [13-15]. Therefore, feasibility of this type of energy harvesting is already proved. The aim of this study is to develop an energy harvester based on environmental vibrations, considering factors such as availability, abundance and feasibility. The types of vibration based energy harvesting are explained in detail in the following subsections.

#### **1.3.1. Electrostatic (Capacitive) Energy Scavengers**

Electrostatic (Capacitive) energy harvesting depends on the change in capacitance with an external vibration, which leads to separation of previously charged plates. Hence, mechanical energy is converted into electrical energy. The output voltage of a capacitance is basically denoted by  $V = q/C$  where,  $q$  is the charge and  $C$  is the capacitance, respectively.

Depending on the function, capacitive energy harvesters are configured as both current and voltage sources. By keeping the charge on the plates or the voltage across the plates constant, capacitive energy harvesters operate as voltage or current sources, respectively. However, for both cases, additional sources are necessary. On one hand,

to design a harvester as a current source, voltage between the plates should remain constant, which is provided by external voltage sources. Then, capacitance change is balanced with the variation of the charge on the plates. On the other hand, to design a harvester as a voltage source, charge on the plates should be kept constant. In this case, an electret, which is a dielectric material having quasi-permanent electric charge on itself, is needed. For this type of usage, balance of capacitance change is provided by the voltage variation across the capacitor plates. Independent from the configuration used, an extra component is compulsory for proper operation of the capacitive energy harvesters.

Electrostatic energy harvesters show better performance, especially in micro-scale [16]. Since this type of harvesters are suitable for low frequency and low amplitude vibrations. A MEMS based electrostatic energy harvester design is shown in Figure 1.2.

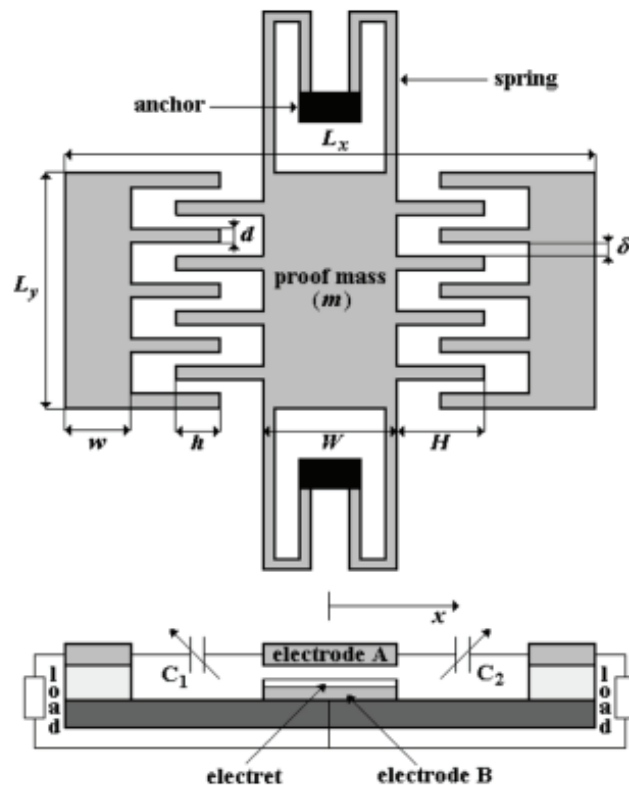


Figure 1.2: An electret based electrostatic energy harvester with top and side views [17].

The design above is an example of an electrostatic harvester to be used as a voltage source. Another design for low frequency and high output performance is proposed by Naruse [18]. This generator provides 40  $\mu\text{W}$  output power at 2 Hz and 0.4 g acceleration amplitude.

Electrostatic energy harvesters are advantageous in terms of their low frequency performance and easy fabrication in micro-scale. However, their output power is not high enough. Additionally, the need for extra voltage or charge sources is another disadvantage of this type of harvesters. Our aim is to harvest high output energy from low frequency excitations. From this perspective, electrostatic energy harvesters are out of the scope of this thesis study.

### **1.3.2. Piezoelectric Energy Scavengers**

Piezoelectric materials convert mechanical stress into electricity. The meaning of piezoelectricity is electricity resulting from applied pressure. This conversion between mechanical and electrical energy is a reversible process. That is, by applying electrical energy, physical form of the piezoelectric material can also be changed. The overall process explained above defines the operation principle of the piezoelectric energy harvesters. Figure 1.3 shows the schematic representation and operation of the piezoelectric energy harvester.

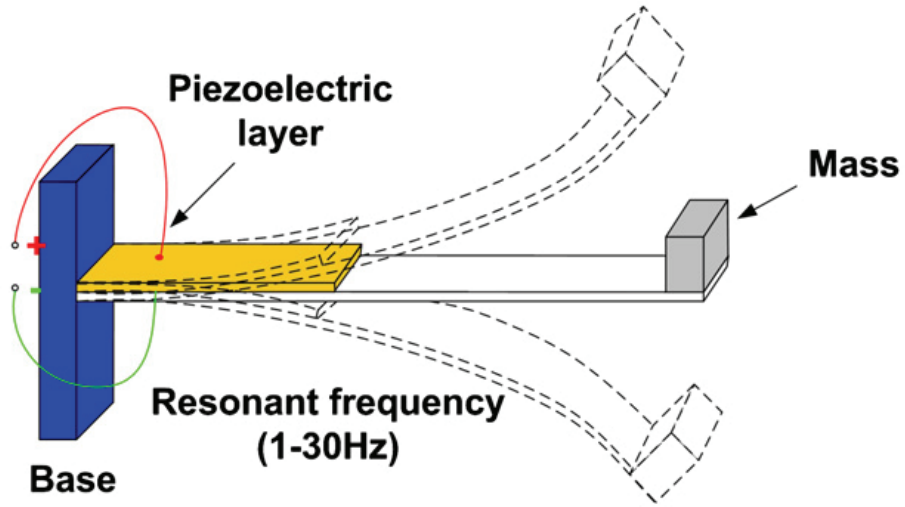


Figure 1.3: A piezoelectric cantilever energy and its response to the excitation [19].

There exist various studies in literature to investigate piezoelectric energy harvesters [19, 20]. This type of generators are advantageous in terms of their high energy densities. However, their fabrication is difficult and they have relatively low conversion efficiency. Also, material degradation is another drawback for this type of energy harvesters [21]. For high frequency vibration sources, piezoelectric energy harvesting is more suitable. Since we focus on low frequency excitation sources, the piezoelectric energy harvesting is out of scope.

### 1.3.3. Electromagnetic (Inductive) Energy Harvesters

Operation principle of electromagnetic (EM) energy harvesters is based on Faraday's law of induction, which explains how electromotive force (*emf*) is produced by a change in the magnetic flux ( $d\phi_B/dt$ ) passing through a closed conductor. The generated *emf*,  $\varepsilon$ , across the coil is represented as:

$$\varepsilon(t) = -\frac{d\phi_B}{dt} = -\left(\frac{dB}{dt}A + \frac{dA}{dt}B\right) \quad (1.1)$$

In (1),  $\phi$  is the magnetic flux,  $B$  is the magnetic flux density,  $A$  is the area of the coil and  $t$  is time. Equation (1.1) can be used to express *emf*  $\varepsilon$  an across N-turn coil:

$$\varepsilon(t) = -\left(\sum_i^N \frac{d\phi_{Bi}}{dz}\right) \left(\frac{dz}{dt}\right) \quad (1.2)$$

where  $\phi_{Bi}$  is the magnetic flux for the  $i^{th}$  coil turn and  $dz/dt$  is the relative velocity between coil turn and the magnet. The flux variation  $d\phi_B/dt$  passing through each coil turn is different, which is taken into account in equation (1.2).

Figure 1.4 shows the structure of the proposed EM energy harvester module. The harvester is composed of a fixed magnet attached to the bottom cap, a moving magnet in a cylindrical tube and a pick-up coil wound around the designated cavity on the tube. Magnets provide repulsive forces to each other, where the moving one stays at the equilibrium position as long as there is no disturbance. Environmental excitation causes an acceleration, which forces the moving magnet to relocate in the direction of excitation. Consequently, the spacing between the magnets changes and repulsive forces begin to accelerate the moving magnet. Therefore, the moving part of the system begins to oscillate inside the cylindrical tube. Electrical energy is generated across the coil terminals by magnetic induction, resulting from this relative motion between the coil and the moving magnet. In other words, an external vibration in the direction of motion causes an alternating voltage induced on the coil due to the variation in the magnetic field. In the proposed structure, a periodic excitation is necessary for continuous power generation.

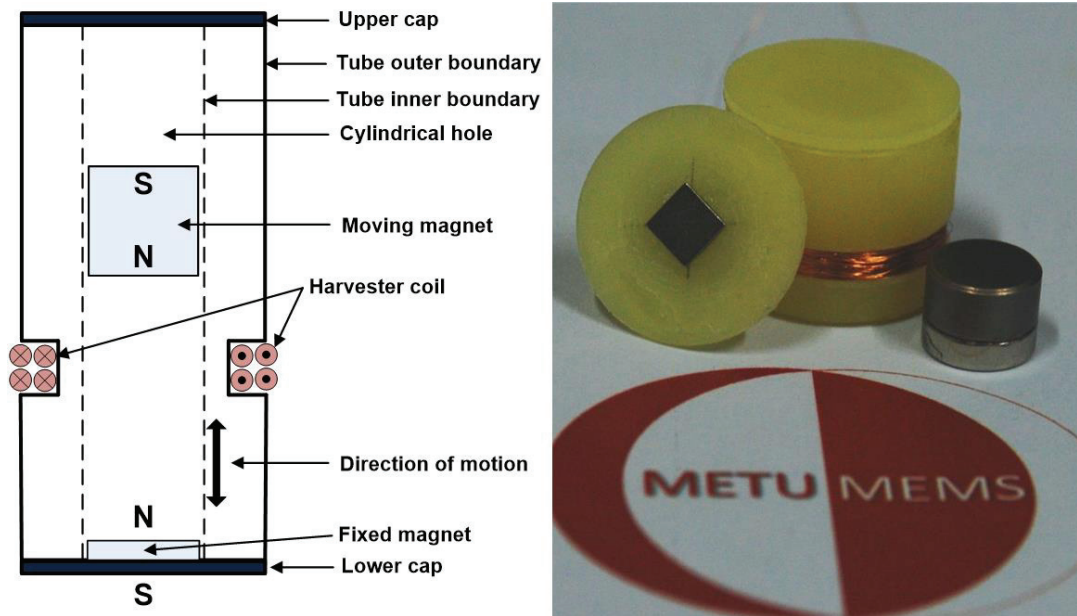


Figure 1.4: Schematic diagram of the proposed electromagnetic energy harvester.

Among the three described harvesting techniques, the low resonance frequency due to high inertial mass and the low input impedance, which enables collection of almost all of the harvested voltage at the output, make EM harvesting technique the most attractive one. The electrostatic energy harvesting technique has main disadvantages compared to other ones. In this technique, output power density is relatively low and separate voltage source or electret is necessary for proper operation. These disadvantages make this technique unfavorable and dissatisfactory for our case. In terms of the induction mechanism, piezoelectric and electromagnetic energy harvesting techniques resemble each other. However, operation frequency of piezoelectric energy harvesters are relatively high compared to the EM energy harvesters. Additionally, conversion efficiency of piezoelectric energy harvesters are lower and their fabrication processes are more complex than that of EM harvesters. A good comparison study is performed by Poulin between piezoelectric and electromagnetic energy harvesting systems as shown Table 1.2 below.

Table 1.2: Comparison of electromagnetic and piezoelectric systems in terms of their operation specifications [22].

System	Electromagnetic	Piezoelectric
Constraint	Low	High
Displacement	High	Low
Voltage	Adjustable	High
Current	Adjustable	Low
Resonance Frequency	Adjustable	High
Output Impedance	Resistive	Capacitive
Adapted Load	Adjustable	High

Electromagnetic induction is the most appropriate technique to be used for macro-scale, low frequency and high power density energy harvesting. According to the table above, excitation amplitude (displacement) is high and resonance frequency is adjustable. Additionally, output voltage and current is adjustable which means output power is also adjustable. Possible constraints are lower for EM energy harvesters compared to piezoelectric designs. Under the effect of these considerations, it is decided to investigate electromagnetic energy harvesting for high power and low frequency applications.

#### 1.4. Review of Electromagnetic Energy Harvesters

The aim of this study is to harvest energy from low frequency and high amplitude vibration sources. Based on this, electromagnetic induction technique is chosen, which best suits our considerations. There exist several studies in literature. These studies are subdivided into two categories as micro-scale and macro-scale energy harvesters. In order to provide an alternative for batteries and power sources, macro-scale EM energy harvesters are considered since the output power of micro-scale designs are not sufficiently high. For the macro-scale designs, depending on the vibration nature,

the designs are categorized in again two groups, linear and nonlinear EM energy harvesters. For all types of EM harvesters, fixing natural frequency of the harvester with the ambient vibration frequency is the main challenge. The reason behind this is that most of the vibrations in nature exist within the low frequency band ( $< 10$  Hz).

Portable autonomous systems require miniaturized harvesters, which are functional at low-frequency ambient vibrations. However, they should be well-optimized to operate efficiently with these size and frequency limitations [23, 24]. Several attempts have been reported in the literature for EM energy harvester optimization. Cepnik *et al.* [25], obtained a mathematical model of an EM energy harvester, where the harvester is optimized by considering this model and utilized coil parameters to achieve maximum output power. The proposed generator has  $20.6 \mu\text{W}$  output power at 50 Hz with 1 g acceleration amplitude. In the model, instead of single magnet structure multiple magnets are used as shown in the Figure 1.5.

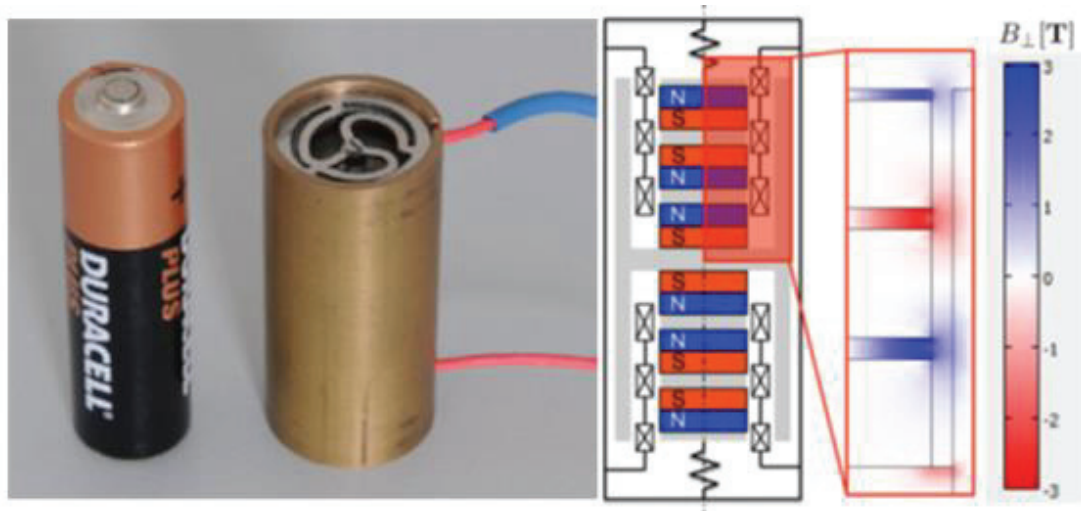


Figure 1.5: Picture and drawing of the prototype design [25].

In this model, output power is tried to be maximized by increasing magnetic flux passing through coil surface. In this AA battery sized design, the multiple magnets are placed as their poles face with each other. The facing poles results in larger magnetic flux gradients and so output power is maximized.

Shahosseini *et al.* proposed a hallbach array structure for the power optimization of the EM energy harvester [26]. The design is in volume of  $53 \text{ cm}^3$  (D-type battery) and capable of generating 15 mW power with 0.8 g excitation amplitude at 8 Hz frequency. The design with cylindrical hallbach array is as shown in Figure 1.6.

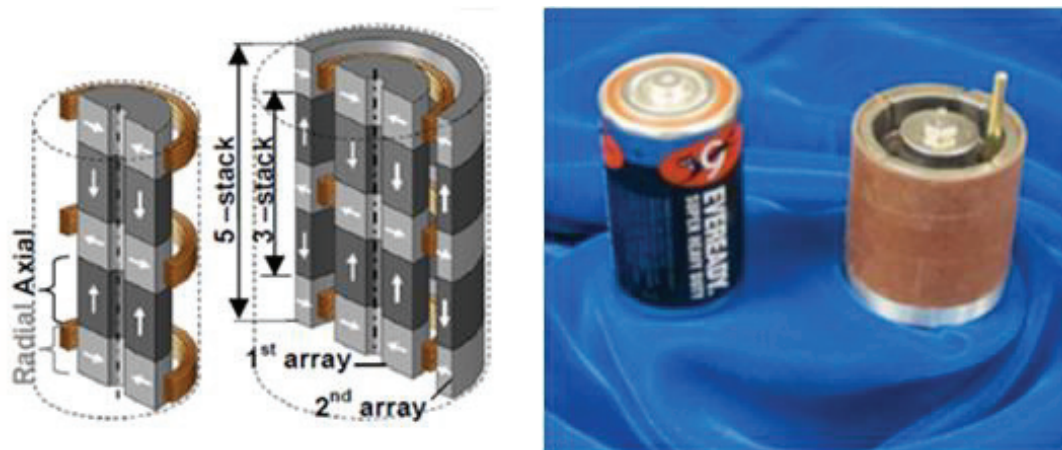


Figure 1.6: Single cylindrical and double-concentric hallbach array of D-cell sized design. [26].

In the design above, quite different magnetic configuration is proposed. With this structure, compared to single magnetic structure, at least three times greater magnetic flux density is observed. The reason behind this improvement is contribution of radial flux density to axial one which cannot be observed with single magnetic structure.

The study presented by Munaz *et al.* includes modeling and optimization of a non-resonant EM harvester, where the results are verified through experiments [27]. The volume of the proposed design is  $30 \text{ cm}^3$  which can generate 4.84 mW output power with 2 g excitation amplitude and 6 Hz resonance frequency. The FEA analysis of the model with magnetic field and flux lines is as shown in Figure 1.7.

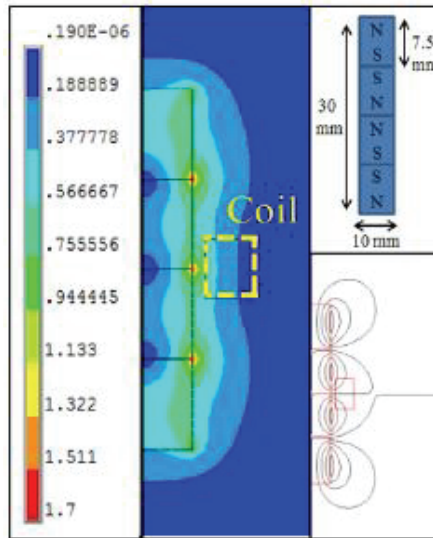


Figure 1.7: FEA model of the design proposed by Munaz with magnetic flux lines [27].

The model above consists of four single magnets where they are attached to each other in axially oriented way. When flux lines are investigated at the pole faces, it is observed that significant flux changes occur at these points.

There exist several studies in literature to increase magnetic flux gradients by oppositely facing magnets. However, magnetic flux improvement is not the only way to harvest maximum power from the environment. The nature of excitation is also important and there are also non-resonant vibrations in the environment. Human body vibrations are good example to these kind of excitation sources and several studies are performed on this topic. Rao *et al.* focused on human body vibrations and proposed an EM energy harvester model as shown in Figure 1.8.

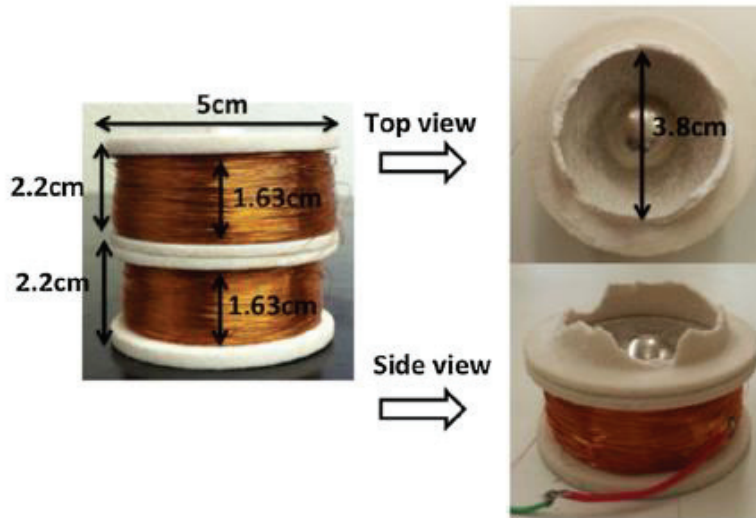


Figure 1.8: Non-resonant EM energy harvester design with top and side views [28].

In this model, a spherical magnet is used since the direction of motion generated by human body can exist in all x, y and z directions. Also, rechargeable battery is attached and overall system has  $100 \text{ cm}^3$  volume. System operates at low frequency band (1-6 Hz) and capable of generating  $3 \mu\text{W}/\text{cm}^3$  power density.

Similar to the human body vibrations, Fondevilla *et al.* concentrates on vibration created by ocean, wind and tides. To provide suitable design for randomness of these vibrations, spherical magnet and cylindrical coil is used as depicted in Figure 1.9.

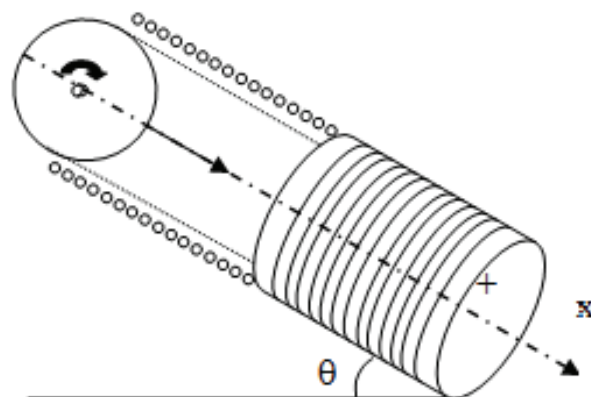


Figure 1.9: Schematic description of the EM harvester design proposed by Fondevilla [29].

Inclination angle changes with the vibrations, which leads movement of the spherical magnet inside the tube. The rotation of the magnet, while it is in motion, changes magnetic flux passing through coil surface and voltage is induced between the coil terminals.

Vibration generated from the cars and vehicles exists whenever they are in motion. From instrument panel to the engine compartment, vibration is continuous, high frequency and high amplitude. Bonisoli *et al.* presents a novel design by the consideration of vibration existed on the wheels of the cars. The design is as illustrated in Figure 1.10.

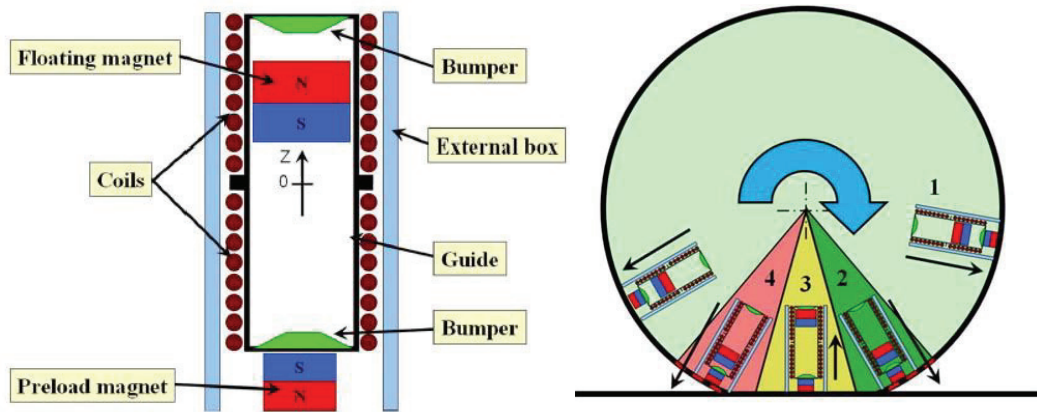


Figure 1.10: The EM energy harvester design to be attached on the wheels and operation principle [30].

The harvester is attached on the wheel as shown on the above and whenever harvester hits the ground oscillation occurs. Because the excitation amplitude is so high bumpers are attached to the bottom and top cap or the tube. Depending on the velocity of the car, applied excitation frequency changes. Therefore, tuning the device for appropriate velocity is easily adjustable.

Vibration generated by vehicle suspension is also important energy source for EM harvesters. Li [31] performs a study to convert vibration existed on vehicle suspension into electricity. According to the design, around 20 W energy is harvested from one

shock absorber, while the vehicle is being driven at 48 km/h. Another model for bridge monitoring application is designed and proposed with fabrication and experimental verification by Khan [32]. In the model, both PCB fabricated and wound coils exist where magnets are placed onto the Latex membrane. The elements used in this design is not familiar with the conventional EM energy harvesters. However, operation principle is based on Faraday’s Law of Induction as in general. The resultant output power of 18 mm x 18 mm harvester is 4  $\mu$ W at 27 Hz with 3 g excitation amplitude. Many of the studies in literature are based on vibration characteristics, which are ambient in nature. Belonging to the continuity of the vibration, EM harvesting devices are modified as observed from the studies explained up to now. For the designs, frequency and amplitude of the sources are the two main quantities to designate how to design the EM energy harvester. Najafi *et al.* summarizes the ambient vibration sources and miniature microsystem energy harvesting devices by presenting their relation on the graph shown below [23].

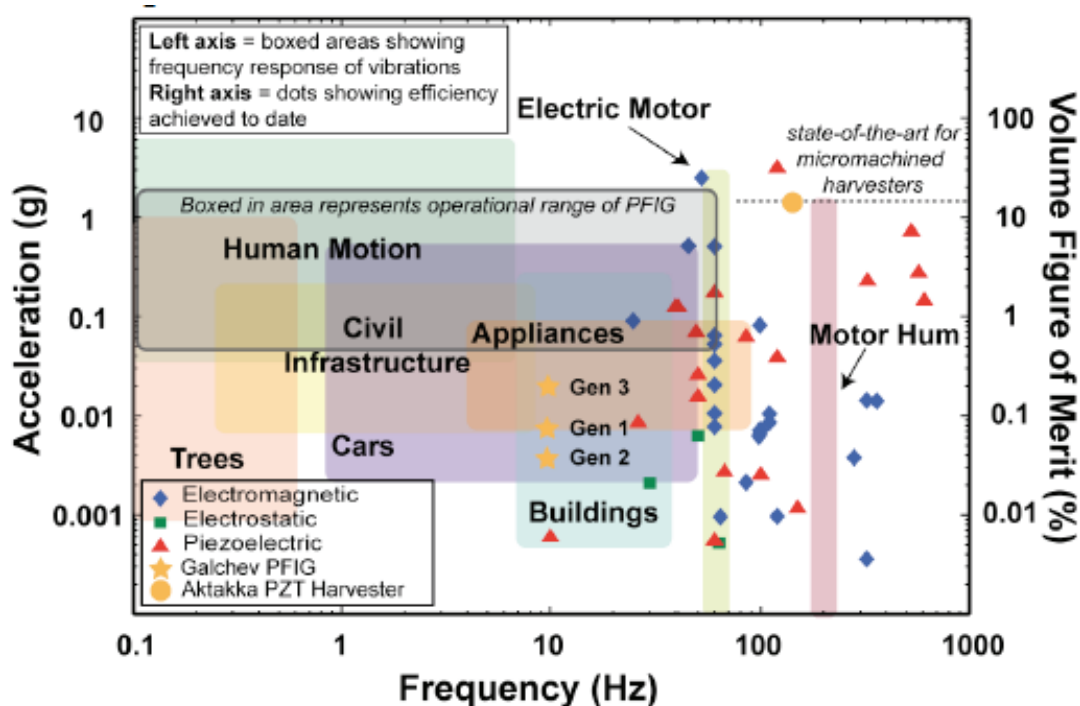


Figure 1.11: Acceleration vs frequency characteristics of vibration sources, found in various applications, and types of energy harvesters designed for these sources [23].

According to the figure above, there are not any designs for low frequency vibrations. The reason behind this is that the figure indicates microsystem applications. Especially for micro-scale designs, it is difficult to benefit from low frequency vibrations. Therefore, studies are concentrated on higher frequencies. However, for macro-scale case, frequency and acceleration range of the vibration sources given in the figure provide beneficial information to the low frequency designers. Addition to this study, Roundy presents acceleration and frequency values of the common ambient vibration sources in tabular form as shown in Table 1.3 [9].

Table 1.3: Ambient vibration sources with acceleration amplitude and excitation frequencies.

Vibration Source	$a = m/s^2$	$F_{Peak}$
Car engine compartment	12	200
Base of 3-axis machine tool	10	70
Blender casing	6.4	121
Clothes dryer	3.5	121
Person nervously tapping their heel	3	1
Car instrument panel	3	13
Door frame just after door closes	3	125
Small microwave oven	2.5	121
HVAC vents in office building	0.2-1.5	60
Windows next to a busy road	0.7	100
CD on notebook computer	0.6	75
Second story floor of busy office	0.2	100

Belonging to the table above, human body movement and car instrument panel are main vibration sources for low frequency designs. Appliances, buildings and civil infrastructures are also considerable source of vibrations. These examples are the proof of the fact that most of the vibrations in the environment have low frequency property. This is one of the reasons why low frequency vibrations are investigated in this thesis study.

Optimization studies in literature, mostly depend on maximizing output power through magnetic field and proper design for proper vibration characteristics.

Optimization through mathematical representations is also a popular idea. However, these studies do not focus on decreasing the operation frequency or optimizing the inertial mass of the harvester to get maximum performance at low frequency vibrations. Besides, most of the vibrations occur at low frequencies in nature, which makes optimizing the resonance frequency of the harvester a keystone for maximizing the output power. In this thesis study, optimization is performed on output power, resonance frequency and size of the harvester. In the next section, the aim of this thesis study is explained in detail.

### **1.5. Objective of the Thesis Study**

The purpose of this thesis study is to design, fabricate and test low frequency and high power output EM energy harvester for wireless system applications. The device dimension is limited with  $8 \text{ cm}^3$  to make the design convenient for portable systems. Similarly, targeted excitations are ambient ones which exist in low frequency level ( $< 10 \text{ Hz}$ ). With these limitations, the aim is to harvest larger output voltages at low excitation amplitudes and frequencies with smaller volume structures ( $< 8 \text{ cm}^3$ ).

Under the consideration of the studies reviewed in the previous section, the objectives of this thesis study is listed as,

1. Design, fabricate and test the macro-scale EM energy harvester,
2. Optimize the parameters to maximize the output power,
3. Modify the internal structure of the harvester to get larger output voltage,
4. Improve low frequency performance of the harvester with novelty,
5. Present proper designs for several vibration types available in the environment,
6. Provide linear and nonlinear designs suitable for ambient vibration characteristics,
7. Generate a model to predict resonance frequency of the device via simulations,

8. Introduce AA battery sized EM energy harvester design operating at low excitation frequency & amplitude.

The objectives were determined during the literature survey. There are many macro-scale EM energy harvester designs, operating at low frequencies. Additionally, very few optimization studies exist to decrease resonance frequency of the harvester. Device dimension plays a critical role on the resonance frequency of the EM energy harvester. There are few examples of low frequency harvester designs in smaller volume. As concluded in the previous section, for microsystems there exists no electromagnetic energy harvesting study for low frequency vibrations. Since the device dimensions are scaled down, interaction between the magnets increases, which yields to a greater stiffness and a higher resonance frequency. In literature, resonance frequencies of the harvesters are predicted using several assumptions and basic mathematical calculations. There is no proper model available for the detection of resonance frequency. This problem is attempted to be solved via a simulator generated using MATLAB. With this simulator, the actual motion of system is simulated and the actual resonance frequency is predicted. Working principle of the simulator is explained in detail in Chapter 3.

## **1.6. Outline of the Thesis**

In this chapter, energy necessity of the wireless sensor systems is discussed. By the electromagnetic induction technique, energy is planned to be supplied to these systems for their continuous operation. Several electromagnetic energy harvesting studies are analyzed. According to the weak and the strong sides of these studies, design objectives of the harvester, to be proposed in this thesis, are prepared.

In the second chapter, theory behind the electromagnetic energy harvesting is explained. To maximize output power, several designs are proposed with the help of

theoretical knowledge and mathematical expressions. These designs are investigated via simulations conducted on COMSOL Multiphysics.

One of the main weaknesses of the EM energy harvester design is the prediction of the resonance frequency. Chapter 3 presents a new analysis method and a simulator to detect the resonance frequency of the harvester before fabrication and experimental tests.

Chapter 4 is the experimental validation process of the simulations performed in the second and the third chapters. Initially, the fabrication and the test setup for EM energy harvester are explained. Then, the performance analyses of the harvesters are provided through experimental results. Finally, similar sized EM energy harvesters existing in the literature are listed and an overall performance comparison is demonstrated in tabular form.

The thesis studies are summarized in Chapter 5 with concluding remarks. Future works to be performed under this thesis subject are recommended at the end.

## **CHAPTER 2**

### **DESIGN MODELLING AND SIMULATION**

One of the aims of this thesis study is to present a device that converts vibration into electricity by using electromagnetic energy harvesting. The conversion is provided by Faraday's Law of Induction. This law bases on magnetic flux variation passing through a closed conducted. To achieve this, relative motion between a magnet and a coil is used in electromagnetic harvesting technique. With this relative motion, continuous magnetic flux change on the coil surface is achieved. Depending on the vibration characteristics, several designs are presented in literature. These designs are categorized as linear and nonlinear energy harvesters. Within the scope of this thesis study, different designs are presented according to the usage area of the harvesters.

In this part, theory behind the design of the EM energy harvesters is explained. Initially, theoretical knowledge on EM energy harvesters is given. Then, mathematical modelling of the system is presented. With respect to this model, how system parameters affect output power is studied. Finally, theoretical and mathematical information are combined and several designs are proposed. Analyses of these designs are performed by simulations, conducted via COMSOL Multiphysics.

## **2.1. Properties of Magnetic Levitation System**

Magnetic levitation is a terminology, which represents macro-scale electromagnetic energy harvesting. In this section, general information about magnetic levitation system is given. These systems are classified in two groups namely, resonant (linear) and non-resonant (non-linear) EM energy harvesters. Initially, working principles of the linear and the non-linear EM energy harvesters are explained. Then, their advantages and disadvantages are compared. Finally, why we prefer to design non-linear energy harvesters rather than linear ones is explained.

### **2.1.1. Linear & Non-linear EM Energy Harvesters**

In the design of EM energy harvesters, maximum output power is achieved by tuning resonance frequency according to the frequency of ambient vibrations. Similarly, linear EM energy harvesters are design to harvest energy from certain vibrations. Therefore, the frequency band of linear energy harvesters are narrow and specific for certain vibrations. In general, proposed linear EM energy harvesters are in micro-scale. For micro-scale designs, in order to maximize output power following methods are used: maximize inertial mass, minimize mechanical losses and increase the bandwidth of the harvester [33]. With these considerations, several designs and optimization strategies are presented. As a design example, in [34], rotary EM energy harvester design is preferred for high-power density acquirement. Apart from this, optimization procedure to maximize output power is presented in [35]. In this study, linear EM energy harvester is described by basic equations and optimization is performed by mathematical calculations.

In optimization of linear EM energy harvesters, researchers realize non-linear effects of the harvesters. In fact, these non-linear effects are deeply analyzed to maximize output power of the designs. Besides, some of the environmental vibrations

show non-linear characteristic such as wind, wave and human body sources. The frequencies of this kind of vibrations are changeable, so linear energy harvesters are not suitable due to their narrow bandwidth. As a result, all these facts turn the idea of the designers to non-linear energy harvesters.

The stiffness of the designs determines the linearity and non-linearity of the harvesters. In literature, several studies are presented to show benefits of the non-linear devices [36, 37]. Additionally, a significant performance comparison between linear and non-linear energy harvesters is provided by Mann and Sims as shown in Figure 2.1.

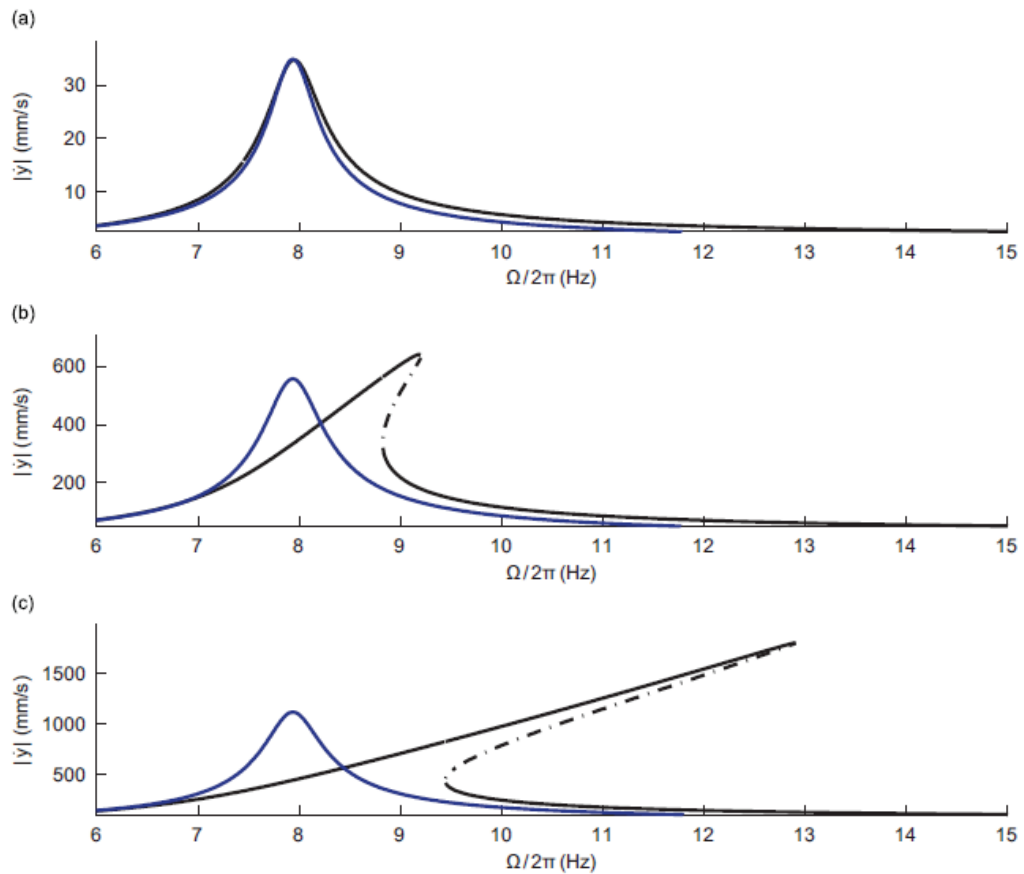


Figure 2.1: Frequency response curves of the relative velocity for the non-linear and a linear oscillator for several excitation amplitudes, (a) 0.1 m/s<sup>2</sup> (b) 2 m/s<sup>2</sup> and (c) 4 m/s<sup>2</sup> [6, 38].

According to the figure above, performances of both of the oscillators are nearly same up to certain level of excitation amplitude. With the increase in amplitude, both of the designs give positive reaction at the output. However, for non-linear energy harvesters, better output performance is observed with increase in resonance frequency. The reason behind these facts is the non-linear response includes harmonics.

### **2.1.2. Preference of Non-linear Systems**

Up to now, general information about the EM energy harvesters is given. At this point, design process begins with the choice of non-linear EM energy harvesting. The advantages of non-linear systems compared to linear ones are listed below,

- Provides larger output voltages compared to exactly same linear designs [38]
- Frequency bandwidth is larger
- Resonance frequency of non-linear systems is tunable with excitation amplitude
- Larger excitation amplitudes increases bandwidth
- Linear harvesters are generally in micro-scale, which results in design challenges.

Additionally, any fabrication error on dimensions leads to another resonance frequency for linear systems [39].

In the following sections, optimization procedure is explained. Several designs are proposed to maximize output performance of the harvester. In the meantime, harvester system is mathematically modelled to see the effect of design parameters on the output.

## 2.2. Modeling of Magnetic Levitation System

In this section, how to model the magnetic levitation system is explained. Initially, the system is mathematically represented. The aim here is to define system parameters clearly. Then, effects of these parameters on the output is observed. By doing so, priorities on optimization process are defined and ordered. At the end of this section, our milestones on the design of EM energy harvester is prepared step by step.

### 2.2.1. Mathematical Representation of the System

The EM energy harvesting systems are mathematically represented as second order spring, mass, damper system as illustrated on Figure 2.2.

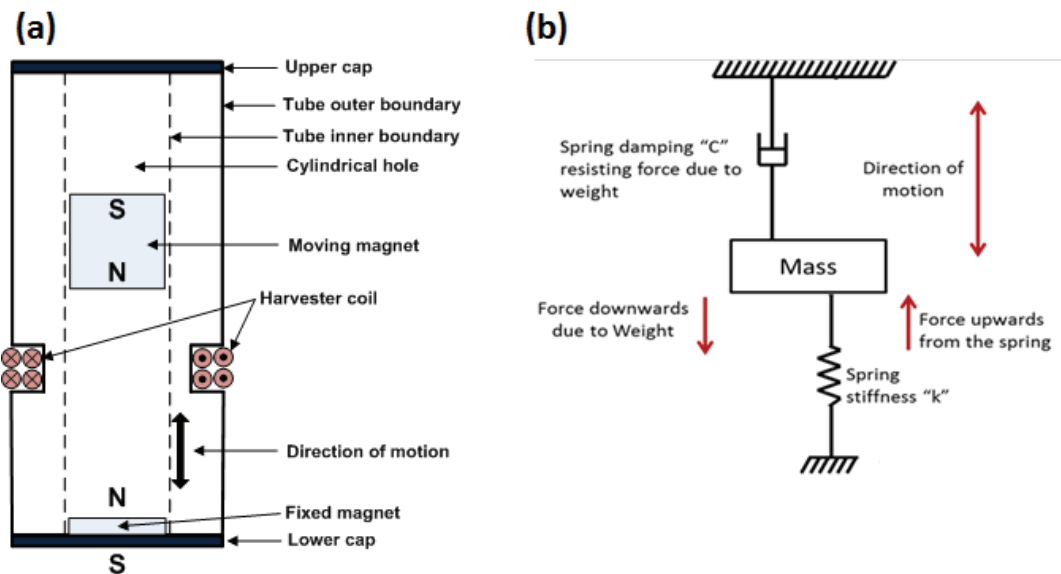


Figure 2.2: (a) Schematic diagram of electromagnetic energy harvester. (b) Model of the resonant electromagnetic energy generator.

In the figure above, interaction between the fixed and the moving magnets is resembled to a mass spring system. The repulsion between magnets are modeled with virtually assigned spring and  $k$  represents stiffness of this spring. Addition to magnetic forces, there exist gravitational and damping forces. The gravitational force is related with the weight of the mass and always constant. During the oscillation, the moving part feels force opposite to its direction of movement. These forces are called damping forces and they are taken into account in the model with the damping constant  $c$ . The damping has two coefficients namely, electrical and mechanical damping coefficients. The electrical damping exists due to Lenz's Law, which states that when an *emf* is generated on closed conductor by magnetic variation, a current exists to oppose that magnetic flux change. This existing current creates a mechanical force to resist the motion. For EM energy harvesters, generated voltage is in mV to V levels where internal resistance is in  $\Omega$  to  $k\Omega$  levels. Therefore, generated current is in  $\mu A$  to mA levels so electrical damping contribution is negligible compared to mechanical damping force. The mechanical damping is created by air friction (drag) force. At this point, damping and magnetic forces become mathematically representable. Apart from these, acceleration of the moving part is determined by law of inertia. All of these forces are result of applied excitation. To represent whole system mathematically, force balance equation is written as shown below.

$$F_{Acceleration} + F_{Damping} + F_{Magnetic} = F_{Excitation} \quad (2.1)$$

$$m_{magnet}a + cv + kz = F_{Excitation} \quad (2.2)$$

$$m_{magnet} \frac{\partial^2 z}{\partial t^2} + c \frac{\partial z}{\partial t} + kz = A m_{magnet} \sin(2\pi ft) \quad (2.3)$$

With the equation (2.3), the motion of the moving part is mathematically represented. Here,  $m$  represents mass of the magnet,  $k$  represents stiffness of magnetic force and  $c$  represents the damping constant.

In the following section, output power of the system is derived from Faraday's Law of Induction. Then, parameters effecting output power is analyzed.

### 2.2.2. Effect of System Parameter on Output Power

Operation principle of electromagnetic (EM) energy harvesters is based on Faraday's law of induction, which explains how electromotive force (*emf*) is produced by the changing rate of magnetic flux ( $d\phi_B/dt$ ) passing through a closed conductor. The generated *emf*,  $\varepsilon$  across the coil is represented as:

$$\varepsilon(t) = -\frac{d\phi_B}{dt} = -\left(\frac{dB}{dt}A + \frac{dA}{dt}B\right) \quad (2.4)$$

In (4),  $\phi$  is the magnetic flux,  $B$  is the magnetic flux density,  $A$  is the area of the coil and  $t$  is time. Equation (1) can be used to express *emf*  $\varepsilon$  an across N-turn coil:

$$\varepsilon(t) = -\left(\sum_i^N \frac{d\phi_{Bi}}{dz}\right)\left(\frac{dz}{dt}\right) \quad (2.5)$$

where  $\phi_{Bi}$  is the magnetic flux for the  $i^{th}$  coil turn and  $dz/dt$  is the relative velocity between the coil turn and the magnet. The pick-up coil is wounded around a cavity and some of the turns are wounded on top of previously wounded ones. Therefore, some of the turns have larger surface area. As e result, the flux  $\phi_B$  passing through coil is not same for each turn because area of the turns are different. Hence, the generated voltage  $\varepsilon$  is represented as a summation of voltage generated on each coil turn. Harvesting larger output power is aimed, while designing the EM energy harvester. Output power  $P_{out}$  is given in (2.6), where  $R_{Coil}$  and  $R_{Load}$  are coil and load resistances of the harvester, respectively.

$$P_{out} = \left\{ \left( \sum_i^N \frac{d\phi_{Bi}}{dz} \right)^2 \right\} \left\{ \frac{R_{Load}}{(R_{Load} + R_{Coil})^2} \right\} \left\{ \left( \frac{dz}{dt} \right)^2 \right\} \quad (2.6)$$

According to the equation (2.6), effect of the system parameters on output power is defined as follows;

- Coil resistance should match with load resistance.
- Magnetic flux variation on z axis should be maximized.

- Larger sized magnets provide larger magnetic flux gradients.
- Number of coil turns should be well defined.
  - Increase in number of coil turns result in larger coil resistance.
  - Maximum coil turn should be achieved with minimum usage of copper wire. To do so, coil should be wounded around smaller diameter tube.
- Relative velocity between coil turns and the magnet should be maximized
  - Enough distance should be provided to the moving part.
  - Stiffness of the system should be well defined. Otherwise, oscillation distance reduces.

The analyses above states that any improvement on each of the parameter shows adverse effect on the other ones. As an example, number of coil turns is directly related with coil resistance, where number of the turns has positive and coil resistance has negative effect on output power. Similarly, in order to make coil resistance as small as possible, diameter of the harvester should be decreased. Then, magnet sizes and magnetic flux gradients decreases. On the contrary, increase in magnet size results in greater stiffness value, which restricts oscillation distance on the moving part. In conclusion, under the effects of several design parameters, optimum design is provided. The design procedure is explained in the next section.

### **2.3. Analysis and Simulation Results of Proposed System**

The following rules should be applied in order to maximize the power generated by an EM harvester [41]:

- i. Spring constant,  $k$ , should be set in a way that resonance frequency of the system becomes equal to the excitation frequency.
- ii. Damping and stray losses should be as small as possible
- iii. Mass of the moving part,  $m$ , should be as large as possible
- iv. Load impedance  $R_{Load}$  should match source impedance  $R_{Coil}$ .

It is clear from equation (2.6) that the position of the coil, the number of turns and the coil size directly affect output power as well as the magnetic field. The position of the coil is related to the relative motion between the coil and the magnet. Harvested power is proportional to the square of the number of coil turns. However, increasing the number of coil turns increases the coil resistance, which decreases the output power. Therefore, there is a trade of between the number of coil turns and the coil resistance. Summarizing, the harvested power of the electromagnetic induction device is controlled by three main factors [26]:

- i. Coil parameters (number of turns, resistance, position, etc.)
- ii. Relative motion between the coil and the magnet
- iii. Flux linkage

Above factors support the mathematical expression in (2.6), where matching source and load impedances maximizes the second term. Square of the flux linkage and the number of turns are directly proportional to the output power. Moreover, the relative motion between the coil and the magnet is represented as  $dz/dt$ , as stated before.

Our aim is to harvest larger output power at low excitation frequencies with compact structures ( $< 8 \text{ cm}^3$ ). In our previous work [42], natural frequency of the system is formulated as  $f_n = (1/2\pi)\sqrt{k/m}$ , where  $k$  is the stiffness of the system and  $m$  is the mass of the moving part. The natural frequency decreases by adding a non-magnetic mass to the moving part. The additional mass does not affect the stiffness  $k$ , where it increases the total mass of the system  $m$ . Consequently, the natural frequency of the system decreases. With the underlined design considerations, several optimization procedures are executed on the previously designed EM energy harvester to provide maximum output power.

Various magnetic structures are analyzed for macro-scale energy harvesters: single-magnet (Figure 2.3(a)), magnet with inertial mass (Figure 2.3(b)), inertial mass in between axial magnets (Figure 2.3(c)), and ferromagnetic spacer between oppositely faced magnets (Figure 2.3(d)). In Figure 2.3, harvesters' volume is  $7 \text{ cm}^3$

with 14 mm diameter and 46 mm height. Cylindrical magnets used in the moving parts have 5 mm diameter, various heights and 1.2 T axial magnetization. By increasing the height of the single-magnet in Figure 2.3(a), the output power is expected to increase due to the increase at the flux linkage. Simultaneously, an increase in the magnet height leads to an increase in the magnetic stiffness  $k$ , which has an adverse effect on the resonance frequency. According to (2.3), the relative velocity between the coil and the magnet has a significant effect on the output power as the flux linkage. However, an increase in the magnet height reduces the displacement of the moving part, as well as the relative motion between the magnet and the coil. Figure 2.3(b) presents a solution to this problem by adding a tungsten inertial mass to the moving part. In [42], it is underlined that instead of increasing the magnet height, addition of a tungsten inertial mass to the magnet yields to better results at the output, at lower excitation frequencies. In contrast, increased height results in larger flux linkage leading to greater repulsive forces and larger stiffness. Thus, larger amplitude excitations are necessary to overcome these repulsive forces. Additionally, higher repulsive forces reduce the amplitude of oscillation. To remove all these negative effects, a tungsten inertial mass, due to its higher density, is attached to the moving part. By doing so, the oscillation distance is protected, the resonance frequency is lowered and the output power is increased.

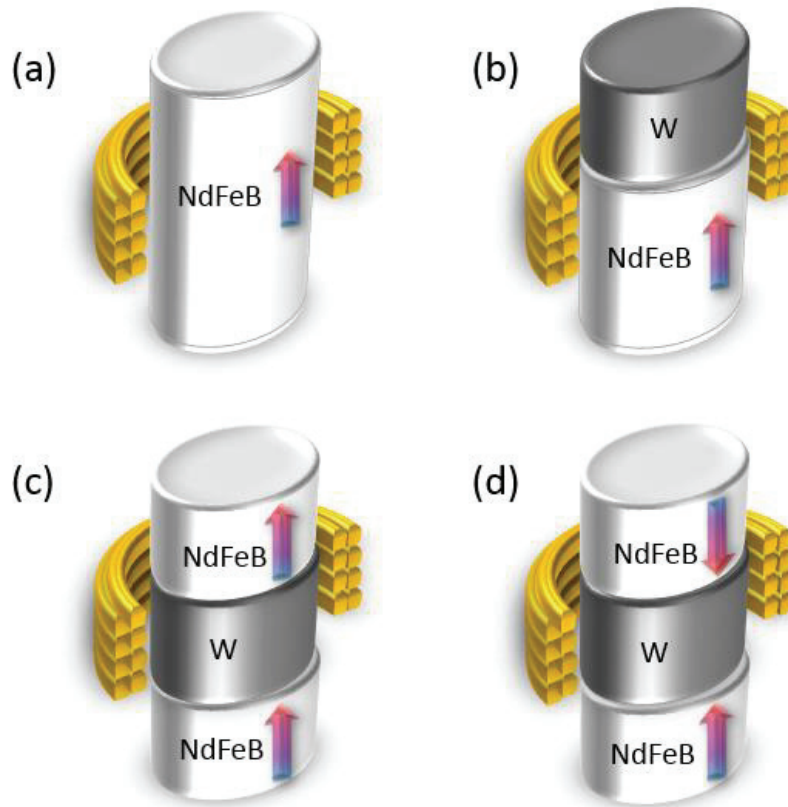
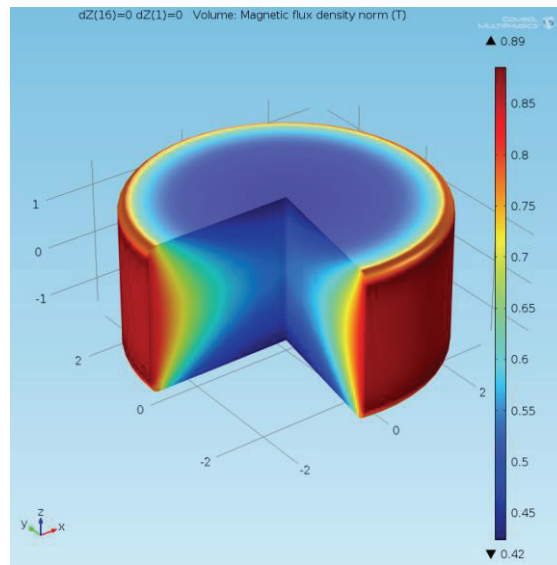


Figure 2.3: Schematic models of analyzed magnetic structures: (a) single-magnet, (b) magnet with inertial mass, inertial mass between (c) axial & (d) oppositely faced magnets.

The shape of our previously designed energy harvester is not suitable for improvements since its height is not sufficiently large. Therefore, any addition to the moving part or an increase in the magnet height restricts the amplitude of the oscillation. To achieve improvements, dimensions of the harvester are modified, that is its diameter is reduced (20 mm to 14 mm) and its height is increased (20 mm to 46 mm), which is close to a regular AA-sized battery dimensions with a  $7 \text{ cm}^3$  volume. At the beginning of the study, the moving magnet dimensions and the coil parameters are determined through FEA performed using COMSOL Multiphysics. The height and the width of the magnet are determined according to the magnetic flux density norm calculated through simulations. The largest magnetic flux linkage occurs at the corners of the magnet as shown in Figure 2.4.

(a)



(b)

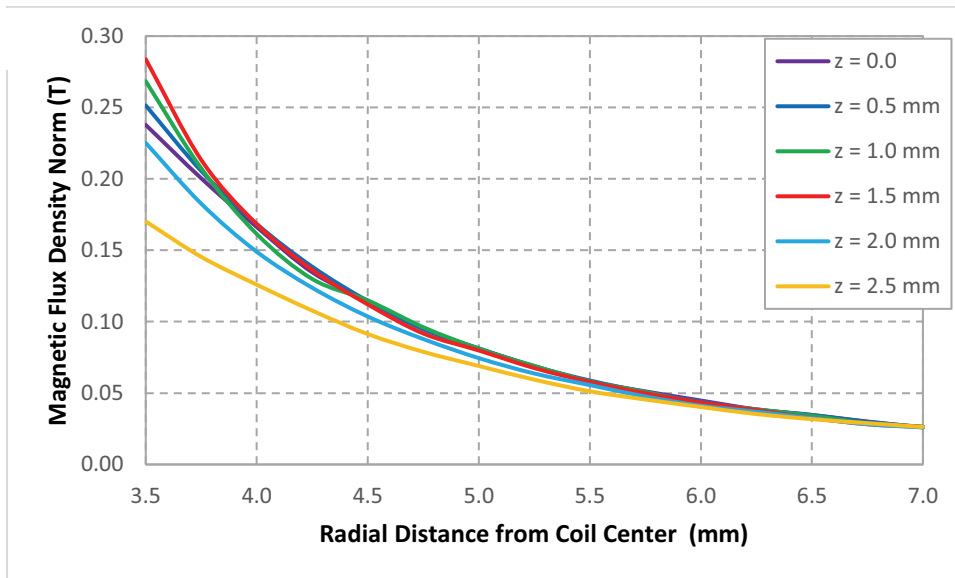


Figure 2.4: (a) 3D view of the finite element model, showing magnetic flux density norm of stationary magnet ( $\varnothing$ : 2.5 mm h: 3 mm) at  $z=0$ . (b) Variation of magnetic flux density norm on the coil surface with magnet displacement.

A magnet with 3 mm height is placed at  $z = 0$ . In Figure 2.4(b), it is observed that the maximum value of the magnetic flux density occurs at  $z = 1.5$  mm, which corresponds to the corner of the magnet. In order to observe the magnetic flux variation more clearly, simulations are performed, when magnet corner and coil surface are at the

same position. Figures 2.5(a) and 2.5(b) present the magnetic flux density norms of the magnets with different heights, where magnet diameter is randomly set as 6 mm.

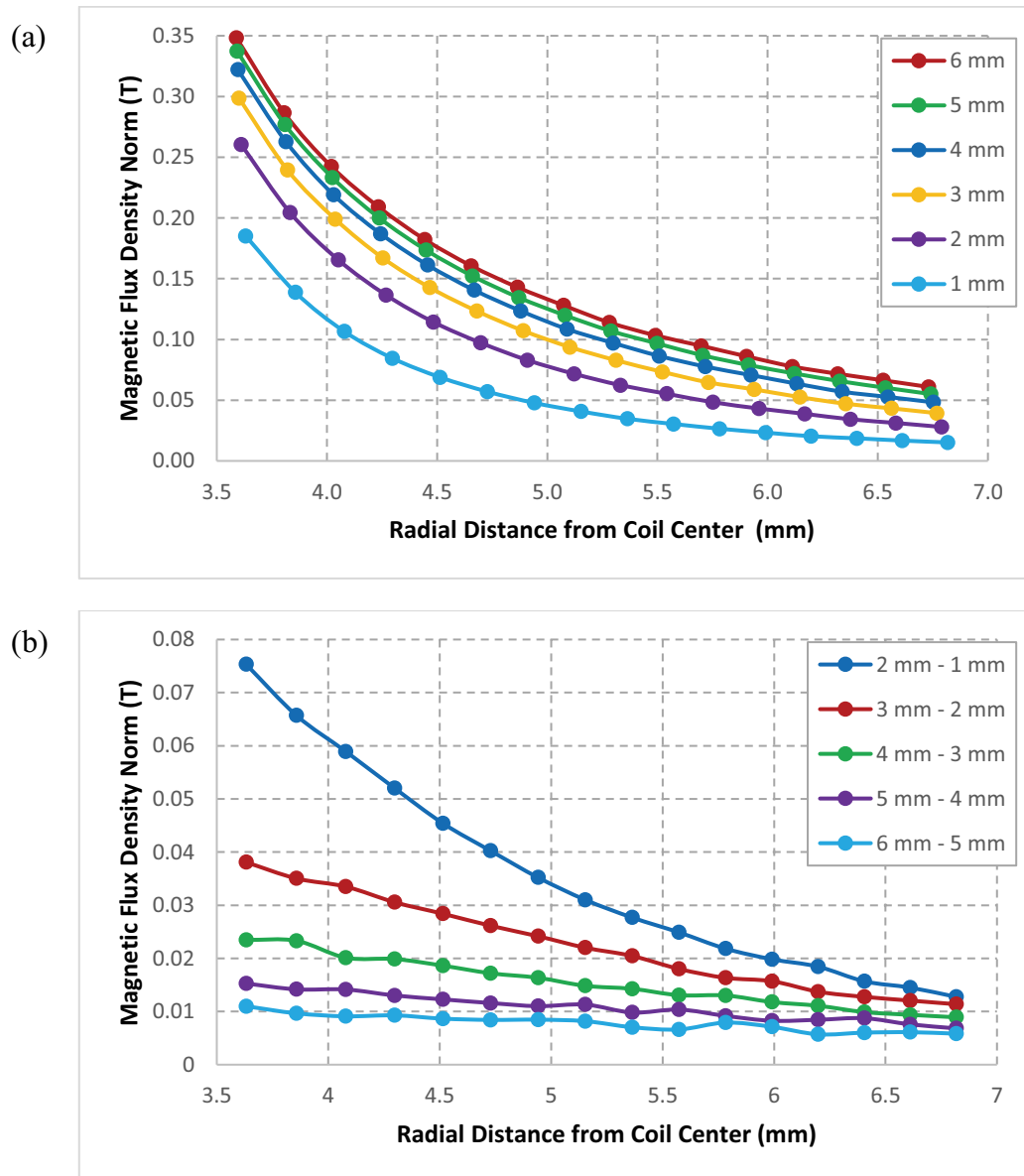


Figure 2.5: (a) Magnetic flux density norm change on the coil surface. (b) Variation of the magnetic flux density norm on the coil surface with the increasing magnet height.

Magnet height affects flux linkage and oscillation distance simultaneously by providing a trade-off, where both have the same influence on the output power. Figure 2.5(a) presents magnetic flux change on a virtually assigned coil surface with respect to the magnet height. Difference of the flux density between several heights can be observed more clearly in Figure 2.5(b). As magnet height increases, the resultant magnetic flux change dramatically decreases, especially at smaller radial-coordinate values of the coil surface. Considering the magnets with 3 mm and 6 mm height, the magnetic flux density variation on the coil surface is at most 0.05 T. In other words, duplication of magnet height results in only a 0.05 T magnetic flux contribution. Therefore, as concluded in [42], instead of increasing the magnet height of a single-magnet structure, using the modified structures is more effective for both higher output voltage and lower resonance frequency. In [25], it is stated that the output power of the harvester can be increased by modifying the geometry. In the system, magnets in the moving part are placed in such a way that poles provide repulsive forces to each other. The design, where magnets provide repulsive forces to each other is better by a factor of 2 compared to the single-magnet structure in terms of magnetic flux density [26]. Similarly, in [40, 43], a modification is done by axial orientation of the magnets to provide repulsive forces to each other. Maximization of magnetic flux density is easier by repulsive forces compared to attractive forces. Therefore, modified structures are preferred as illustrated in Figures 2.3(c) and 2.3(d). Height of the moving magnet to be used in these modified structures, is determined as 3mm according to the results of the analysis on Figure 2.4.

The total diameter of the system includes the magnet diameter and the coil thickness. The trade-off between the diameter of the magnet and the coil thickness is analyzed in terms of magnetic flux density via COMSOL as shown in Figure 2.6.

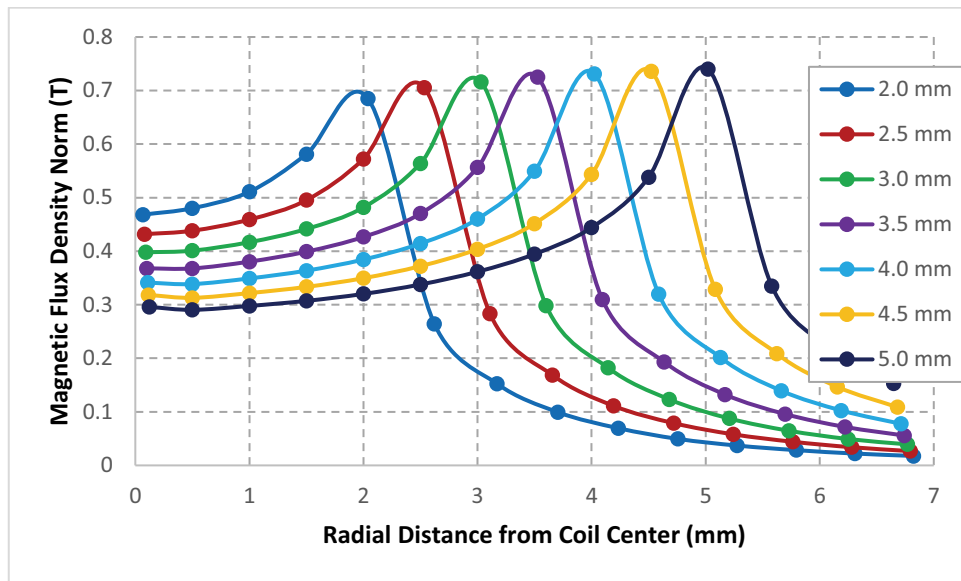


Figure 2.6: Variation of the magnetic flux density norm on the coil surface with the change in the magnet radius.

Radial-coordinate of the harvester is 7 mm, which is also limited by the 0.5 mm air gap and the 0.5 mm container thickness. With 60  $\mu\text{m}$  diameter copper coil, it is possible to wound 345 coil turns at a 1 mm thick 3 mm long coil cavity. Area under the curves presented in Figure 2.6 and the resulting coil turns are listed in Table 2.1. Note that, larger sized magnets provide larger magnetic flux as expected. On the contrary, flux change rates significantly reduce with increasing the size. Output voltage is directly related to the product of the flux change and the magnet velocity. Assume that in the next position of the magnet, a 10% percent decrease in magnetic flux is observed on coil surface. It is already concluded that, the magnetic flux change with position for larger sized magnets are lower compared to smaller sized magnets. By assuming 10% percent reduction for all cases, the worst case assumption is performed for smaller radius magnets. Additionally, velocity of the moving parts is the same for all cases. As a result, resultant output voltage can be calculated between the two consecutive positions of magnet. Results clearly demonstrate that the number of coil turns has a greater effect on the output power compared to the magnetic flux

variations. With optimum result consideration, coil thickness and magnet diameter are assigned as 3.5 mm and 5 mm, respectively.

Table 2.1: Comparison of magnet and coil parameters according to their effect on output voltage

<b>Coil Thickness</b>	<b>Number of Coil Turn</b>	<b>Magnet Radius</b>	<b>Area Under the Curve</b>
4.0 mm	1370	2.0 mm	0.00166 T
3.5 mm	1200	2.5 mm	0.00189 T
3.0 mm	1030	3.0 mm	0.00206 T
2.5 mm	860	3.5 mm	0.00220 T
2.0 mm	685	4.0 mm	0.00232 T
1.5 mm	515	4.5 mm	0.00239 T
1.0 mm	345	5.0 mm	0.00243 T

Coil length also has a significant effect on the number of coil turns. Coil length simulations are completed by using the ‘Induced voltage of moving magnet’ model of COMSOL. Several excitation amplitudes at 8 Hz are applied to the model with various coil lengths. The proper coil length for the proper excitation amplitude is determined in terms of the resultant output power. Figure 2.7 shows the effect of coil length on the output power for several excitation amplitudes.

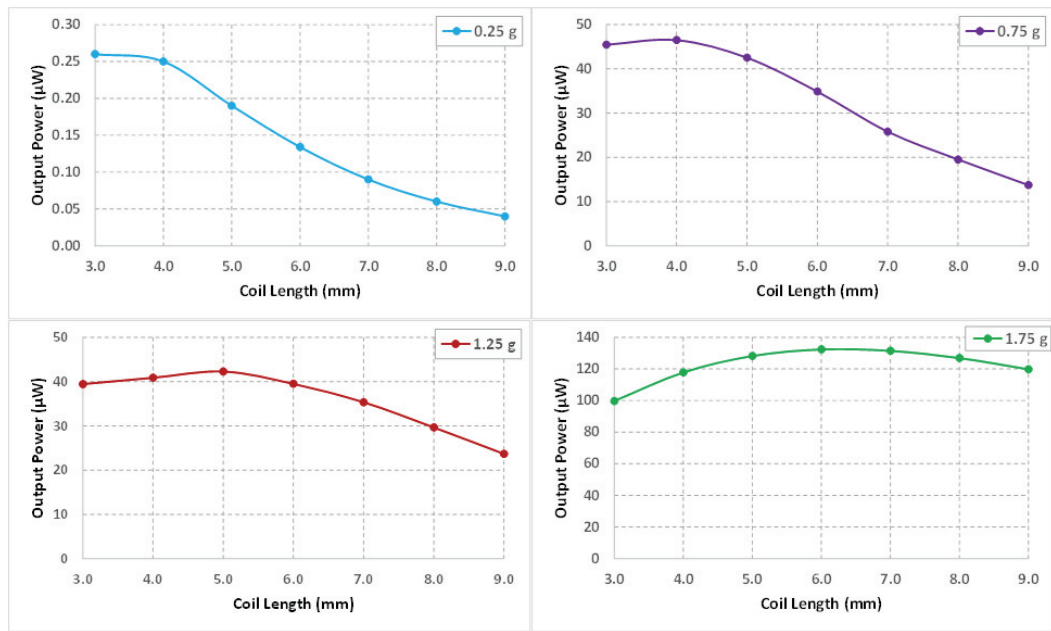


Figure 2.7: Calculated output power for various coil lengths at low frequency (8 Hz) vibrations.

Figure 2.7 indicates that at low vibration amplitudes the 3 mm coil length best suits for maximum output power requirement. When the excitation amplitude increases, the coil length for maximum power also increases. Aim is to design a harvester to operate at low frequency and low excitation amplitude vibrations (< 4 mm & < 10 Hz), for which coil length should be 3 mm. Design specifications of the moving magnet for an AA battery sized energy harvester are presented in tabular form in Table 2.2.

Table 2.2: Design specifications of the moving magnet for low frequency and low excitation amplitudes

Parameters	Values
Magnet Diameter	5.0 mm
Magnet Height	3.0 mm
Coil Thickness	3.5 mm
Coil Length	3.0 mm
Coil Turns	1200

Analyses show that for an AA battery sized design at low amplitude excitations, 5 mm diameter and 3 mm height magnet best suits to modified structures. With various modifications on the moving part, more efficient results at the output can be observed.

Figure 2.3(c) illustrates a tungsten inertial mass in between the two magnets. With this approach, twofold magnetic flux existence is expected in one turn of periodic motion. To do so, the sinusoidal wave at the output voltage in one period of time is expected to be doubled. Tungsten mass provides a connection between the magnets and increases the mass of the moving part. Additionally, due to its nonmagnetic nature, the interaction between the magnets is expected to reduce. Otherwise, the results would be worse than the structure with increased magnet height. In literature, it is stated that, repulsive forces results in larger magnetic flux density norms [25-26,40,43]. In Figure 2.3(d), the magnetic flux passing through the coil surface is expected to increase with opposite orientation of the magnets. To validate the expectations, a magnetic field analysis is performed for three different structures via COMSOL Multiphysics. Two of the magnetic structures in Figure 2.8 (c) and (d) resemble the models in Figure 2.3 (c) and (d), where the ones in Figure 2.8 (a) and (b) are as in Figure 2.3 (a) and (b), respectively. All these structures have the 5 mm diameter and a total thickness of 10 mm.

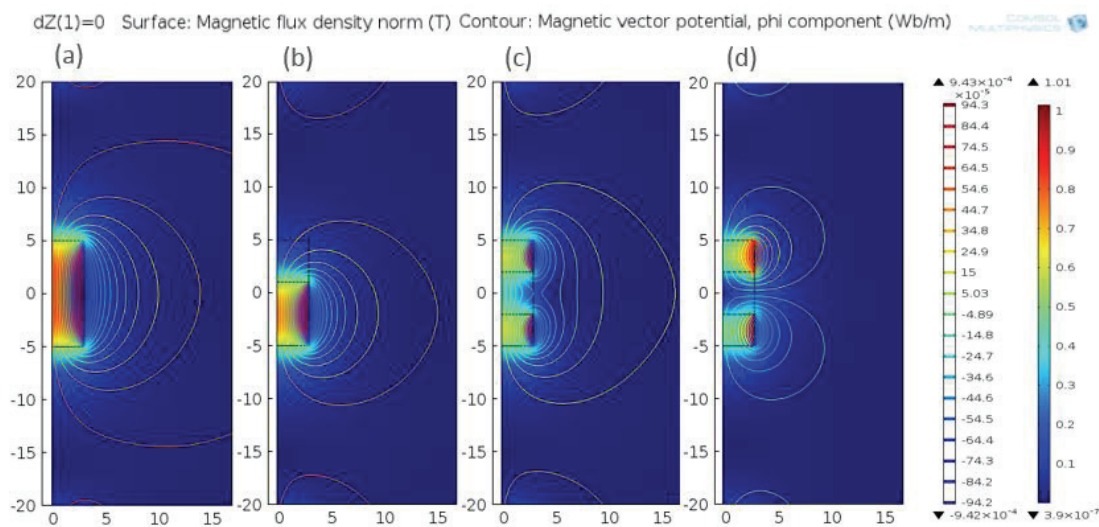


Figure 2.8: Finite element analysis results showing flux lines for (a) single-magnet, (b) inertial mass placed on top of magnet, inertial mass placed between (c) axial & (d) oppositely faced magnets.

Figure 2.9 indicates magnetic flux density norm of the moving structures, displayed in Figure 2.8, on the coil surface, which is virtually placed at  $z = 0$ .

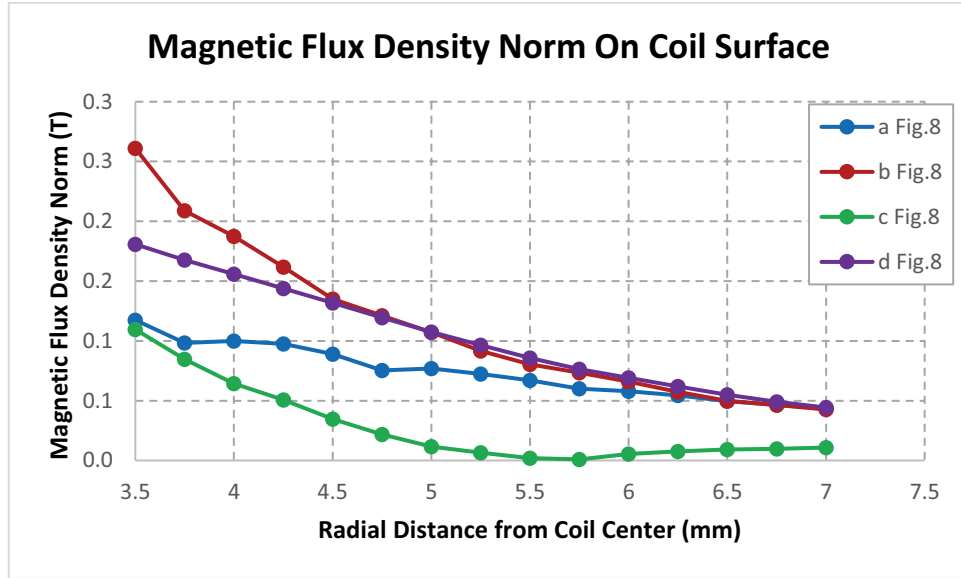


Figure 2.9: Plot of the magnetic flux density norm along the radial component of the coil surface.

In [44], it is stated that for larger output power it is necessary to get larger magnetic flux gradients, which is easily provided by repulsive forces. Magnetic flux gradients shown in Figure 2.9 support this idea. Instead of a single magnetic structure, modified structures provide larger flux gradients. According to the Figure 2.9, 4 mm height tungsten with 6 mm height magnet system provides greater magnetic flux change compared to other ones. However, this is due to the fact that coil is placed at  $z = 0$  which is very close to the magnet corner. If the coil is placed in between the edges of the magnet (just like other systems), axially oriented system provides the greatest magnetic flux change. With this consideration, optimization analysis using COMSOL concludes that the best design for maximum output power is the oppositely oriented magnetic structure shown in Figure 2.3(d), especially for low frequency and low excitation amplitude applications.

In our previous work, only one fixed magnet is placed to the bottom cap to increase the displacement of the moving part. Compared to both ends-fixed magnet system, the resonance frequency is lower and the displacement of the moving part is greater. In this case, magnetic stiffness of the system decreases, and consequently the resonance frequency reduces as emphasized in [40]. Apart from this, for EM energy harvesters, very few studies are performed on coil optimization [42-43,45]. In the Chapter 4, experimental verification of the coil optimization is explained.

## **2.4. Conclusion**

In this chapter, design procedure of the EM energy harvester is explained. Compact EM energy harvester design, capable of providing high output power at low frequency and low amplitude excitations, is aimed.

Initially, system is mathematically represented to analyze effects of input parameters at the output. Then, this analyses are combined with our previous work and literature survey. By doing so, design steps are determined and modelling begins.

In the modelling section, simulation analyses are performed via COMSOL Multiphysics. According to the simulation results, magnet dimensions and coil parameters are determined. Each of the parameters related with the moving magnet and coil, are deeply studied with several simulations and calculations. Additionally, several studies from literature are taken into account in the determination of these parameters.

In order to optimize design, four different moving magnet structures are proposed. From the first to the last, developments and improvements are applied to the moving magnet. In Chapter 4, similar process is performed by experimentally. The analyses in this design and modelling section is experimentally validated.

## **CHAPTER 3**

### **MATLAB SIMULATOR**

In this chapter, resonance frequency detection techniques for the proposed generator designs are explained. Initially, the operation principle of the simulator is described. Then, two different techniques are proposed referring to operation principle. Finally, resonance frequencies of several designs are estimated with the output of simulator model.

#### **3.1. Operation Principle of the Simulator**

Resonance frequency is one of the main design parameters of EM energy harvesters. The resonance frequency of the energy harvesters are estimated through the analysis of output voltage versus frequency plot. In practice, excitation comes and under the effect of magnetic forces, the moving part of the system begins to oscillate. In order to simulate this action via COMSOL, excitation should be applied to the overall system and resultant motion of magnet should be recorded. However, expected motion cannot be simulated in COMSOL. Since motion can be assigned only one

component of model providing that other ones should remain stationary. Therefore, FEA through COMSOL is inadequate to model the operation of EM energy harvester. Consequently, simulator design is necessary to solve this problem so that frequency response of generators to the applied excitation can be recorded. According to the records, resonance frequency of the harvester can be determined and design will be performed belonging to ambient energy source frequencies.

Motion of the moving part under the effect of acceleration, damping and magnetic forces is already formulized in literature. With the applied excitation, magnet feels acceleration and moves out of equilibrium position. At that instant, distance between the fixed and the moving magnets changes. Hence, magnetic forces begin to act on the moving magnet and affect its motion. Whole process repeats itself with the excitation frequency and continues to the end of the excitation. This process for each period of time is modeled by using MATLAB.

System begins its operation with sinusoidal excitation. Initially, input should be sampled to detect the response of the moving magnet at the first instant. Between the first and the second sampled points of input, acceleration is assumed as constant. Then, for the next point, forces acting on the moving magnet should be defined. Since, addition to disturbance coming from outside, magnetic forces begin to act on the magnet. With the contribution of magnetic forces, new acceleration value of the magnet is calculated. The next position is determined under the effect of final acceleration value. The position of the magnet changes continuously with acceleration. Similarly, variation of position changes magnetic forces acting on the moving magnet and indirectly acceleration. Therefore, at the end of each instant, corresponding magnetic force and excitation are revised. Then, acceleration value is updated with the addition of the next value to the previous one. To sum up, acceleration is defined at first, and then the next position of the moving magnet is calculated.

In order to define magnetic forces for each instant in the model, magnetic force versus displacement characteristics is modeled via COMSOL. Then, this discrete data

is transferred into continuous function by using 'lsqcurvefit' command of MATLAB. By doing so, continuous function of the magnetic force versus displacement plot is obtained. Finally, for any values of displacement, resultant magnetic force can be calculated in Newton (N) through mathematical equation.

Flowchart of the operations handled by the model is illustrated in Figure 3.1.

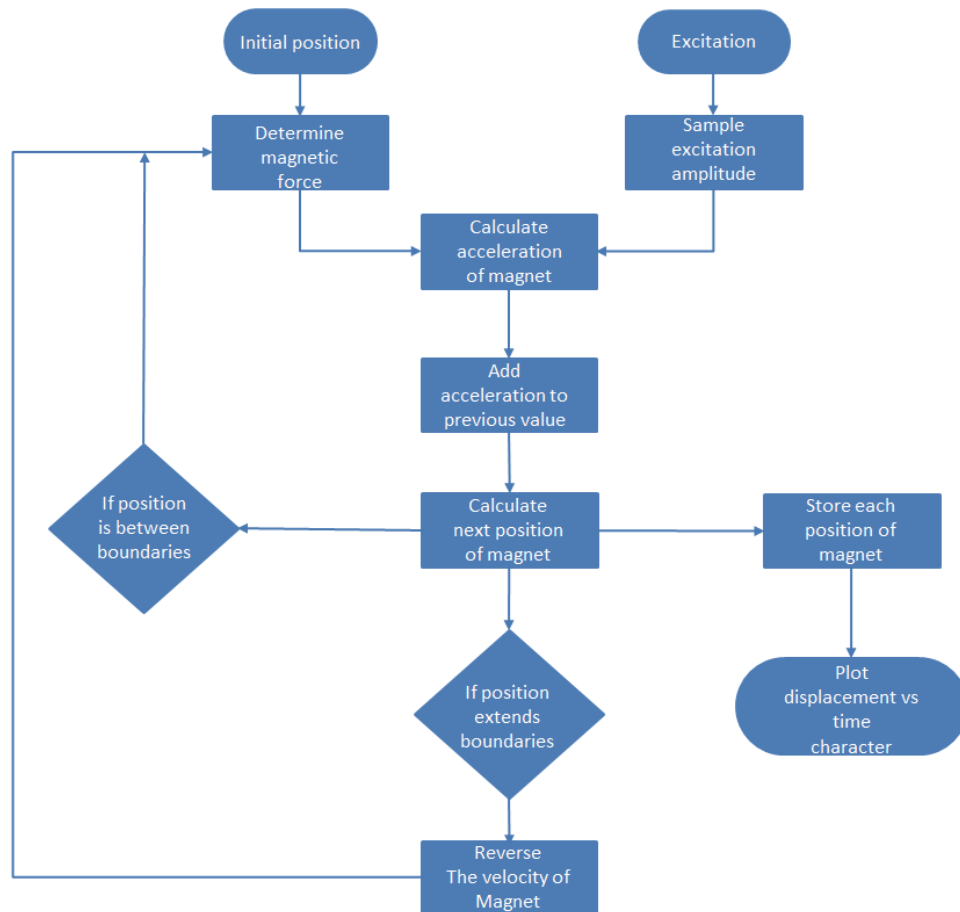


Figure 3.1: Flowchart of the operation introduced to MATLAB model for detection of the resonance frequency.

With the analysis explained on the figure above, displacement versus time characteristic of the moving part is found. It is known that maximum displacement occurs at resonance. Then, frequency sweep is applied to the excitation and resultant

displacement margins are recorded. To do so, frequency response of the excitation is analyzed and natural frequency of the system is determined.

### 3.2. Discrete Time Analysis

In the discrete time analysis, aim is to get displacement versus time plot with basic physical and mathematical calculations. At the beginning, initial positions are determined and resultant magnetic force is calculated. Simultaneously, applied excitation is sampled and its contribution to the system is determined.

When there is no excitation, system is at equilibrium and only gravitational force exists. The moving part stays at equilibrium position, where magnetic force and weight of the moving part equal to each other. Until excitation comes, system remains its rest position and velocity of the system is zero. With the excitation, magnet moves out of equilibrium position and oscillation begins.

The displacement versus time character of the moving part is attempted to be found from applied sinusoidal acceleration. For the sake of simplicity, excitation coming from outside is sampled and between two successive sampled points acceleration is assumed to be constant. That is sinusoidal wave is assumed as combination of square waves. With this way, instead of sinusoidal integration processes, displacement can be derived with basic physical and mathematical equations. For each sampled point, acceleration of the magnet is calculated as follows,

$$m_{magnet}a_{magnet} = F_{Excitation} + F_{Magnetic} - F_{Gravitational} \quad (3.1)$$

at the first instant  $F_{Magnetic}$  equals to  $F_{Gravitational}$ , so,

$$m_{magnet}a_{magnet} = F_{Excitation} \quad (3.2)$$

$$a_{magnet} = \frac{F_{Excitation}}{m_{magnet}} \quad (3.3)$$

with the acceleration system begins to move. The displacement travelled over up to next sampled point is found by two times integration of acceleration with respect to time.

$$a_{magnet} = \frac{\partial v_{magnet}}{\partial t} = \frac{\partial^2 z_{magnet}}{\partial t^2} \quad (3.4)$$

Since sampled excitation is considered as constant between two successive sampled points, physical laws are carried out with basic mathematics as follows,

$$a_{magnet} = \frac{v_{magnet}}{\Delta t} = \frac{2z_{magnet}}{\Delta t^2} \quad (3.5)$$

### 3.2.1. Determination of Initial Conditions

In order to get expected results from the MATLAB model, initial conditions should be well defined. Otherwise, the resonance frequency of the harvester is determined with certain amount of errors. Center of the harvester is defined as origin,  $z = 0$ . If there were no gravitation and excitation forces, center of the moving part would be at the origin, which is equilibrium case. In reality, gravitation exists and excites the moving part to move on downward direction. Simultaneously, repulsive magnetic force prevents the moving part to come closer with the fixed magnets. Up to certain point, where gravitational and magnetic forces become equal to each other, the magnet moves down. Then, it remains stable at this equilibrium position. At the equilibrium position, until excitation is applied, displacement, velocity and acceleration of the magnet is zero. Figure 3.2 shows how the equilibrium position of magnet is detected.

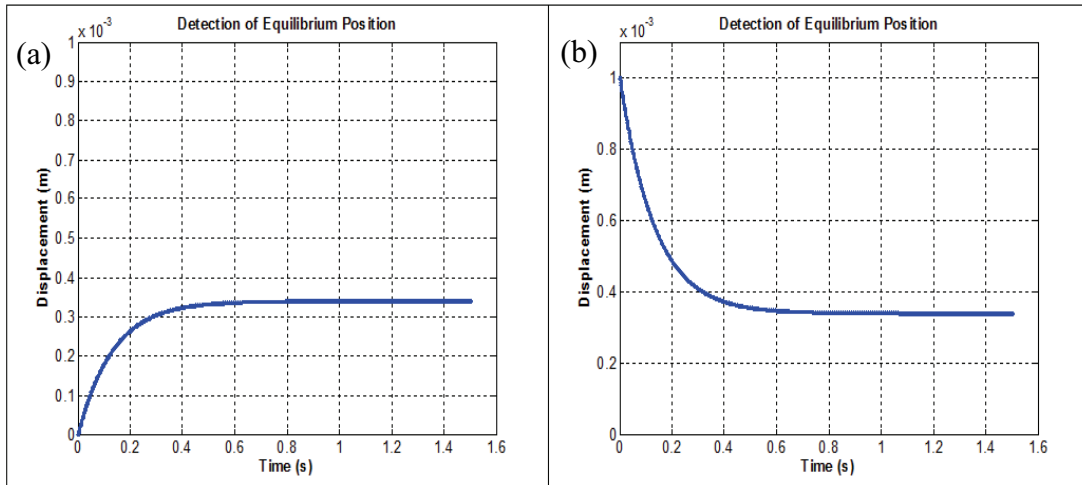


Figure 3.2: Rest position determination of magnet placed below (a) and above (b) of equilibrium position.

In the figure above, stabilization between gravitational and magnetic forces is observed. Here, magnetic force and gravitational force become equal when magnet reaches the position, where  $z = 0.34$  mm. Rest position (equilibrium position) of the magnet for this design is determined as 0.34 mm. Initial position of displacement should be 0.34 mm, where velocity and acceleration are zero without excitation.

For determination of initial conditions, magnetic force acting on the moving magnet is taken into account. Through FEA tool, magnetic force versus displacement plot is extracted and this discrete data converted into continuous function via MATLAB. At the end, displacement dependent continuous function of magnetic force is obtained. By doing so, for each value of displacement, resultant magnetic force is easily calculated. In the next section, this process is explained in detail.

### 3.2.2. Magnetic Force Definition of the System

Magnetic repulsion between magnets defines the resonance frequency of the system. The repulsion force between magnets is modeled as virtual spring and spring constant  $k$  defines natural frequency of the system. Figure 3.3 is an example of the standard magnetic force versus displacement character of basic EM energy harvester.

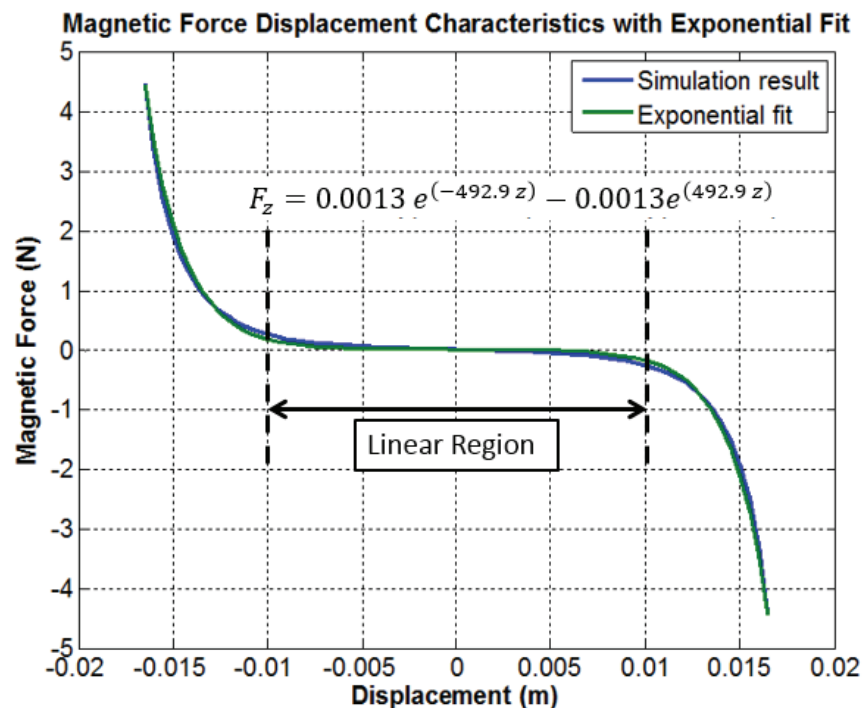


Figure 3.3: Exponential data fit to magnetic force versus displacement data extracted from COMSOL.

The magnetic force characteristic of AA battery sized EM energy harvester is shown above, where there exists two fixed magnets at the top and bottom cap of the harvester. Blue colored data represents simulation results, where for each 0.5 mm increment of oscillation interval resultant magnetic force is recorded. This discrete data is converted into continuous function, which is shown in green color on the figure above. Here magnetic force can be calculated for any point of  $z$  by using the equation on the Figure 3.3. As observed, fitted data is very close to original data extracted from COMSOL.

The equation on the Figure 3.3 proves that magnetic stiffness of the system cannot be constant. That is, magnetic force cannot be represented as multiplication of constant stiffness with displacement for whole operation region. As a result, linearity of the differential equation is disturbed. Therefore, actual resonance frequency of the system cannot be determined through linear differential solution. In [38], for mathematical solution, operation region of the moving magnet is limited as shown in the figure above. In this linear region, stiffness of the system is assumed constant and resonance frequency is calculated via linear differential equation solution. This solution is valid as long as magnet oscillates inside linear region. However, depending on excitation amplitude and frequency, the moving magnet exceeds this linear region, where stiffness is no more linear. As a result, at each instant of time, displacement changes and directly stiffness changes. Since stiffness of the system is also  $z$  dependent parameter. For total oscillation interval, stiffness does not remain constant and determination of resonance frequency with constant stiffness assumption is not valid. The work performed in this thesis study is to provide solution to this problem.

For each instant of time, resultant stiffness is calculated and magnetic force is found by the formula  $F_{Mag} = kz$ . Resultant displacement for that instant is calculated. Right after, for the next cycle, next stiffness value is calculated again. In other words, for each instant of time, derivative of magnetic force is taken with respect to corresponding  $z$  value to find stiffness. Then, result is inserted to the linear differential equation. By doing so, magnetic stiffness of the system is represented as a combination of various linear stiffness values and for each instant corresponding value is inserted to the equation. To sum up,  $z$  dependency of stiffness is accepted, meanwhile linear differential equation solution is performed. This approach will be explained in detail in section 3.3.2.2.

Up to now, how MATLAB model works to detect the resonance frequency of the harvester is explained. In the next section, weaknesses of the model are discussed.

### 3.2.3. Deficiencies of the model

Determination of initial conditions, magnetic force and sampling of the excitation are explained. Through the flowchart of the model, deficiencies of the discrete time analysis are explained in this part.

Movement of the moving magnet begins with excitation so, sampling process of the applied excitation should be performed at first. Excitation is sinusoidal and to simplify integral operation mathematically, sinusoidal wave is converted to column graph. The conversion process is as explained in Figure 3.4.

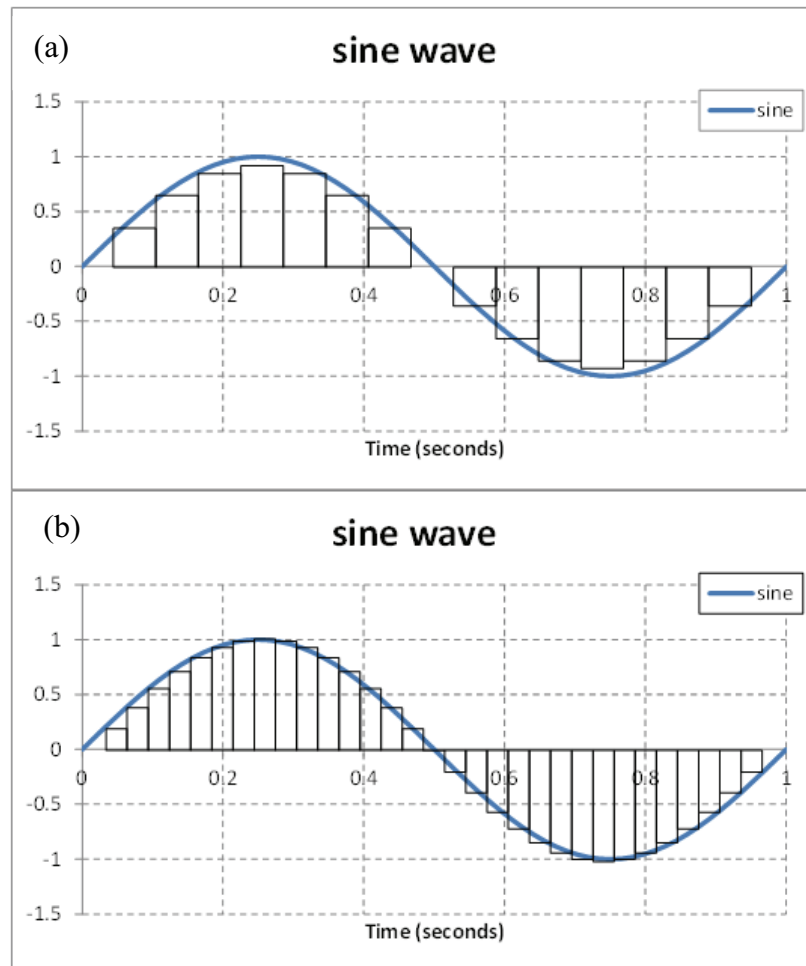


Figure 3.4: Sampling operation of sine wave for (a) smaller and (b) larger sampling frequencies.

Sinusoidal excitation represents acceleration applied to the system and to get displacement versus time character, two times integral operation should be applied to this sine wave. With the assumption of sinusoidal wave as a combination of square waves, mathematical analyses become much easier. However, depending on sampling frequency, area calculated under the curve changes, which has adverse effect on calculations. Resonance frequency of the system is detected by applying frequency sweep. However, for each frequency, sampling frequency will also changes automatically. Therefore, comparison of the displacements becomes impossible because resultant area under the curve changes for each value. According to Figure 3.4, sampling frequency in (b) is twice of that of in (a). Frequency sweep is done from 5 Hz to 15 Hz, final value of sampling frequency becomes three times of initial value.

Increasing sampling frequency as large as possible is considered as a solution to this problem. By doing so, sampling frequency will become so high and will not be affected from frequency sweep. To validate this assumption, displacement character is extracted from sinusoidal acceleration with larger sampling frequencies and results are compared with actual value. Sinusoidal wave with 1 m amplitude is sampled with different frequencies and resultant displacement time plots are as shown in Figure 3.5.

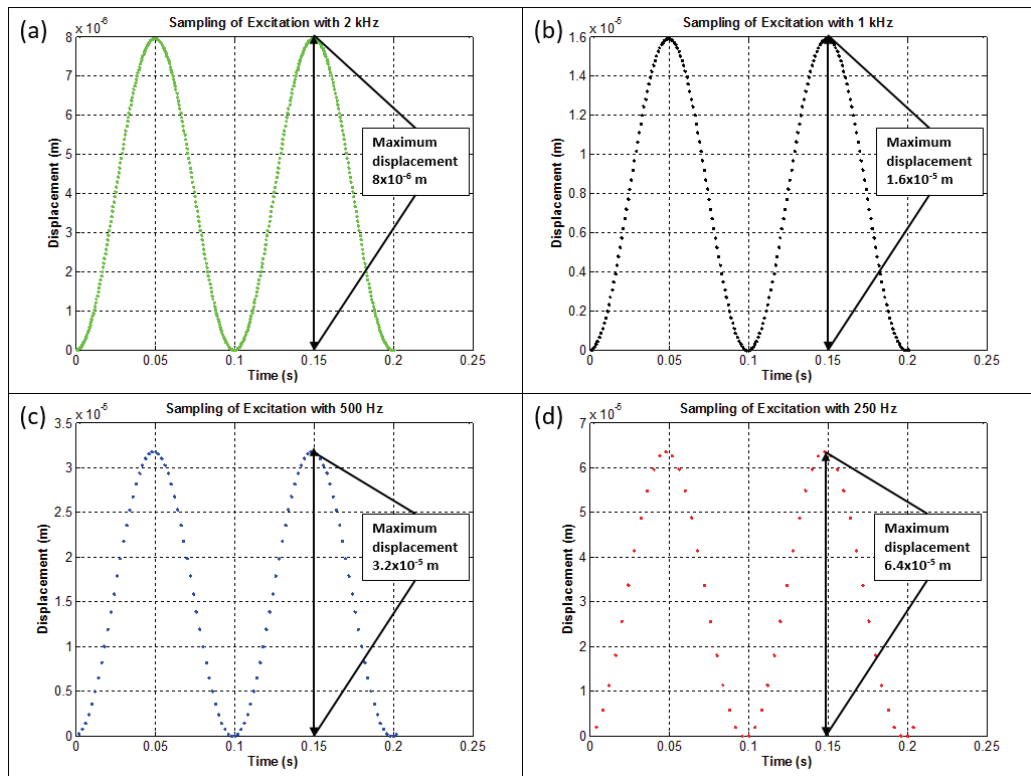


Figure 3.5: Displacement characteristics of the moving magnet under 1 m 10 Hz sinusoidal excitation for several sampling frequencies (a) 2 kHz, (b) 1 kHz, (c) 500 Hz and (d) 250 Hz.

In Figure 3.5, 1 m 10 Hz sinusoidal excitation is applied to our discrete time model and from this acceleration, displacement versus time plots belonging to different sampling frequencies are exhibited. Here, increasing sampling frequency, meaning that taking greater number of data points for one period of time, results in smaller displacement interval. However, these results are totally opposite to our expectation. Actually, 1 m 10 Hz sinusoidal acceleration results in 0.5 mm peak to peak displacement. Rather than larger sampling frequencies, results of smaller sampling frequencies are closer to this value. The reason behind this fact is related with our mathematical assumptions. Increasing sampling frequency prevent data miss because time interval between the successive points become smaller and number of data taken from one period of time increases. However, outcome of this idea affects results

negatively because displacement is found by multiplication of acceleration with square of time as follows,

$$z_{magnet} = a_{magnet}\Delta t^2 \quad (3.6)$$

as the time interval ( $\Delta t$ ) decreases, resultant displacement is affected negatively by square term. As a result, as sampling frequency increases, results become further away from actual displacement value.

To sum up, there existed several problems in discrete time analysis due to simplifications in mathematical operations. This analysis will no more help us to detect the resonance frequency of the system. In order to solve this problems, mathematical analyses, between acceleration and displacement, should be well organized. In the next section, new approach called as continuous time analysis is explained, where *definition of limit in calculus* is used to model mathematical calculations.

### 3.3. Continuous Time Analysis

Aim is to remove deficiencies of the discrete time analysis with continuous time analysis. Operation principles of both of the analyses are very similar except from mathematical computations. Previously it is concluded that representation of sinusoidal wave as combination of several column graphs results in serious and unsolvable problems. To present solution, integral operations are taken through sinusoidal wave under the guidance of *the definition of limit*, in calculus.

$$a_{magnet} = \frac{\partial v_{magnet}}{\partial t} = \frac{\partial^2 z_{magnet}}{\partial t^2} \quad (3.7)$$

$$a_1 = \frac{v_2 - v_1}{\Delta t} \quad (3.8)$$

$$v_1 = \frac{z_2 - z_1}{\Delta t}, \quad v_2 = \frac{z_3 - z_2}{\Delta t} \quad (3.9)$$

$$z_3 - 2z_2 + z_1 = a_1 \Delta t^2 \quad (3.10)$$

here, *definition of limit* helps us to provide connection between displacement and acceleration. To find out the value of  $z_3$ , unknowns in the equation  $z_2$ ,  $z_1$  and  $a_1$  should be defined at first. These unknowns are related with the initial conditions and sampling of input acceleration. In the next subsections, determination of initial conditions, sampling of sinusoidal acceleration and flowchart of the continuous time analysis are explained in detail.

### 3.3.1. Determination of Initial Conditions

Initially system is at rest and maintains its rest position up to excitation comes from outside. Determination of the equilibrium position is already explained in discrete time analysis, which is exactly same in this approach. To clarify, system is at rest, when gravitational and magnetic forces acting on the moving magnet equal to each other. The initial point of displacement is determined with the help of MATLAB as explained previously in section 3.1.1. Equilibrium position changes belonging to designs under the effect of magnetic repulsion and weight of the moving part.

Up to the first instant of acceleration, velocity of the magnet is zero. With this consideration and by using definition of limit second position of displacement  $z_2$  is found as follows:

$$v_1 = \frac{z_2 - z_1}{\Delta t} = 0 \quad (3.11)$$

$$z_2 - z_1 = 0 \quad (3.12)$$

The equations above proves that first and second position of displacement equals to equilibrium position.

Having determined the first and the second instants of displacement, only unknown is the first instant of acceleration. After all unknowns are determined, inside for loop next positions of the moving magnet are calculated. Hence, displacement versus time characteristic of the harvester design is obtained. To determine the first instant of acceleration, sampling process should be applied to sinusoidal excitation, which is explained in the next section.

### **3.3.2. Sampling Process and Magnetic Force Definition**

Acceleration acting on the moving part is defined by the input excitation, magnetic forces and gravitational force. Here, excitation is sinusoidal and should be sampled with small time intervals to see its contribution to the next position of displacement. With the input excitation, displacement between the magnets begins to vary, which makes magnetic force contribute to acceleration of the moving magnet. Unlike input excitation and magnetic force, gravitational force is always constant and acts in the downward direction.

Sampling is very critical here because any data missing results in corruption, which results in wrong determination of the resonance frequency. This process is explained in the next subsection.

#### **3.3.2.1. Sampling Process**

The number of data taken in one period of time is crucial. Since any data miss results in deformation on sine wave. At first, the necessary data number taken in one period of time should be determine. Then, from applied acceleration, displacement versus time character of the moving part is plotted. Finally, this plot is compared with

the actual wave. Figure 3.6 displays the comparison of calculated and original waves where 0.1 g peak amplitude 5 Hz sinusoidal acceleration is applied to the system.

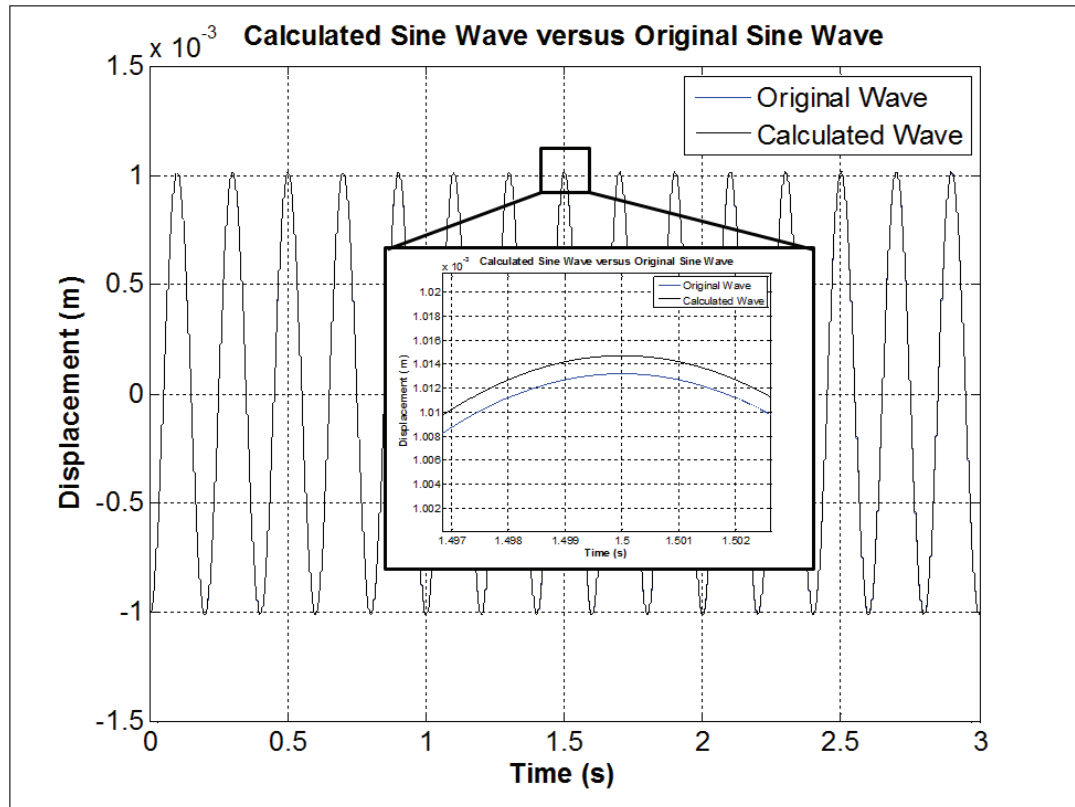


Figure 3.6: Comparison of original and calculated sine waves when number of data taken in one period of time is  $10^5$ .

Color of original wave is blue and calculated wave is represented with black. Here, fifteen period of waves are observed. The conclusion is that calculated and original waves are nearly coincide. Only very small difference is observed when portion indicated by black square in the figure is magnified. If the number of data taken is smaller than  $10^5$ , difference between the waves gradually increases by the time passes. However, at this time, this minor difference always remains constant.

The study performed in this section helps us to settle exact number of data points should be taken in one period of time. By doing so, corruption on sinusoidal wave and

data missing are prevented. In the next section, effect of magnetic force on acceleration is studied.

### 3.3.2.2. Magnetic Force Definition

Contribution of the magnetic force on the motion of the moving magnet is already discussed in the previous chapters. In general, magnetic force is modeled by multiplication of stiffness  $k$  with displacement  $z$  as follows;

$$F = kz \quad (3.13)$$

In literature, generally, magnetic stiffness value  $k$  is assumed as constant and resonance frequency detection is provided by basic mathematical representations. Apart from these, in [38], magnetic stiffness is accepted as displacement dependent parameter. In the discrete time analysis section, it is underlined that, stiffness  $k$  cannot be considered as constant parameter throughout the whole displacement interval. As a result, linearity of second order differential equation is disturbed. To make linear differential equation solution be applicable,  $z$  dependent magnetic stiffness  $k$  is represented as a combination of constant stiffness values. Therefore, for each value of displacement, magnetic stiffness is evaluated with respect to corresponding  $z$  value. As a result, in each instant of time, linearity of differential equation is ensured. Figure 3.7 explains the whole process.

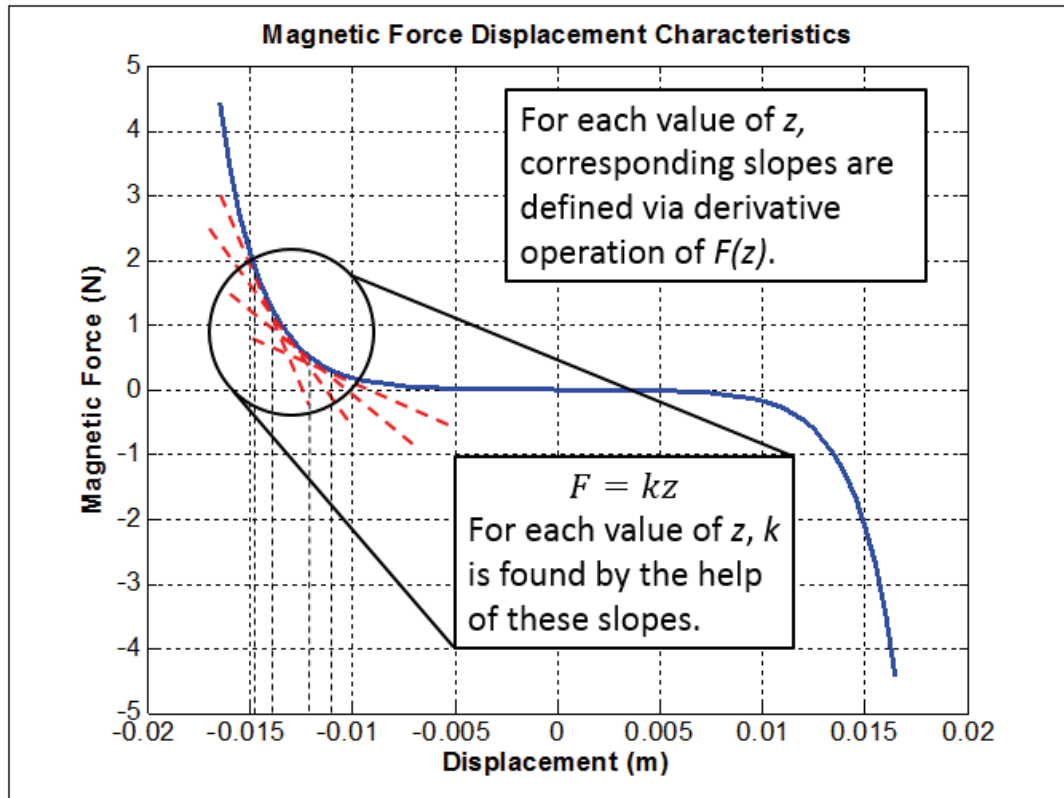


Figure 3.7: Definition of magnetic force acting on suspended part.

In Figure 3.7, for each instant of  $z$  value, resultant stiffness  $k$  is evaluated. Tangents to the magnetic force curve are drawn for each instant. To do so, magnetic stiffness  $k$  is defined as a combination of several constant values.

At this point, all necessary parameters are defined for displacement time characteristic of the moving part of the system. In the next section, how these parameters are used to find the resonance frequency of the system is explained.

### 3.3.3. Flowchart of the Model

Up to now, requirements of continuous time analysis like initial condition determination, sampling of excitation and magnetic force definition are defined. In this section how these requirements are used to reach resonance frequency is explained in detail. Figure 3.8 demonstrates the flowchart of continuous time analysis.

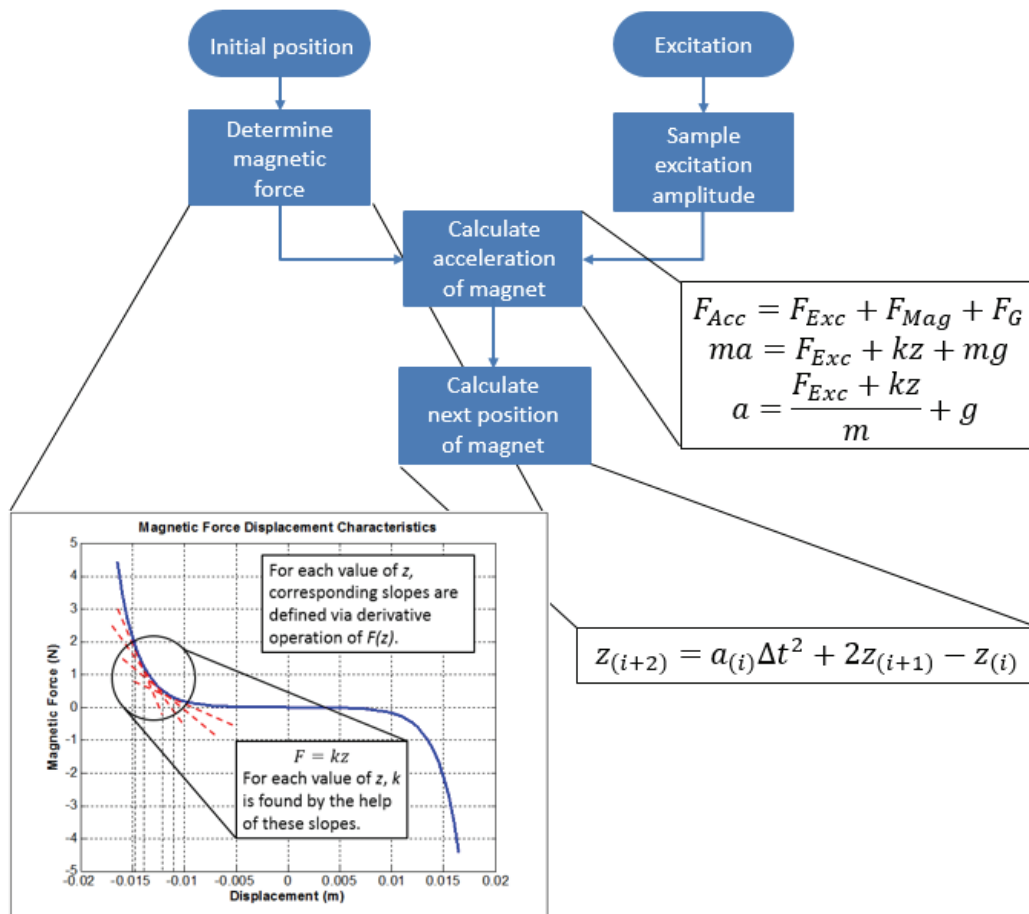


Figure 3.8: Flowchart of continuous time analysis.

At the beginning, initial position of the moving part is found, where magnetic force and gravitational force acting on the moving magnet are equal to each other. Without excitation, there exists no motion so that by *definition of limit* second position of the moving part should be same with initial position.

Applied excitation should be sampled with reasonable sampling frequency. By using the sampled data and *definition of limit*, relation between acceleration and displacement of the moving part is defined.

Under the influence of forces acting on the moving part, acceleration is calculated through the formula given in Figure 3.8. Finally, the first and the second positions of displacement are known and acceleration of the first instant is evaluated. With these values the next value of displacement is calculated as illustrated in the Figure 3.8.

The flowchart explains only one cycle of this analysis. Inside for loop, next and subsequent positions of displacement are evaluated and each of these values is recorded. These recorded values shows displacement versus time plot of the moving part under the applied excitation. The general flow of the analysis is already illustrated in Figure 3.1.

### **3.4. Simulation Results of MATLAB Simulator**

In this subsection, resonance frequencies of the designs proposed in section 2 are estimated through MATLAB simulator. Experimentally, resonance frequency of the EM harvester systems is detected by frequency sweep. That is, for constant amplitude, frequency of the excitation is swept. For each frequency, resultant output voltage is recorded and maximum output voltage occurs at resonance. Therefore, resonance frequency is detected with the analysis of output voltage versus frequency characteristics. Similarly, instead of output voltage, displacement of the moving part is recorded in MATLAB simulator. The frequency, at which maximum displacement occurs, represents resonance of the system.

Displacement versus frequency plots of the designs are as follows,

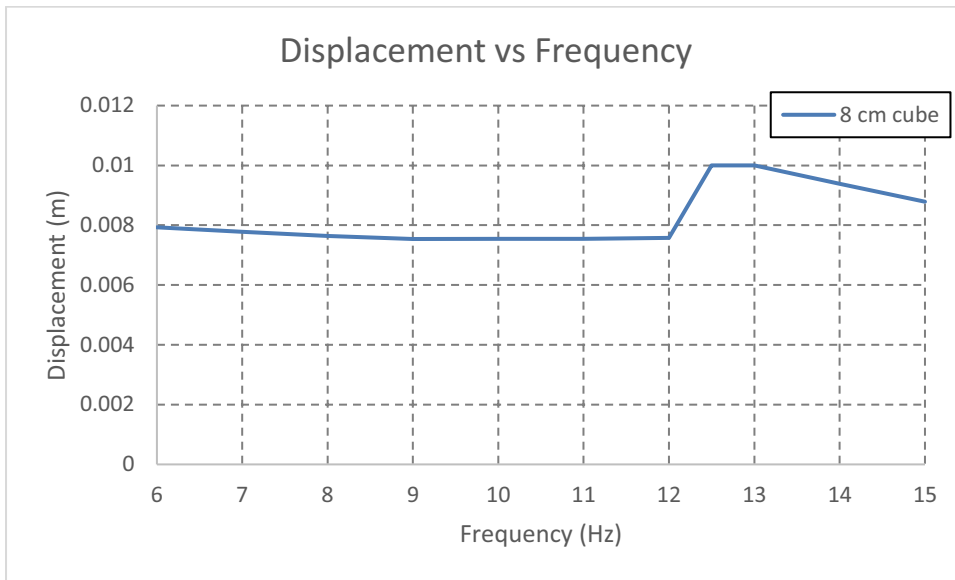


Figure 3.9: Frequency response plot of displacement for 8 cm<sup>3</sup> cube design.

Resonance frequency of the 8 cm<sup>3</sup> cube design is estimated as 12.5 Hz.

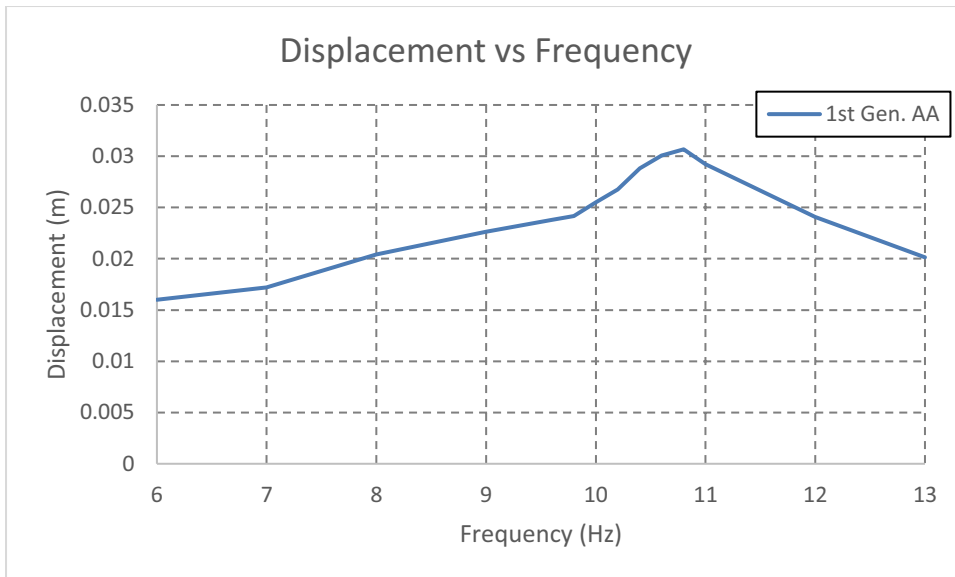


Figure 3.10: Frequency response plot of displacement for 1<sup>st</sup> generation AA battery design.

Resonance frequency of the 1<sup>st</sup> generation AA battery design is estimated as 10.8 Hz.

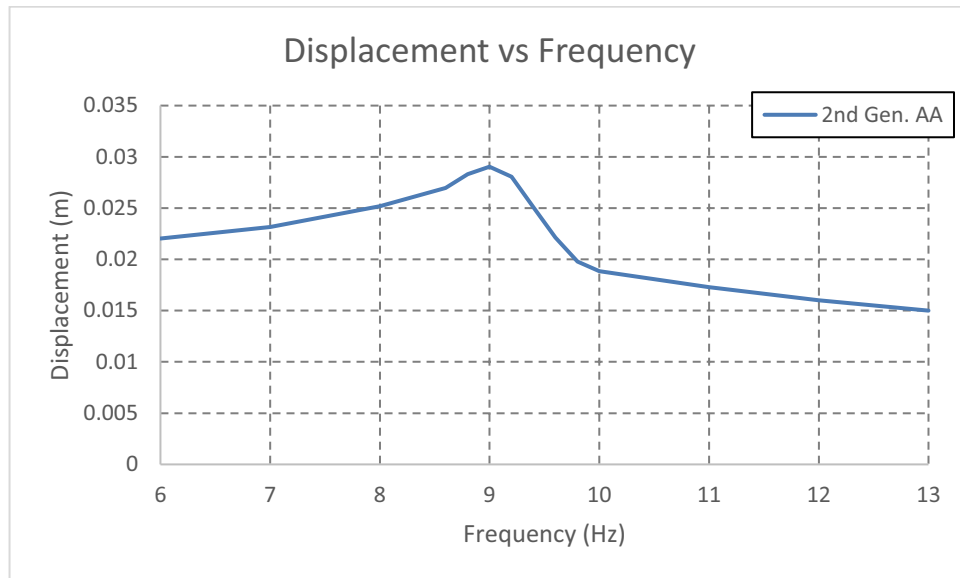


Figure 3.11: Frequency response plot of displacement for 2<sup>nd</sup> generation AA battery design.

Resonance frequency of the 2<sup>nd</sup> generation AA battery design is estimated as 9 Hz.

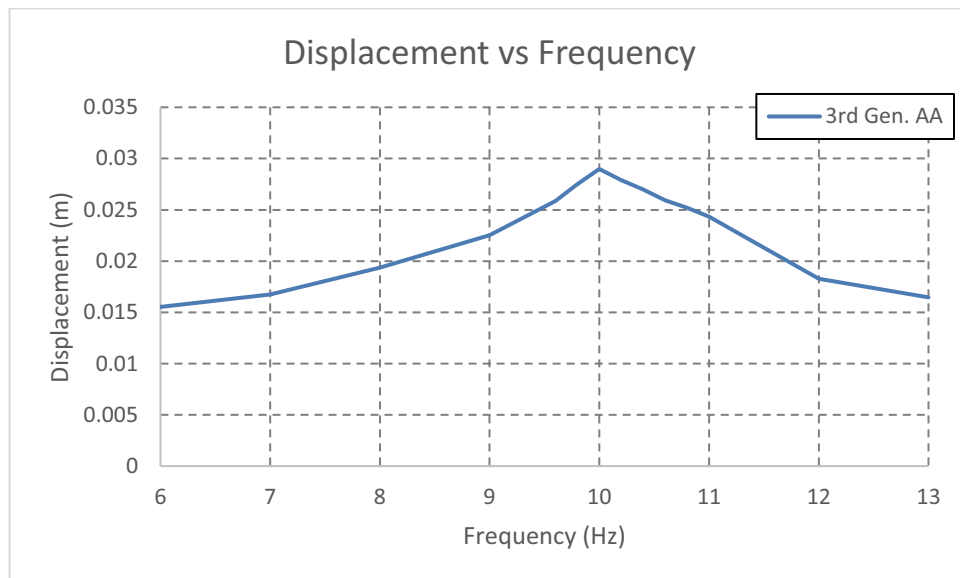


Figure 3.12: Frequency response plot of displacement for 3<sup>rd</sup> generation AA battery design.

Resonance frequency of the 3<sup>rd</sup> generation AA battery design is estimated as 10 Hz.

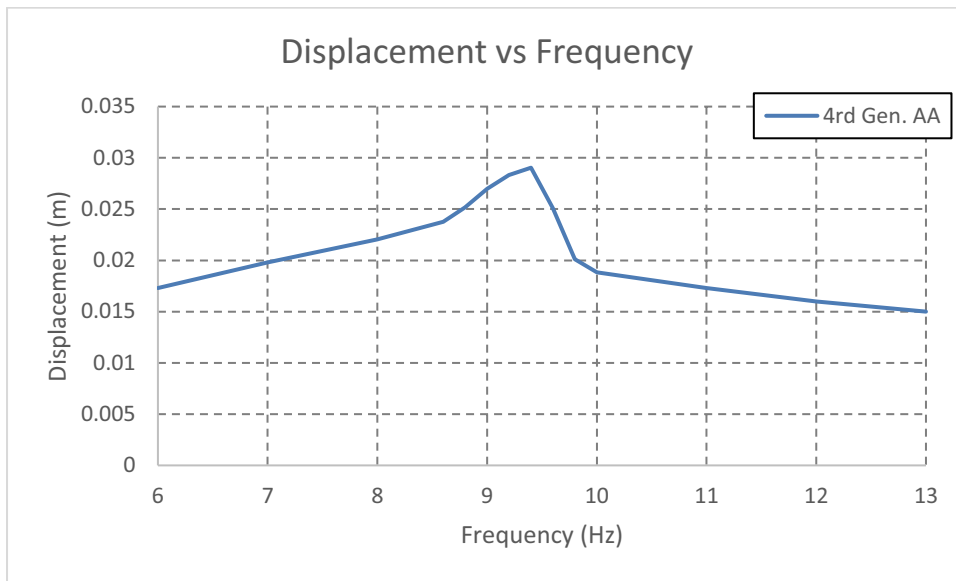


Figure 3.13: Frequency response plot of displacement for 4<sup>th</sup> generation AA battery design.

Resonance frequency of the 4<sup>th</sup> generation AA battery design is estimated as 9.4 Hz.

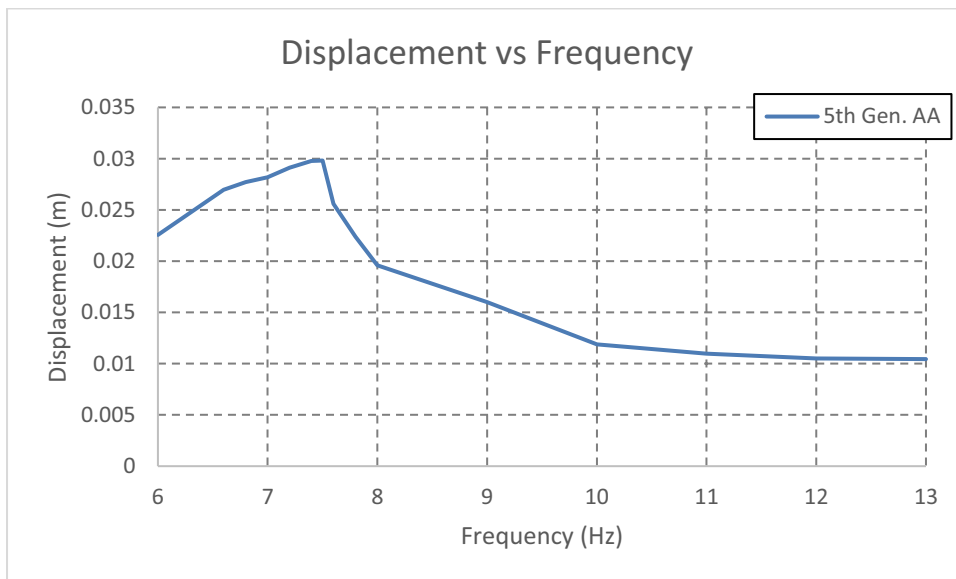


Figure 3.14: Frequency response plot of displacement for 5<sup>th</sup> generation AA battery design.

Resonance frequency of the 5<sup>th</sup> generation AA battery design is estimated as 7.5 Hz.

### 3.5. Conclusion

In this chapter, the resonance frequency detection techniques are explained. Aim is to find out the resonance frequency of the harvester via the displacement versus time plot of the moving part in the harvester. FEA tools are not sufficient enough to compute desired analyses in determination of resonance frequency. Therefore, to detect the resonance frequency, simulator model is designed and improved via MATLAB. At first, the discrete time model is suggested in which integral operations are modeled with basic mathematical calculations. Sinusoidal wave of excitation is assumed as a combination of several square waves. Data conversion from acceleration to displacement is intended to be provided by basic calculus through constant amplitude square waves for each time interval. Nevertheless, expectations are not satisfied due to mathematical simplifications. To come up with a solution, continuous time analysis is presented, where mathematical operations are carried out with the *definition of limit* in calculus. By doing so, general operation principle of the MATLAB model is not violated, only difference is related with integral operations to govern displacement character of the moving magnet.

Required information is inserted to the finalized version of the model and results are analyzed. According to the results, expected resonance frequencies for various EM energy harvester models are recorded and compared with the actual results. In the next chapter, fabrication process, test setup and comparison of tests with simulation results are presented. In addition, validation of the MATLAB model in detection of the resonance frequency is also proved.



## **CHAPTER 4**

### **FABRICATION AND EXPERIMENTAL TEST RESULTS**

In this section, experimental analyses are explained and the test results are analyzed. The efficiency of simulator performances and the design procedure are verified through experimental results. In design modelling and simulation section, optimization procedure for maximum output power is explained. Several simulations are performed and improvements are applied to reach the finalized model. In this section almost the same procedure as Chapter 2 is applied. This chapter starts with the fabrication procedure of EM energy harvesters, continues with the description of test setup and concludes with the presentation of individual test results of proposed designs. The experimental results are compared with the simulation results at the end.

#### **4.1. Fabrication and Test Setup**

The container of the electromagnetic energy harvester system is made of a castermid material. After the design parameters, such as magnet and coil sizes, are determined cylindrical castermid materials are put into process. In order to get maximum power output, six several designs are examined. Similarly, various coil positions are studied to get the highest output power. Designs are geometrically

classified two groups, in which the first design group has 20 mm diameter, 20 mm height and the second one has 14 mm diameter, 46 mm height as shown in Figure 4.1.

The material is cylindrically drilled with specified dimensions to provide sufficient oscillation distance to the moving part. Then, a copper coil is wrapped around a cavity on the tube. A fixed magnet is attached to the bottom cap and an oscillating one is placed inside the cylindrical hole, such that the magnets provide repulsive forces to each other. The top cap is pasted with the rest of the fabricated parts and system is constructed as depicted in Figure 4.1.

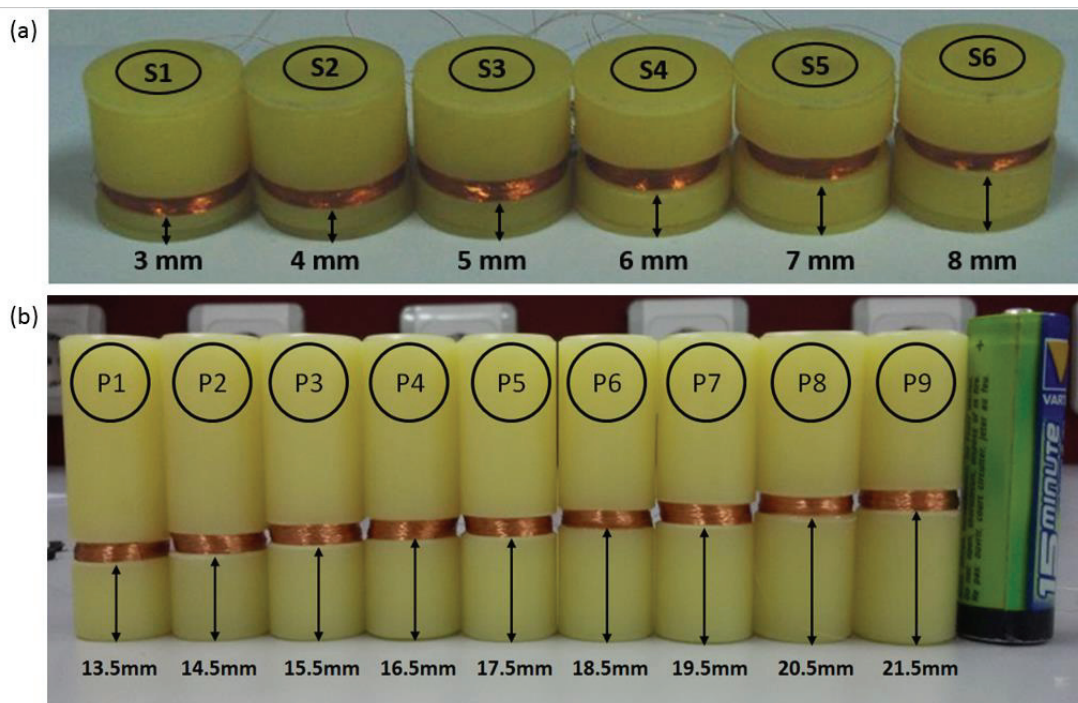


Figure 4.1: Fabricated EM harvester prototypes (a) h:19 mm, Ø:20 mm, 6 cm<sup>3</sup> , N:1500 (b) h:46 mm, Ø:14 mm, 7 cm<sup>3</sup> , N:1200

In Figure 4.1 (a), 6 cm<sup>3</sup> harvester prototypes with several coil positions are presented. In this design, four internal structures are analyzed to get maximum output power at low resonance frequency excitations. In order to achieve further improvements on the performance of the EM energy harvester, the internal structure is modified by changing harvester dimensions as shown in Figure 4.1 (b).

Figure 4.2 shows the schematic representation (a) and corresponding photos (b) of the experimental test setup. The test setup consists of a PC, a control system, a shaker table and an oscilloscope. Fabricated energy harvesters are placed onto the shaker table, which is controlled by the software on the PC. Excitation amplitude and frequency to be applied to the harvester is assigned via the software tool. The amplifier activates the shaker table, which gives feedback to the controller system via an accelerometer. The feedback loop directs the shaker table to oscillate in favor of the assigned values and the induced voltage is observed on the oscilloscope screen.

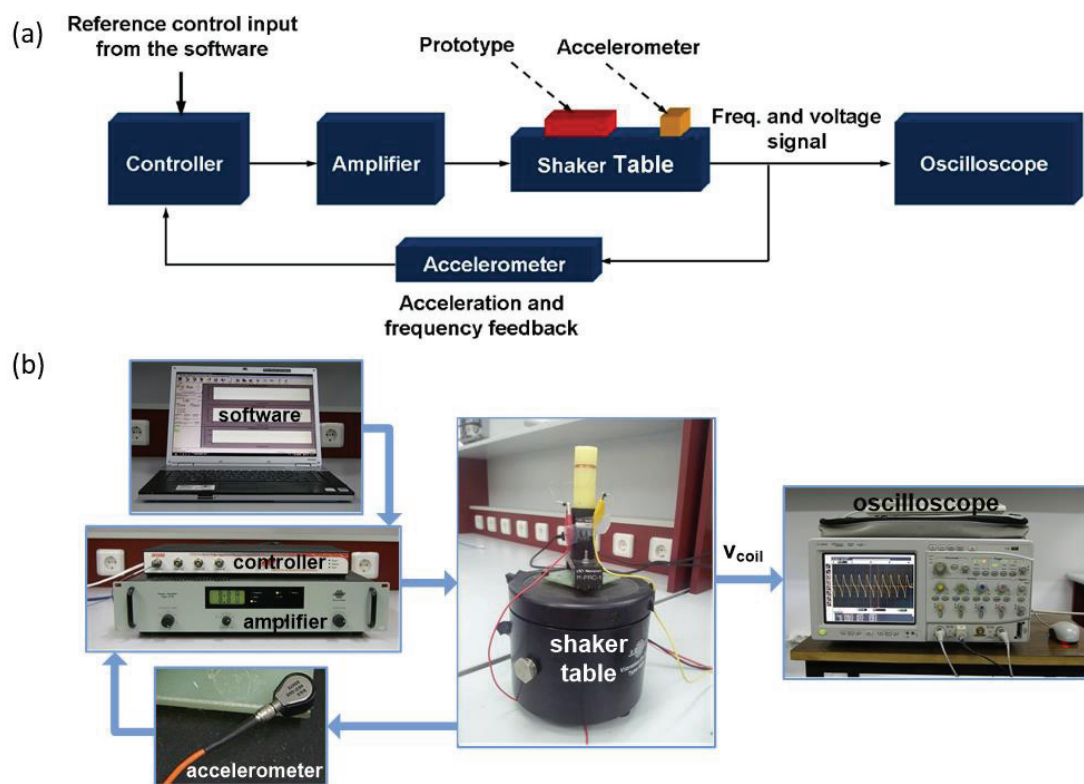


Figure 4.2: Block diagram (a) and schematic representation (b) of the test setup.

Induced voltage is recorded for open-loop case and then, output power is defined by hand calculation for maximum power transfer case. As observed in the following sections, maximum RMS value of induced voltage is 0.57 V, where internal resistance is 265  $\Omega$ . As a result, output current for maximum power transfer case is around 1

mA. However, my load which converts AC signal to DC it has 3 k $\Omega$  resistance. For this case, the current value reduces to 170  $\mu$ A which contributes negligibly small damping force.

The performances of the designs are presented with representative plots and tables in the following sections. Additionally, the most appropriate prototypes of each design are compared and the optimization process is validated through experimental results.

#### 4.2. Testing of Proposed 8 cm<sup>3</sup> Energy Harvester

The designed energy harvesters can fit into 8 cm<sup>3</sup> volume. The proposed designs through simulations are tested. Outcomes of the improvements on the interior designs are validated with tests.

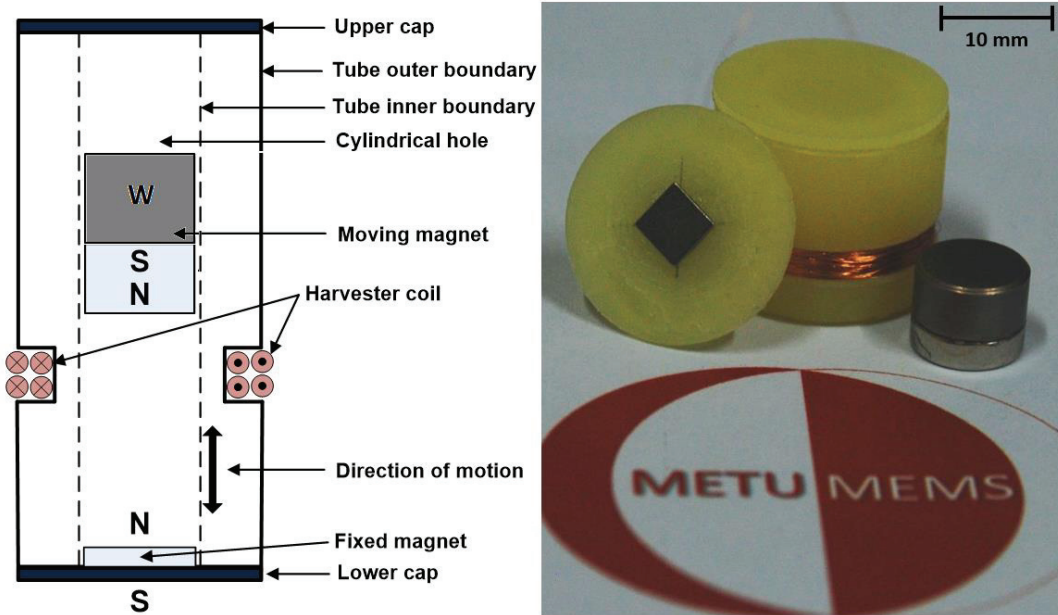


Figure 4.3: (a) Structure of the EM energy harvester and (b) the fabricated prototype where the inertial mass is composed of  $\varnothing$ : 10 mm, h: 3 mm, 1.7 gram NdFeB magnet and  $\varnothing$ : 10 mm, h: 5 mm, 6.8 gram tungsten-copper mass. (S3 on Figure 4.1. (a))

EM harvester prototypes are fabricated and tested on the shaker table to validate the optimum coil position and performance. Figure 4.1 (a) presents the fabricated EM harvester prototypes, where prototypes from P1 to P6 have coils located 3 mm to 8 mm from the bottom of the harvester, with 1500 coil turns. All of the harvesters have 19 mm of height and 20 mm of diameter, which corresponds to 6 cm<sup>3</sup> of volume. The optimum energy harvesting device operating in 8 cm<sup>3</sup> cube volume is presented in Figure 4.3.

Figure 4.4 presents the peak-to-peak output voltages ( $V_{PP}$ ) of 6 prototypes at 8 Hz and 0.4 g vibration which corresponds to non-resonant operation. Both simulations and test results yield to an optimum coil position of 5 mm above the bottom of the harvester. This result is further proved by for resonance condition of the harvesters. Figure 4.5 presents the frequency response of the prototypes where S3 yields the maximum output.

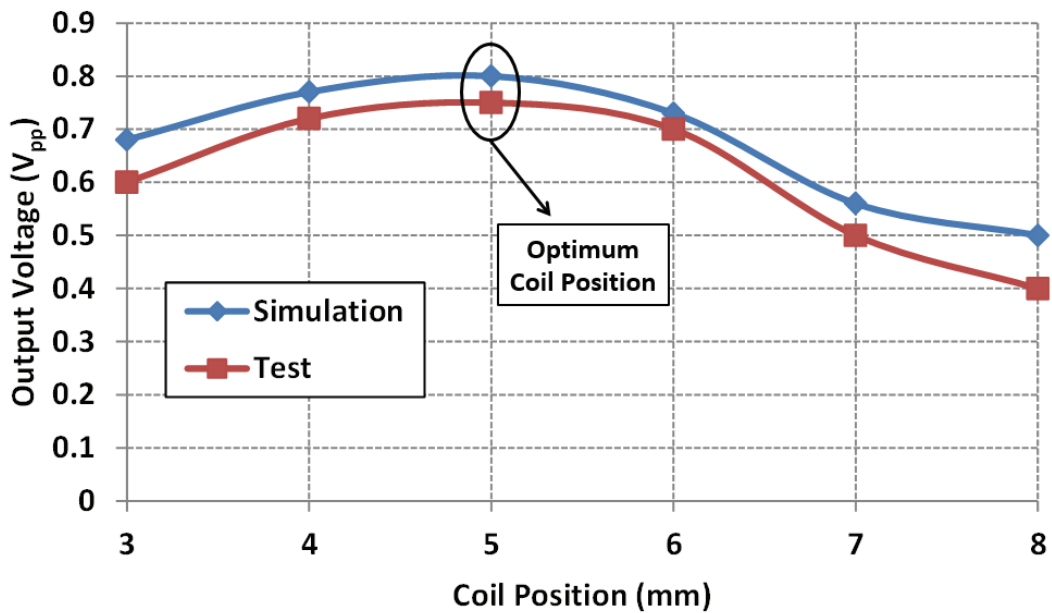


Figure 4.4: Simulation and test results of the harvester output for different coil position. (8 Hz, 3 mm peak-to-peak vibration with 0.4 g peak acceleration).

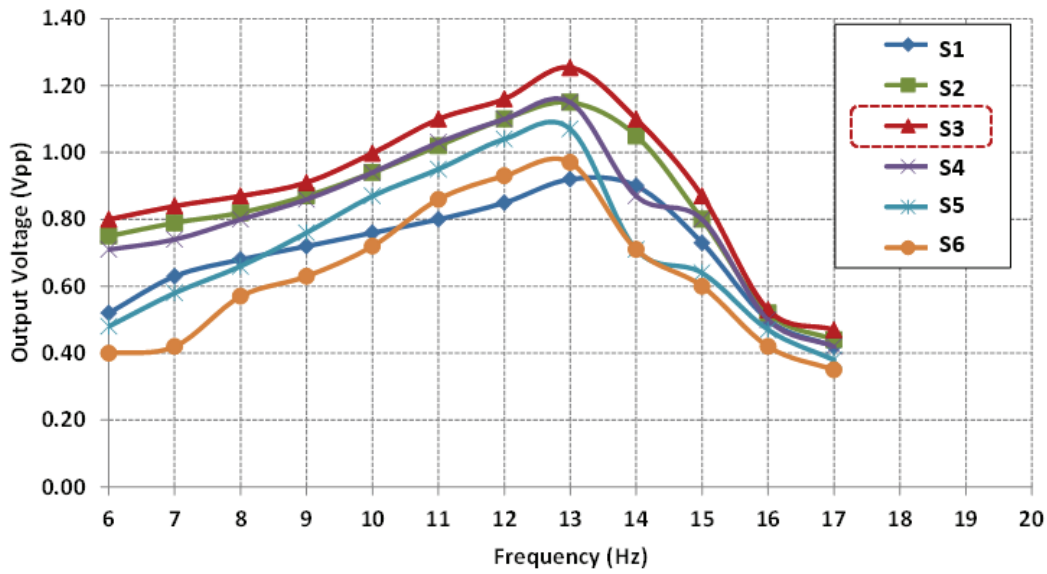


Figure 4.5: Frequency response of EM harvester prototypes (S1-S6) at 0.5 g peak vibration acceleration. S3, where the coil is placed 5 mm above the bottom of the harvester, gives the maximum output.

The decrease at the resonance of frequency and the improvement of the low frequency performance of the harvester with the attachment of tungsten-copper mass is illustrated in Figure 4.6. Increasing the moving magnet size itself (from 3.4 to 4.5 gram) results in an increase in the resonance frequency (from 23 Hz to 27 Hz). The reason is that the magnetic forces and the stiffness increases more than the increase in the inertial mass. Instead, attaching 4.1 and 6.8 gram tungsten-copper masses on a 1.7 gram NdFeB magnet, pulls the resonance frequencies down to 12.5 and 15 Hz, respectively. Simultaneously, generated output voltage increases. Figure 4.7 presents the harvested AC voltage at 15 Hz and 0.7 g acceleration where, 1.61 V<sub>Peak-to-Peak</sub> and 110 μW<sub>RMS</sub> output power is generated. Table 4.1 presents the optimized system specifications. The results show that the presented approach is effective in increasing the harvester performance for low frequency operation within a fixed device volume.

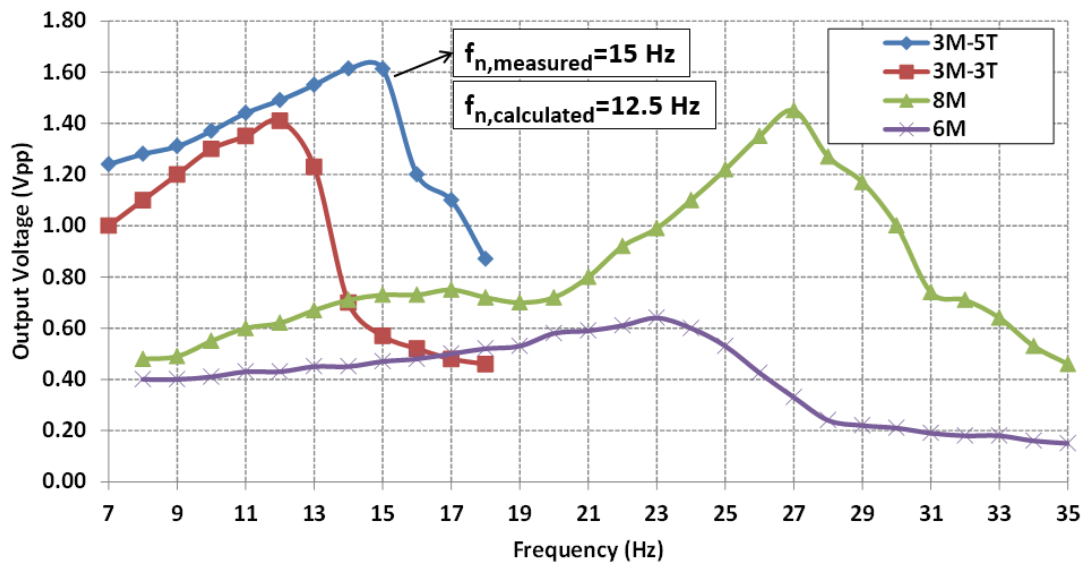


Figure 4.6: Frequency response of S3 at 0.7 g peak vibration acceleration for different inertial masses, where the maximum output voltage is obtained with 1.7 gram magnet and 6.8 gram tungsten-copper mass (Mag1.7-WCu6.8).

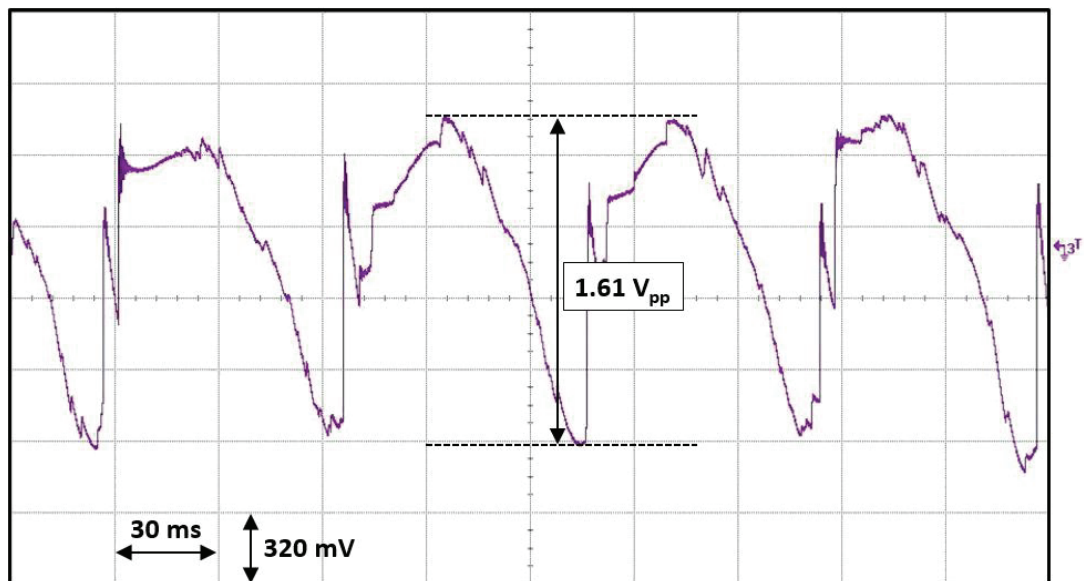


Figure 4.7: Harvested AC voltage from S3 with 1.7 gram magnet and 6.8 gram tungsten-copper inertial mass at 15 Hz and 0.7 g peak acceleration (Oscilloscope screen).

Table 4.1: System specifications of the proposed EM energy harvester

Harvester Dimensions	Ø:20 mm, h:19 mm, 6 cm <sup>3</sup>	Saturation Magnetization	1.2 T
Inertial Mass	NdFeB Ø:10 mm, h:3 mm, 1.7 gram	Coil Turns	1500
	W <sub>80</sub> -Cu <sub>20</sub> Ø:10 mm, h:5 mm, 6.8 gram	Coil Resistance	450 Ω
Input Vibration	15 Hz and 0.7 g peak acceleration	Output Voltage	1.61 V <sub>PP</sub> , 0.45 V <sub>RMS</sub>
Fixed Magnet	5.3x5.3x0.5 mm <sup>3</sup>	Harvested Power Power Density	110 μW <sub>RMS</sub> 18 μW <sub>RMS</sub> /cm <sup>3</sup>

The improvements on this EM harvester design are limited with device dimensions to modify internal structure. Device dimensions are changed for better output power. The proposed designs with the performance tests are presented in the next section.

### 4.3. Tests of Proposed AA Battery Sized EM Energy Harvesters

Proposed EM energy harvesters are designed to be comparable with an AA sized battery in terms of both performance and device parameters. The reason is that one of the most widely used battery type is AA sized ones. In order to maximize the output performance, various designs are investigated. The tests of the AA battery sized designs are demonstrated and performances are evaluated in the following subsections.

### 4.3.1. 1<sup>st</sup> Generation AA Battery Sized EM Harvester

Figure 4.8 illustrates the internal structure and device dimensions of the proposed 1<sup>st</sup> generation AA battery sized design of EM energy harvester.

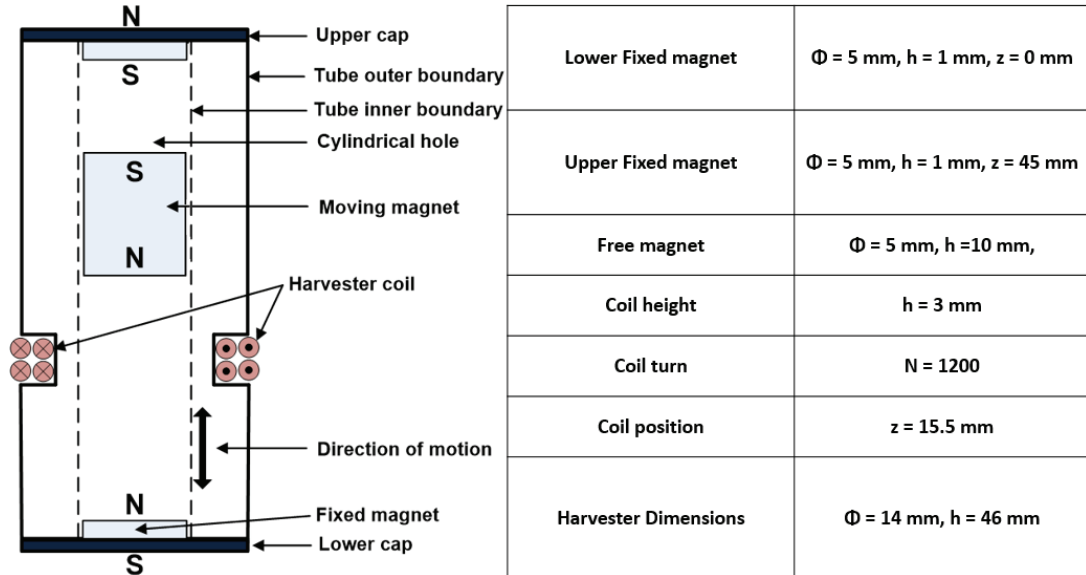


Figure 4.8: System specifications of the 1<sup>st</sup> generation AA battery sized energy harvester.

Several prototypes of the proposed design are fabricated with different coil positions and tested on a shaker table to observe the low frequency performances. Figure 4.1 (b) presents the fabricated EM harvester prototypes, where prototypes from P1 to P9 have coils located 13.5 mm to 21.5 mm from the bottom of the harvester, with 1200 coil turns. All of the harvesters have 46 mm height and 14 mm diameter, which corresponds to a  $7 \text{ cm}^3$  volume.

Figure 4.9 presents the peak-to-peak output voltages ( $V_{PP}$ ) of the 9 prototypes at 10 Hz and 0.5 g vibration, which corresponds to resonant operation. Test results yield to an optimum coil position of 15.5 mm above the bottom of the harvester. This result is further proven by detecting the resonance frequency of the harvesters. Figure 4.10

presents the frequency response of the prototypes, where P3 yields the maximum output.

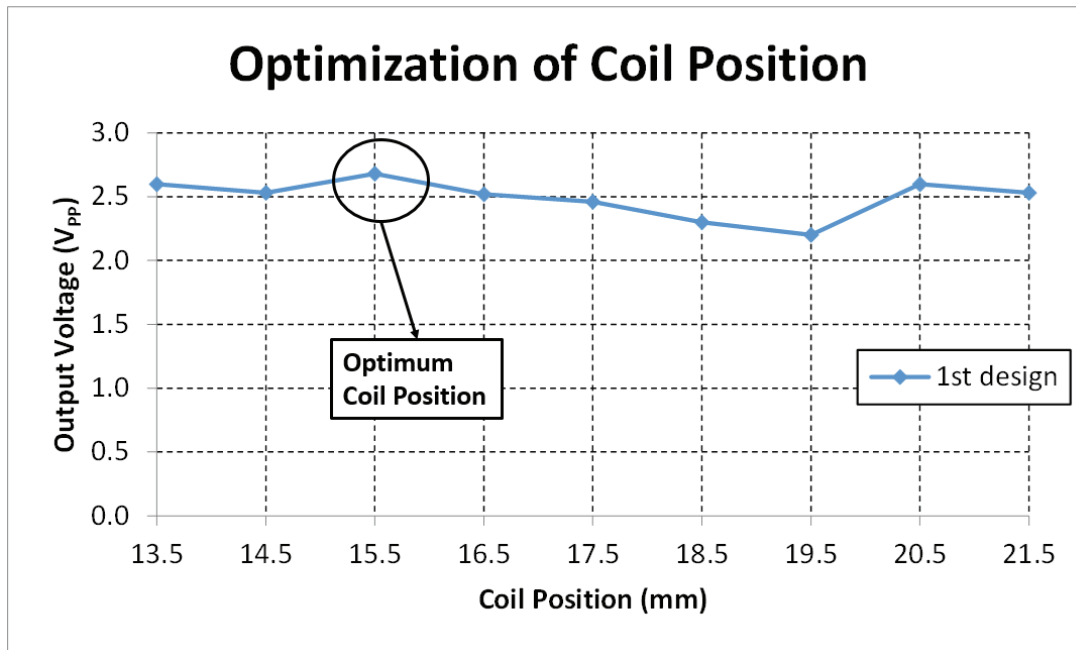


Figure 4.9: Test results of the harvester output for different coil position. (10 Hz, 2.5 mm peak-to-peak vibration with 0.5 g peak acceleration).

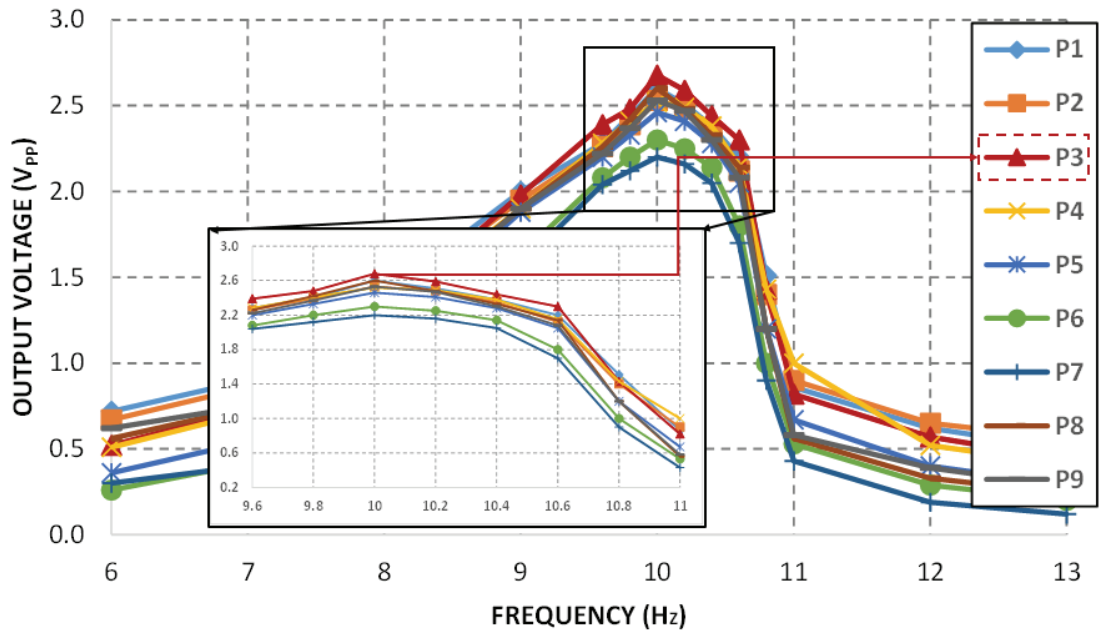


Figure 4.10: Frequency response of EM harvester prototypes (P1-P9) at 0.5 g peak vibration acceleration. P3, where the coil is placed 15.5 mm above the bottom of the harvester, yields the maximum output.

In the frequency response plot, the resonance frequency is indicated as 10 Hz.

Table 4.2: The performance comparison of the 1<sup>st</sup> generation AA battery sized and 8 cm<sup>3</sup> volume designs.

	<b>8cm<sup>3</sup> Square Prism Design</b>	<b>1<sup>st</sup> AA Battery Sized Design</b>
Device Dimensions	Ø:20 mm, h:19 mm, 6 cm <sup>3</sup>	Ø:14 mm, h:46 mm, 7 cm <sup>3</sup>
Inertial Mass	NdFeB W <sub>80</sub> -Cu <sub>20</sub>	NdFeB W <sub>80</sub> -Cu <sub>20</sub>
	Ø:10 mm, h:3 mm, 0.9 cm <sup>3</sup>	Ø:5 mm, h:10 mm, 0.8 cm <sup>3</sup>
	Ø:10 mm, h:5 mm, 1.5 cm <sup>3</sup>	-
Input Vibration	0.7 g peak acceleration	0.5 g peak acceleration
Resonance Frequency	15 Hz	10 Hz
Coil Turn	1500	1200
Coil Resistance	450 Ω	265 Ω
Output Voltage	1.61 V <sub>PP</sub> , 0.45 V <sub>RMS</sub>	2.52 V <sub>PP</sub> , 0.57 V <sub>RMS</sub>
Harvested Power	110 μW <sub>RMS</sub>	306.5 μW <sub>RMS</sub>
Power Density	18 μW <sub>RMS</sub> /cm <sup>3</sup>	43.8 μW <sub>RMS</sub> /cm <sup>3</sup>

According to Table 4.2, the volume of the moving magnet and the number of coil turns are reduced. Output power is increased (from 110  $\mu\text{W}$  to 306.5  $\mu\text{W}$ ), while the excitation amplitude (from 0.7 g to 0.5 g) and frequency (from 15 Hz to 10 Hz) are reduced. As a result, without any modifications on internal structure, output power of EM energy harvester can be increased. In the next section, the volume of the moving magnet is reduced to decrease the resonance frequency. At the same time, with the addition of tungsten mass, the output performance is attempted to be increased.

#### 4.3.2. 2<sup>nd</sup> Generation AA Battery Sized EM Harvester

In this design, the moving magnet height is reduced to weaken the effect of magnetic force. Instead of this reduction, tungsten mass is placed as illustrated with device dimensions in Figure 4.11. To do so, the stiffness is reduced and the mass of the moving part is increased. As a result, the resonance frequency of the harvester is reduced.

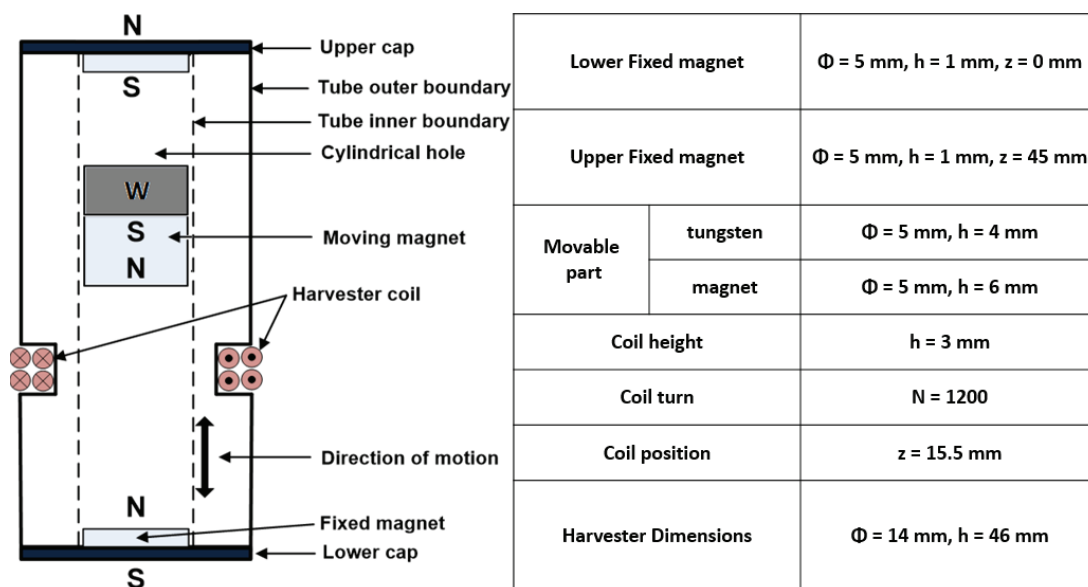


Figure 4.11: System specifications of the 2<sup>nd</sup> generation AA battery sized energy harvester.

Figure 4.12 presents the peak-to-peak output voltages ( $V_{PP}$ ) of the 9 prototypes at 8.6 Hz and 0.5 g vibration, which corresponds to resonant operation. Test results yield to an optimum coil position of 15.5 mm above the bottom of the harvester. This result is further proved by detecting resonance frequency of the harvesters. Figure 4.13 presents the frequency response of the prototypes where P3 yields to the maximum output.

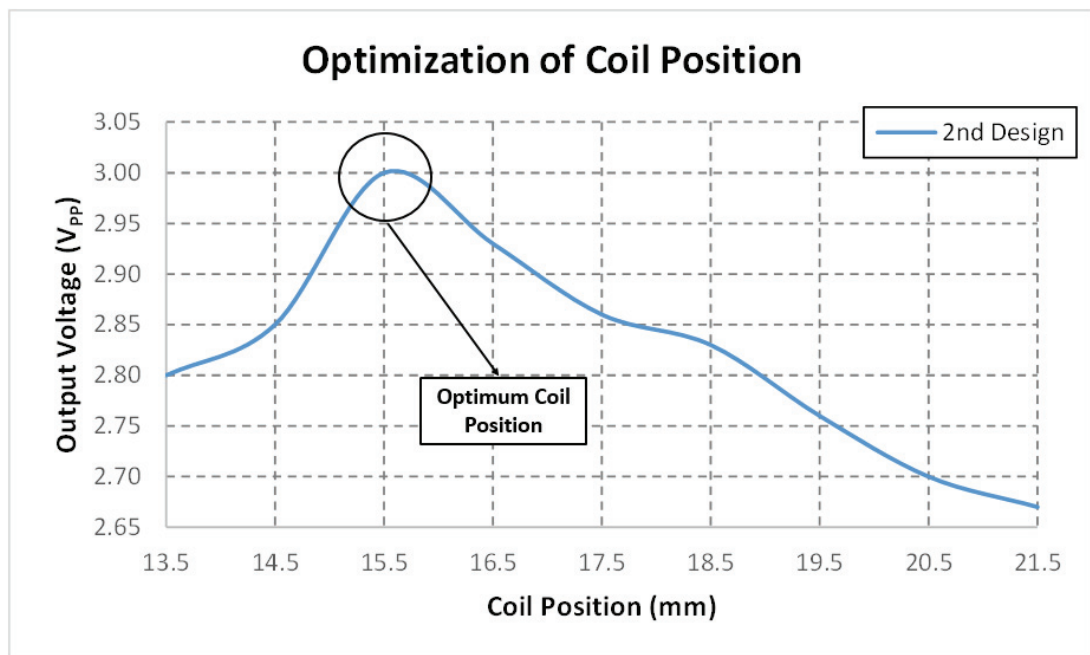


Figure 4.12: Test results of the harvester output for different coil position. (8.6 Hz, 1.7 mm peak-to-peak vibration with 0.5 g peak acceleration).

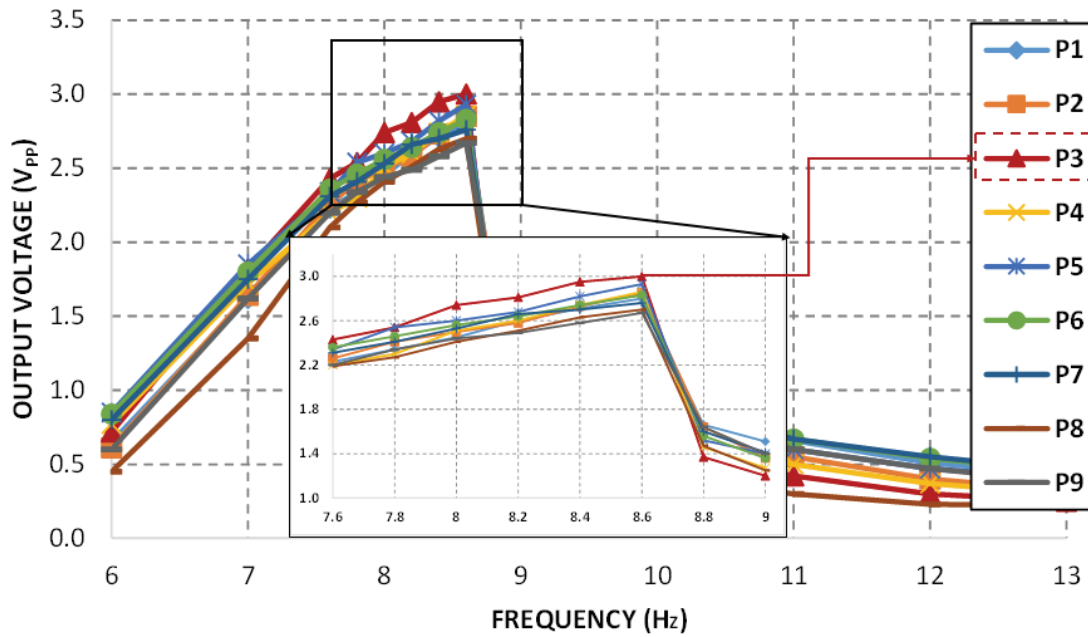


Figure 4.13: Frequency response of EM harvester prototypes (P1-P9) at 0.5 g peak vibration acceleration. P3, where the coil is placed 15.5 mm above the bottom of the harvester, yields the maximum output.

Table 4.3: Comparison of the proposed 1<sup>st</sup> generation AA battery sized design with 2<sup>nd</sup> generation AA battery sized design.

	1 <sup>st</sup> AA Battery Sized Design	2 <sup>nd</sup> AA Battery Sized Design
Device Dimensions	Ø:14 mm, h:46 mm, 7 cm <sup>3</sup>	Ø:14 mm, h:46 mm, 7 cm <sup>3</sup>
Inertial Mass	NdFeB W <sub>80</sub> -Cu <sub>20</sub>	NdFeB W <sub>80</sub> -Cu <sub>20</sub>
	Ø:5 mm, h:10 mm, 0.8 cm <sup>3</sup>	Ø:5 mm, h:6 mm, 0.5 cm <sup>3</sup>
	-	Ø:5 mm, h:4 mm, 0.3 cm <sup>3</sup>
Input Vibration	0.5 g peak acceleration	0.5 g peak acceleration
Resonance Frequency	10 Hz	8.6 Hz
Coil Turn	1200	1200
Coil Resistance	265 Ω	265 Ω
Output Voltage	2.52 V <sub>PP</sub> , 0.57 V <sub>RMS</sub>	3 V <sub>PP</sub> , 0.5 V <sub>RMS</sub>
Harvested Power	306.5 μW <sub>RMS</sub>	238 μW <sub>RMS</sub>
Power Density	43.8 μW <sub>RMS</sub> /cm <sup>3</sup>	34 μW <sub>RMS</sub> /cm <sup>3</sup>

Table 4.3, presents that the resonance frequency is reduced as expected. Here reduction in output power is significant (from 306.5 μW to 238 μW), which is

unexpected. With this approach, the output power is reduced. In order to get a larger output voltage,  $V_{RMS}$  of the output voltage should be increased. In simulations,  $V_{RMS}$  value is increased with modification on internal structure. Validation of this study is investigated in the next section.

### 4.3.3. 3<sup>rd</sup> Generation AA Battery Sized EM Harvester

The moving magnet dimensions are adjusted with the guidance of the simulations. Several modifications are tried instead of a single magnet structure to optimize the output and the resonance frequency. The proposed model consists of two NdFeB magnets with a tungsten mass placed in between as illustrated with device dimensions in Figure 4.14.

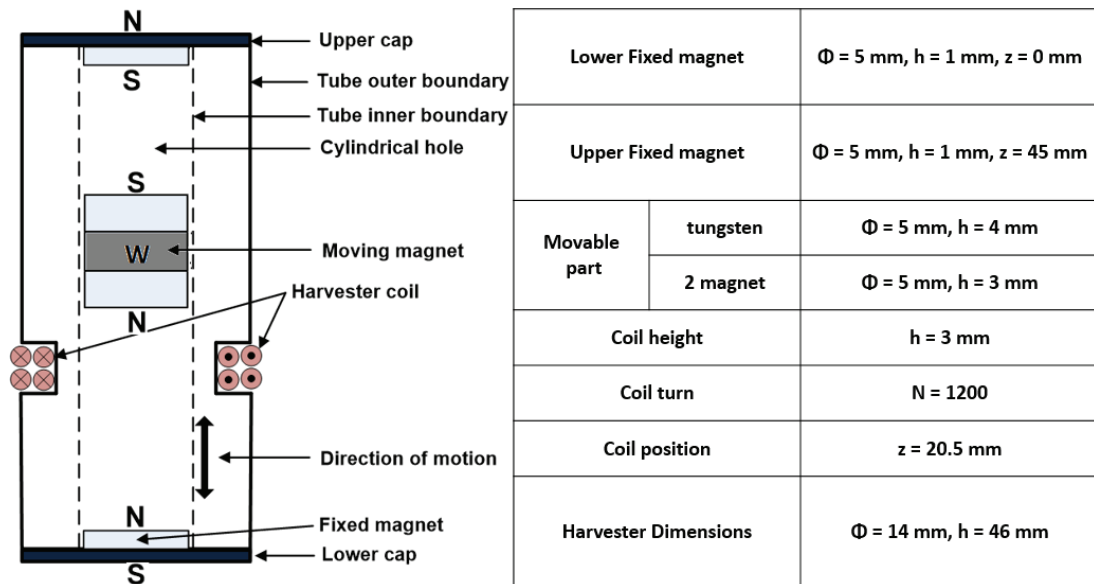


Figure 4.14: System specifications of the 3<sup>rd</sup> generation AA battery sized energy harvester.

Figure 4.15 presents the peak-to-peak output voltages ( $V_{PP}$ ) of the 9 prototypes at 9 Hz and 0.5 g vibration, which corresponds to resonant operation. Test results yield to an optimum coil position of 20.5 mm above the bottom of the harvester. This result

is further proven by detecting the resonance frequency of the harvesters. Figure 4.16 presents the frequency response of the prototypes where P8 yields the maximum output.

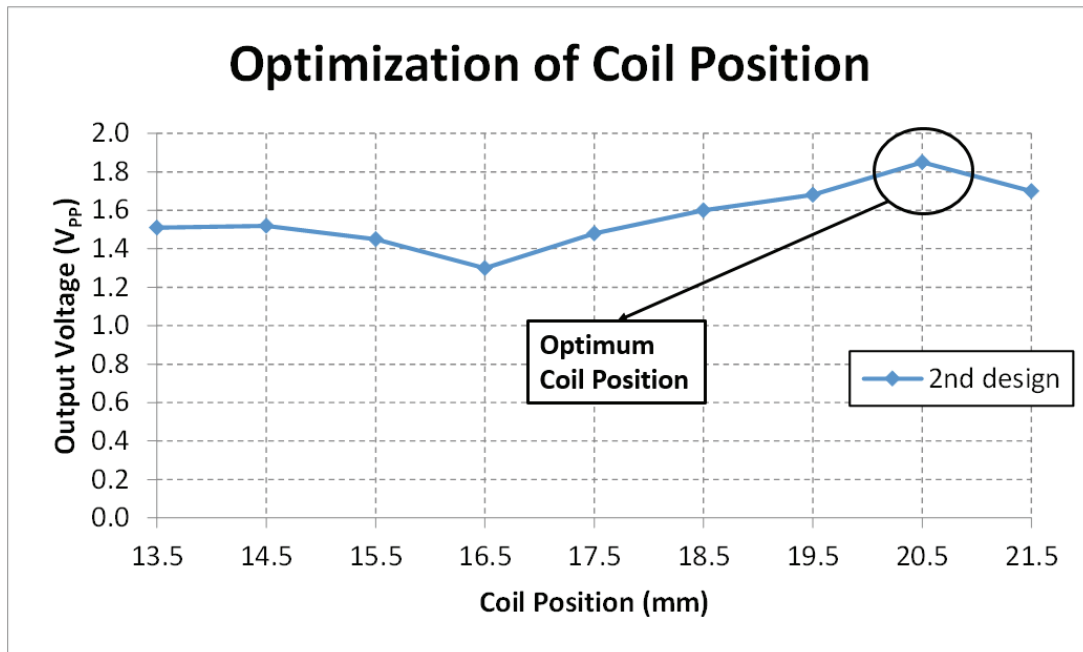


Figure 4.15: Test results of the harvester output for different coil position. (9 Hz, 2.5 mm peak-to-peak vibration with 0.5 g peak acceleration).

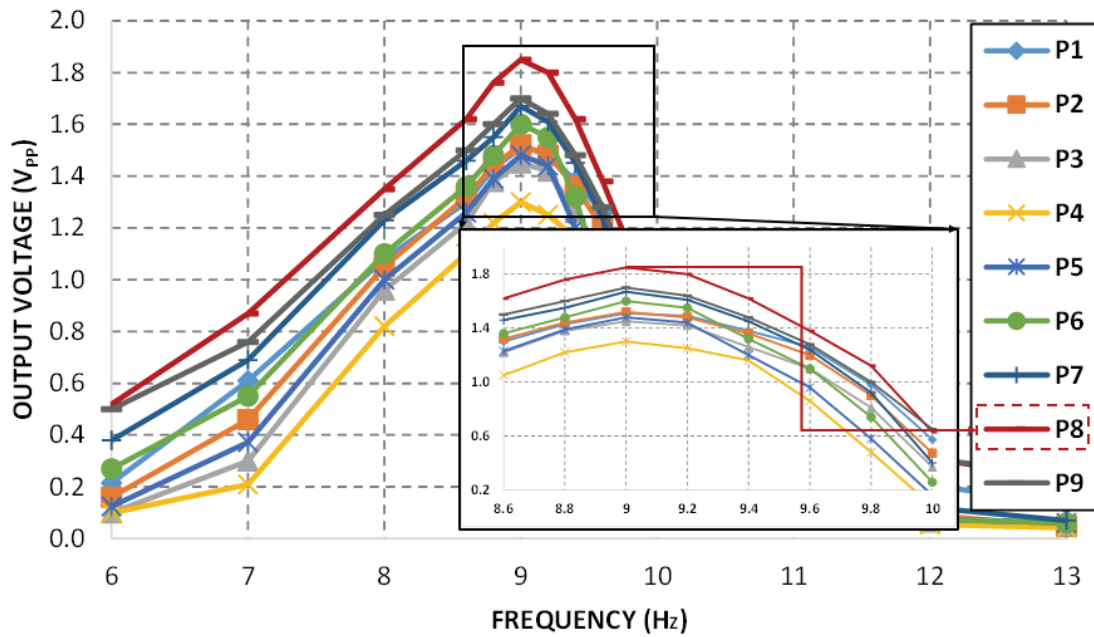


Figure 4.16: Frequency response of EM harvester prototypes (P1-P9) at 0.5 g peak vibration acceleration. P8, where the coil is placed 20.5 mm above the bottom of the harvester, yields the maximum output.

In the frequency response plot, the resonance frequency is indicated as 9 Hz.

Table 4.4: The performance comparison of the 2<sup>nd</sup> generation AA battery sized and 3<sup>rd</sup> generation AA battery sized design.

	2 <sup>nd</sup> AA Battery Sized Design	3 <sup>rd</sup> AA Battery Sized Design
Device Dimensions	Ø:14 mm, h:46 mm, 7 cm <sup>3</sup>	Ø:14 mm, h:46 mm, 7 cm <sup>3</sup>
Inertial NdFeB	Ø:5 mm, h:6 mm, 0.5 cm <sup>3</sup>	Ø:5 mm, h:6 mm, 0.5 cm <sup>3</sup>
Mass W <sub>80</sub> -Cu <sub>20</sub>	Ø:5 mm, h:4 mm, 0.3 cm <sup>3</sup>	Ø:5 mm, h:4 mm, 0.3 cm <sup>3</sup>
Input Vibration	0.5 g peak acceleration	0.5 g peak acceleration
Resonance Frequency	8.6 Hz	9 Hz
Coil Turn	1200	1200
Coil Resistance	265 Ω	265 Ω
Output Voltage	3 V <sub>PP</sub> , 0.5 V <sub>RMS</sub>	1.85 V <sub>PP</sub> , 0.38 V <sub>RMS</sub>
Harvested Power	238 μW <sub>RMS</sub>	136.5 μW <sub>RMS</sub>
Power Density	34 μW <sub>RMS</sub> /cm <sup>3</sup>	19.5 μW <sub>RMS</sub> /cm <sup>3</sup>

Table 4.4 presents that  $V_{RMS}$  of the output is reduced (from 238  $\mu\text{W}$  to 136.5  $\mu\text{W}$ ) with this modification on the internal structure. In design phase, it is considered that if we propose double-magnet structure isolated from each other, we can increase the output power. In simulation, double-magnet structure is isolated from each other by using tungsten mass. The results support that the output power increases with this proposed 3<sup>rd</sup> generation AA battery sized design. However, experimental result contradicts with this analysis. Additionally, the resonance frequency of the system is increased (from 8.6 Hz to 9 Hz). To conclude, 3<sup>rd</sup> generation design causes regression on the performance of harvester in terms of output power and resonance frequency.

#### **4.3.4. 4<sup>th</sup> Generation AA Battery Sized EM Harvester**

In the 4<sup>th</sup> proposed design of AA battery sized EM energy harvester, magnetic flux gradients are stimulated by axially orienting magnets at the moving part. The studies on literature and analyses on COMSOL simulations state that repulsive forces contribute to larger magnetic flux gradients rather than attractive forces. To maximize the output of the harvester, magnets at the moving part are placed in such a way that they repel each other as demonstrated in Figure 4.17

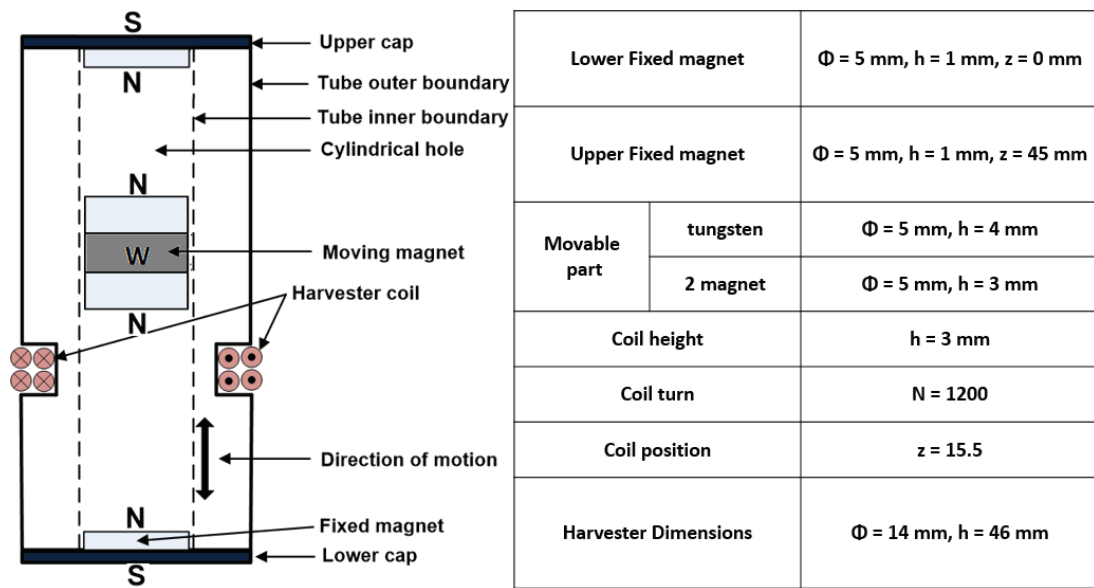


Figure 4.17: System specifications of the 4<sup>th</sup> generation AA battery sized energy harvester.

Figure 4.18 presents the peak-to-peak output voltages ( $V_{PP}$ ) of the 9 prototypes at 8.8 Hz and 0.5 g vibration, which corresponds to non-resonant operation. Both simulations and test results yield to an optimum coil position of 15.5 mm above the bottom of the harvester. Figure 4.19 presents the frequency response of the prototypes, where P3 yields the maximum output.

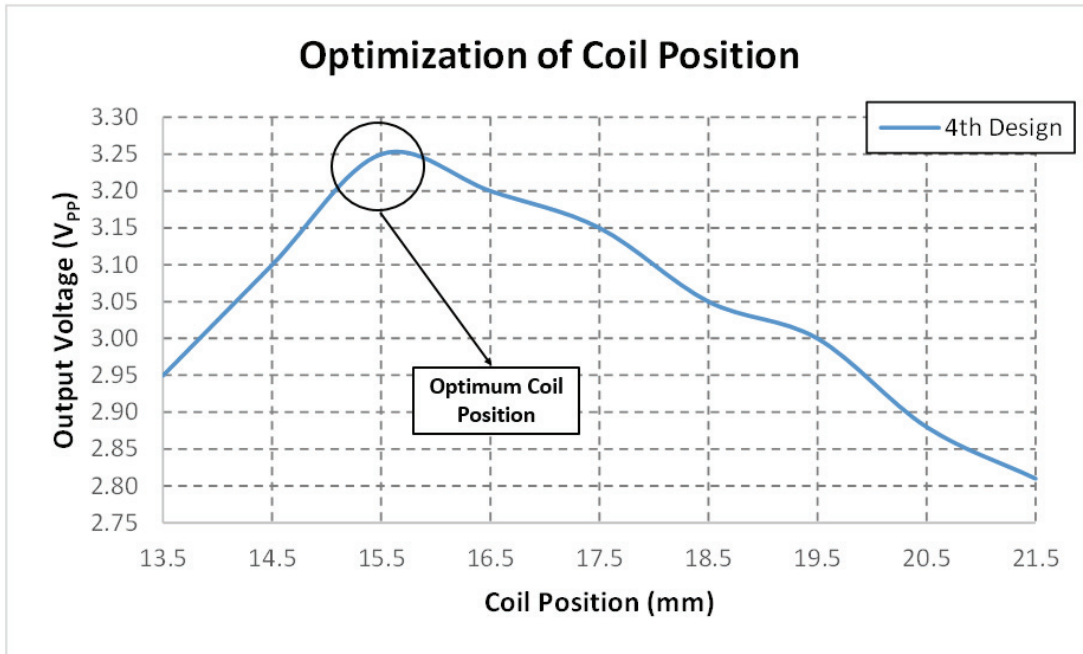


Figure 4.18: Simulation and test results of the harvester output for different coil position. (10 Hz, 1.2 mm peak-to-peak vibration with 0.5 g peak acceleration).

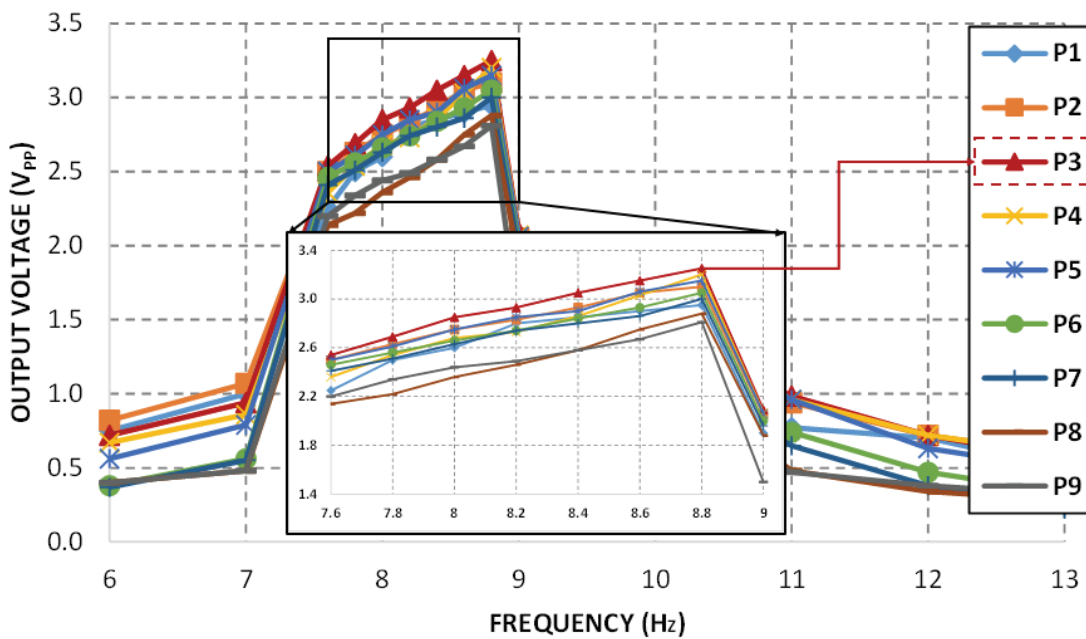


Figure 4.19: Frequency response of EM harvester prototypes (P1-P9) at 0.5 g peak vibration acceleration. P3, where the coil is placed 15.5 mm above the bottom of the harvester, yields the maximum output.

Table 4.5: Comparison of the proposed 3<sup>rd</sup> generation AA battery sized design with 4<sup>th</sup> generation AA battery sized design.

	<b>3<sup>rd</sup> AA Battery Sized Design</b>	<b>4<sup>th</sup> AA Battery Sized Design</b>
Device Dimensions	Ø:14 mm, h:46 mm, 7 cm <sup>3</sup>	Ø:14 mm, h:46 mm, 7 cm <sup>3</sup>
Inertial NdFeB	Ø:5 mm, h:6 mm, 0.5 cm <sup>3</sup>	Ø:5 mm, h:6 mm, 0.5 cm <sup>3</sup>
Mass W <sub>80</sub> -Cu <sub>20</sub>	Ø:5 mm, h:4 mm, 0.3 cm <sup>3</sup>	Ø:5 mm, h:4 mm, 0.3 cm <sup>3</sup>
Input Vibration	0.5 g peak acceleration	0.5 g peak acceleration
Resonance Frequency	9 Hz	8.8 Hz
Coil Turn	1200	1200
Coil Resistance	265 Ω	265 Ω
Output Voltage	1.85 V <sub>PP</sub> , 0.38 V <sub>RMS</sub>	3.25 V <sub>PP</sub> , 0.52 V <sub>RMS</sub>
Harvested Power	136.5 μW <sub>RMS</sub>	250 μW <sub>RMS</sub> ,
Power Density	19.5 μW <sub>RMS</sub> /cm <sup>3</sup>	35.7 μW <sub>RMS</sub> /cm <sup>3</sup>

The output power is increased (from 136.5 μW to 250 μW) and frequency is reduced (from 9 Hz to 8.8 Hz). With axially orientation of the magnets on the moving part output power of EM energy harvester is increased. This result satisfies our expectations from simulation analyses. By the removal of the magnet on the top cap, harvester performance is further improved as explained on the next section.

#### 4.3.5. 5<sup>th</sup> Generation AA Battery Sized EM Harvester

In the 5<sup>th</sup> generation proposed design of AA battery sized EM energy harvester, magnetic flux gradients are enhanced by axially orienting magnets at the moving part. The literature studies and COMSOL simulations conclude that repulsive forces contribute to larger magnetic flux gradients rather than attractive forces. To further increase the output performance of the harvester, fixed magnet at the top cap is removed as demonstrated in Figure 4.20.

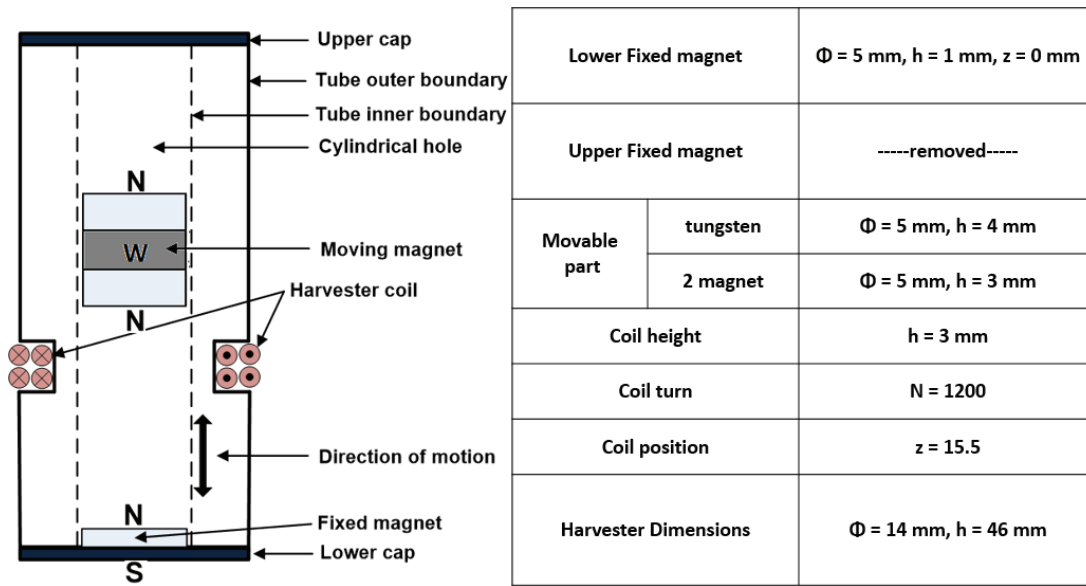


Figure 4.20: System specifications of the 5<sup>th</sup> generation AA battery sized energy harvester.

Figure 4.21 presents the peak-to-peak output voltages ( $V_{PP}$ ) of the 9 prototypes at 10 Hz and 0.5 g vibration which, corresponds to non-resonant operation. Both simulations and test results yield to an optimum coil position of 15.5 mm above the bottom of the harvester. This result is further proven by resonance condition of the harvesters. Figure 4.22 presents the frequency response of the prototypes where, P3 yields the maximum output.

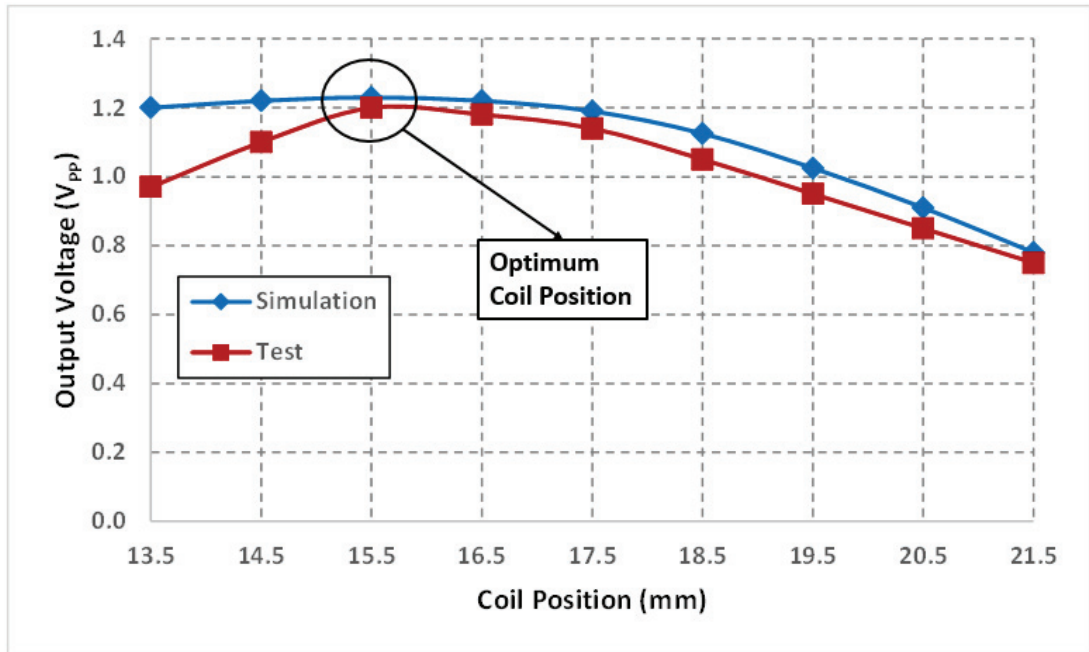


Figure 4.21: Simulation and test results of the harvester output for different coil position. (10 Hz, 2.5 mm peak-to-peak vibration with 0.5 g peak acceleration).

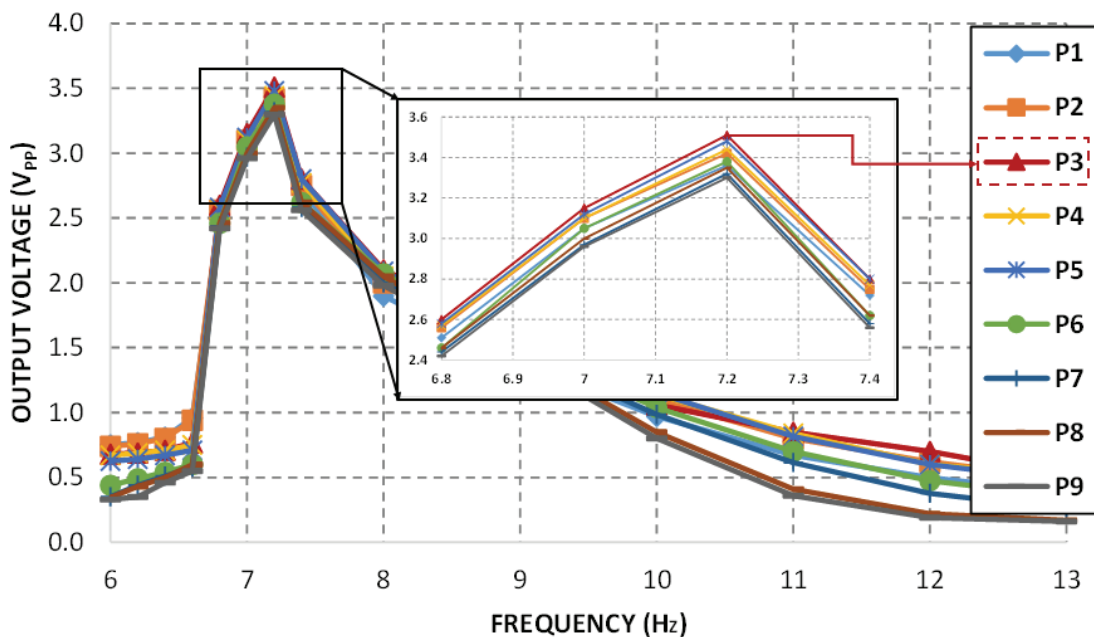


Figure 4.22: Frequency response of EM harvester prototypes (P1-P9) at 0.5 g peak vibration acceleration. P3, where the coil is placed 15.5 mm above the bottom of the harvester, yields the maximum output.

Table 4.6: Comparison of the proposed 4<sup>th</sup> generation AA battery sized design with 5<sup>th</sup> generation AA battery sized design

	<b>4<sup>th</sup> AA Battery Sized Design</b>	<b>5<sup>th</sup> AA Battery Sized Design</b>
Device Dimensions	Ø:14 mm, h:46 mm, 7 cm <sup>3</sup>	Ø:14 mm, h:46 mm, 7 cm <sup>3</sup>
Inertial NdFeB	Ø:5 mm, h:6 mm, 0.5 cm <sup>3</sup>	Ø:5 mm, h:6 mm, 0.5 cm <sup>3</sup>
Mass W <sub>80</sub> -Cu <sub>20</sub>	Ø:5 mm, h:4 mm, 0.3 cm <sup>3</sup>	Ø:5 mm, h:4 mm, 0.3 cm <sup>3</sup>
Input Vibration	0.5 g peak acceleration	0.5 g peak acceleration
Resonance Frequency	8.8 Hz	7.2 Hz
Coil Turn	1200	1200
Coil Resistance	265 Ω	265 Ω
Output Voltage	3.25 V <sub>PP</sub> , 0.52 V <sub>RMS</sub>	3.5 V <sub>PP</sub> , 0.53 V <sub>RMS</sub>
Harvested Power	250 μW <sub>RMS</sub> ,	266 μW <sub>RMS</sub> ,
Power Density	35.7 μW <sub>RMS</sub> /cm <sup>3</sup>	38 μW <sub>RMS</sub> /cm <sup>3</sup>

With this finalized design, a correlation between simulation and test results is validated again. The procedure used in the simulations is exactly applied to the experiments. Our theoretical expectations are experimentally satisfied. All designs are compared with each other in the next part of this chapter.

#### 4.4. Comparison of Test Results with Simulation Results

Figure 4.23 presents the performances of the EM energy harvester designs proposed so far.

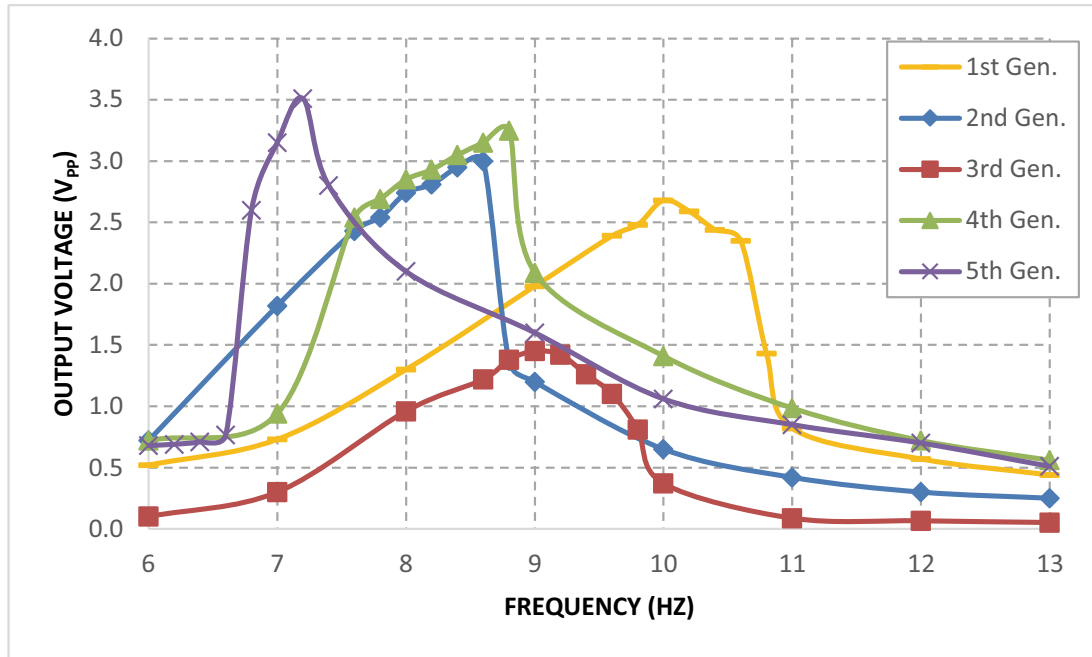


Figure 4.23: Frequency response of the EM energy harvester designs to 0.5 g sinusoidal excitation.

In the figure above, it is clear that the best performance of all five designs is the 5<sup>th</sup> generation AA battery sized EM energy harvester design. Thoroughly, optimization processes of the harvesters are applied to two different volumes namely, AA battery and 8 cm<sup>3</sup> volumes. The best performances of each volume of EM energy harvesters are compared in Table 4.7.

Table 4.7: Comparison of the proposed 8 cm<sup>3</sup> square prism volume energy harvester with 5<sup>th</sup> generation AA battery sized design.

	<b>8cm<sup>3</sup> Square Prism Design</b>	<b>5<sup>th</sup> AA Battery Sized Design</b>
Device Dimensions	Ø:20 mm, h:19 mm, 6 cm <sup>3</sup>	Ø:14 mm, h:46 mm, 7 cm <sup>3</sup>
Inertial NdFeB	Ø:10 mm, h:3 mm, 0.9 cm <sup>3</sup>	Ø:5 mm, h:6 mm, 0.5 cm <sup>3</sup>
Mass W <sub>80</sub> -Cu <sub>20</sub>	Ø:10 mm, h:5 mm, 1.5 cm <sup>3</sup>	Ø:5 mm, h:4 mm, 0.3 cm <sup>3</sup>
Saturation Magnetization	1.2 T	1.2 T
Input Vibration	0.7 g peak acceleration	0.5 g peak acceleration
Resonance Frequency	15 Hz	7.2 Hz
Coil Turn	1500	1200
Coil Resistance	450 Ω	265 Ω
Output Voltage	1.61 V <sub>PP</sub> , 0.45 V <sub>RMS</sub>	3.5 V <sub>PP</sub> , 0.53 V <sub>RMS</sub>
Harvested Power	110 μW <sub>RMS</sub>	266 μW <sub>RMS</sub> ,
Power Density	18 μW <sub>RMS</sub> /cm <sup>3</sup>	38 μW <sub>RMS</sub> /cm <sup>3</sup>

In Table 4.8 all designs are compared with each other in terms of applied excitation (frequency & amplitude), output voltages (V<sub>PP</sub> & V<sub>RMS</sub>) and output power.

Table 4.8: Comparison all of the proposed designs with each other in tabular form.

Designs	Excitation		Output Voltage		Output Power (μW)
	Amp. (g)	Freq. (Hz)	V <sub>PP</sub> (V)	V <sub>RMS</sub> (V)	
<b>8 cm<sup>3</sup> Square</b>	0.7	15.0	1.61	0.45	110
<b>1<sup>st</sup> Gen. AA</b>	0.5	10.0	2.52	0.57	306.5
<b>2<sup>nd</sup> Gen. AA</b>	0.5	8.6	3	0.5	238
<b>3<sup>rd</sup> Gen. AA</b>	0.5	9.0	1.85	0.38	136.5
<b>4<sup>th</sup> Gen. AA</b>	0.5	8.8	3.25	0.52	250
<b>5<sup>th</sup> Gen. AA</b>	0.5	7.2	3.5	0.53	266

Table 4.8 summarizes the performance of the proposed EM energy harvesters. Each of the designs is advantageous depending on the purpose of the usage. If the most important criteria of the design is output power, single-magnet structure usage is more

useful. However, resonance frequency of the design becomes larger compared to multi-magnet structures at this time. With various modifications, the resonance frequency of the harvester can be lowered. In the design of 5<sup>th</sup> generation AA battery sized EM energy harvester, this reduction clearly observed. Similarly, reduction on the output power also exists. However, the highest  $V_{PP}$  voltage is achieved with this design. In the conversion of AC to DC, the peak voltage is important to open the diodes. That is, the higher the input peak voltage, the more efficient the conversion process.

AC voltage waveform of the 5<sup>th</sup> generation AA battery design under  $0.5g \sin(2\pi 7t)$  excitation is as shown on Figure 4.24.

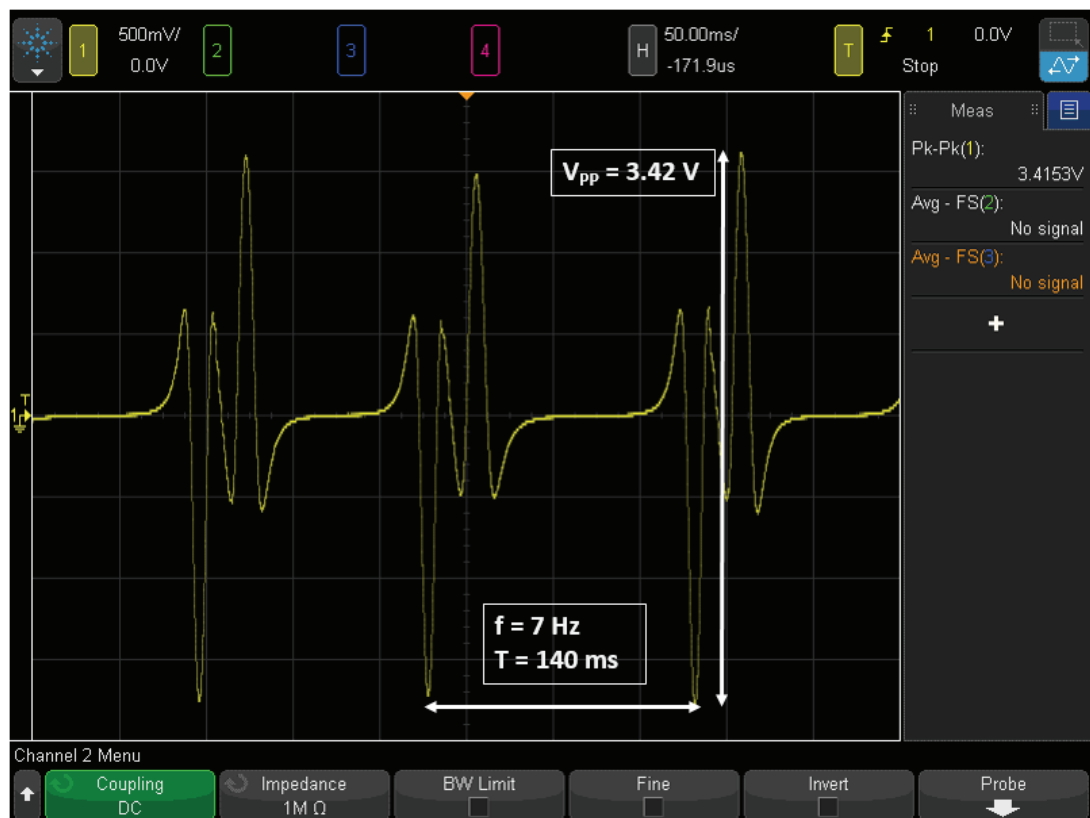
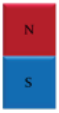
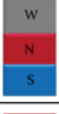
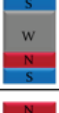


Figure 4.24: Harvested AC voltage from P3 at 7 Hz and 0.5 g peak acceleration (Oscilloscope screen).

#### 4.5. Actual and Estimated Resonance Frequencies of the Designs

Resonance frequencies of the proposed EM harvester designs are estimated via the MATLAB simulator. In this section, a comparison between actual and estimated resonance values are performed and presented in tabular form in Table 4.9.

Table 4.9: Comparison of the predicted and actual values of the resonance frequencies for the proposed EM harvester designs.

EM Harvester Designs	Internal Structures	Predicted Resonance (Hz)	Actual Resonance (Hz)	Percent Difference(%)
8 cm <sup>3</sup>		12.5	13.0	3.8
1 <sup>st</sup> Gen. AA		10.8	10.0	8
2 <sup>nd</sup> Gen. AA		9	8.6	4.8
3 <sup>rd</sup> Gen. AA		10	9.0	11
4 <sup>th</sup> Gen. AA		9.4	8.8	6.8
5 <sup>th</sup> Gen. AA		7.5	7.2	4.2

The percentage difference between the actual and the estimated values is due to the fact that existing operation of the moving part inside the harvester cannot exactly be modeled in simulators.

## 4.6. Conclusion

In this chapter, validation of the simulations with the test results are provided. The optimization procedure is experimentally repeated and similar results are obtained. The studies on the conceptual optimization process turns into practice as expected. The test results reflects the both positive and negative outcomes of modifications on the internal structure of EM energy harvesters. Therefore, robustness of theoretical studies are also experimentally proven.

In 8 cm<sup>3</sup> design output power is 110  $\mu$ W under the sinusoidal excitation of 0.7 g at 15 Hz. In order to improve the output performance of the EM energy harvester, device dimensions are modified. With the modified dimensions, the output power is increased up to 306.5  $\mu$ W under the excitation of 0.5 g at 10 Hz. Apart from output power, resonance frequency and  $V_{PP}$  are also important parameters to define the performance of the EM energy harvester. For low frequency and high output power design under low amplitude vibrations, 5<sup>th</sup> generation AA battery design is the most applicable one compared to other ones. From the beginning to the end, resonance frequency is reduced by nearly %50 from 15 Hz to 7.2 Hz. Additionally, output power is increased by more than %100 from 110  $\mu$ W to 266  $\mu$ W. Simultaneously,  $V_{PP}$  is increased by more than %100 from 1.61 V to 3.5 V. By achieving all these, applied excitation amplitude is also reduced from 0.7 g to 0.5 g.

Additionally, validity of generated MATLAB simulator to detect resonance frequency is evaluated. This is the novelty of this thesis study. The studies in literature, to detect resonance frequency of the harvester, totally depend on mathematical analysis and several assumptions. However, in this model, response of the motion varies under the applied frequency and excitation amplitude. That is, physical analysis, associated with mathematical analysis, is also taken into account. As a result, the resonance frequency of the harvester is determined with small percentage differences before fabrication and test procedure. The reason behind this deviation is that laboratory conditions are not totally modeled in simulations. In detection of the

resonance frequency, the most effective parameter is magnetic stiffness, which is determined via FEA tools. In FEA simulators, magnets are placed on z-directions and there is no radial motion. However, in reality, radial movement is observed because there exists one mm radial distance between the moving magnet and the inner surface of the harvester container. Therefore, when radial motion exists, magnetic force acting on the moving part changes which affects magnetic stiffness and directly the resonance frequency of the system. Additionally, in simulations, friction force between the moving part and the container cannot be modeled. All these facts results in differences between the actual and the estimated values of the resonance frequencies.

The studies of this thesis are concluded at this point with the validation of theoretical analyses on optimization and the resonance frequency estimation. The discussions and future recommendations to the studies performed so far are presented in the next chapter.

## CHAPTER 5

### CONCLUSION AND FUTURE WORK

In this thesis study, macro-scale electromagnetic energy harvesters have been designed, optimized, fabricated and tested. The aim of the thesis study is to present compact EM energy harvester, which operates at low frequency and low amplitude vibrations. In order to optimize the output performance, several designs are proposed and analyzed. The designs, performances and analyses are explained as follows:

1.  $8 \text{ cm}^3$  EM energy harvester design is proposed at first. Here aim is to design a compact energy harvester which fits into square prism with one side 2 cm. In the beginning, the harvester consists of two fixed magnets placed at the bottom and the top caps, a moving single-magnet and a pick-up coil with 1500 turns. The harvester has 20 mm radius and 20 mm height. Due to this limits, oscillation distance of the moving magnet is not sufficient. Additionally, interaction between the magnets are quite high which increases magnetic stiffness and the resonance frequency. In order to recover this negative effects, fixed magnet at the top cap is removed. This makes sense; however, it is not enough to decrease the resonance frequency. Then, the single-magnet is modified by reducing its height. Meanwhile, tungsten mass is attached on top of the single-magnet. The aim here is to maximize gravitational force acting on the magnet so that magnet can compress virtually considered magnetic spring. To do so, oscillation distance is increased and resonance frequency is

decreased. In the end, the proposed 8 cm<sup>3</sup> EM energy harvester generates 110 μW power and 1.61 V<sub>PP</sub> voltage under the sinusoidal excitation of 0.7 g at 15 Hz.

2. Improvements on 8 cm<sup>3</sup> EM harvester are limited due to the device dimensions. In order to get larger output power, the device dimensions are modified, height is increased from 20 mm to 46 mm and diameter is decreased from 20 mm to 14 mm. By doing so, oscillation distance for the moving magnet is increased and interaction between the fixed and the moving magnets are decreased. Additionally, pick up coil is wounded around smaller diameter at this time so that amount of used copper wire to reach same number of turn is reduced. As a result, coil resistance is reduced which has positive impact on output power. The strategies to improve output power is explained by proposed models as follows:
  - a. 1<sup>st</sup> Generation AA Battery Design: This design consists of two fixed magnets placed at the bottom and the top caps, a moving single-magnet and a pick-up coil with 1200 turns. All of the magnets are cylindrical with 5 mm diameter and the fixed ones have 1 mm height where the moving one has 10 mm height. The system is excited with 0.5 g and 10 Hz sinusoidal excitation and 2.52 V<sub>PP</sub> is induced between the coil terminals. The resultant output power is 306.5 μW. By changing only device dimensions, resonance frequency is decreased from 15 Hz to 10 Hz, output voltage is increased from 1.61 V<sub>PP</sub> to 2.52 V<sub>PP</sub> and output power is increased from 110 to 306.5 μW. In fact, all these outcomes are achieved with 0.5 g excitation amplitude rather than 0.7 g.
  - b. 2<sup>nd</sup> Generation AA Battery Design: In this design, effect of tungsten inertial mass is analyzed. The moving magnet height is decreased from 10 mm to 6 mm and 4 mm height tungsten inertial mass with same

diameter is attached on top of it. The expectation is reduction in resonance frequency and improvements on output power and voltage by the reference of the previous work. This modification satisfies our expectations, the resonance frequency is decreased from 10 Hz to 8.6 Hz and output voltage is increased from 2.52  $V_{PP}$  to 3.00  $V_{PP}$ . However, decrease in the output power is observed from 306.5  $\mu W$  to 238  $\mu W$ .

- c. 3<sup>rd</sup> Generation AA Battery Design: The aim is to increase output power by modification on the moving part. The 6 mm height moving magnet is divided into two 3 mm height magnets. This time tungsten inertial mass is placed in between these two magnets. In this way, interaction between these two magnets is expected to be lowered and so they behave like separate single magnets. To do so, output power is harvested by the contribution of two single magnets with 3 mm height. However, experimental results do not reflect simulation results and our expectations. The resonance frequency is increased to 9 Hz, the output voltage is decreased from 3.00  $V_{PP}$  to 1.85  $V_{PP}$  and output power is decreased from 238  $\mu W$  to 136.5  $\mu W$ . These results show that interaction between the moving magnets are not removed, which affects results negatively.
- d. 4<sup>th</sup> Generation AA Battery Design: Studies reported in literature states that repulsive forces between the magnets result in larger magnetic flux gradients compared to attractive forces. By this larger flux gradients, output voltage and power of the system can be improved. To see this effect, the moving magnets in the 3<sup>rd</sup> generation design are axially oriented to provide repulsive forces to each other. According to the results, the resonance frequency is decreased from 9 Hz to 8.8 Hz, the output voltage is increased from 1.85  $V_{PP}$  to 3.25  $V_{PP}$  and the output power is increased from 136.5  $\mu W$  to 250  $\mu W$ .

- e. 5<sup>th</sup> Generation AA Battery Design: In order to decrease the resonance frequency of the system, the fixed magnet at the top cap is removed, which is the only difference from the 4<sup>th</sup> generation AA battery design. To do so, reduction on magnetic stiffness exists, which makes the resonance frequency to decrease. Additionally, oscillation distance of the moving part is enhanced so velocity of the moving part increases. Therefore, magnetic flux passing through coil surface changes more rapidly which increases the output voltage. The results show that the resonance frequency is decreased from 8.8 Hz to 7.2 Hz, the output voltage is increased from 3.25 V<sub>PP</sub> to 3.50 V<sub>PP</sub> and the output power is increased from 250  $\mu$ W to 266  $\mu$ W.

All in all from the 8 cm<sup>3</sup> EM energy harvester design to 5<sup>th</sup> generation AA battery sized EM harvester design the resonance frequency is decreased from 15 Hz to 7.2 Hz, the applied excitation amplitude decreased from 0.7 g to 0.5 g, the output voltage is increased from 1.61 V<sub>PP</sub> to 3.5 V<sub>PP</sub> and the output power is increased from 110  $\mu$ W to 266  $\mu$ W. During this process, the harvester dimensions, the coil turn and position, the fixed magnets and the moving part of the system are optimized. Several EM harvester designs are proposed and several prototypes are fabricated. From single-magnet to various multi-magnet structures are analyzed. Throughout this process, effects of the design changes are reported so that the designers can benefit from this report and use as a guidance to design a macro-scale EM energy harvester. Depending on the satisfactions the architecture changes and the performance of the proposed harvesters can be evaluated belonging to the expectations. In this thesis study, the aim is to propose an EM energy harvester, which provides high output voltage and power under low excitation amplitudes and frequencies. The 5<sup>th</sup> generation AA battery sized EM harvester design best suits these expectations.

In this thesis, a novel study to define the resonance frequency of the EM energy harvesters is presented. Up to now, the resonance frequency of the harvesters are determined through mathematical expressions by 2<sup>nd</sup> order linear differential equation

solutions. These solutions are depending on several assumptions. Linear magnetic stiffness assumption is one of the examples. However, in practice, the stiffness of the system is no more linear. In reality, as the distance between the magnets reduces, magnetic force exponentially increases. Therefore, the physical relation between the magnetic force and the distance can be represented as exponential functions. In this thesis study, the mathematical expressions are equated under the consideration of this physical condition. The expressions are modeled via MATLAB and a simulator is presented to detect the resonance frequency of the system.

Having presented the performance analysis of the proposed designs and the achievements of this thesis study, the comprehensive list of future work is presented below:

1. The proposed EM energy harvester is 46 mm in height and only 3 mm is reserved for coil. If multi-coil structure is analyzed, this height is sufficient to be utilized for larger output power and voltage.
2. During the design of EM energy harvester, simulations are performed via FEA tools. These models work with linear constant values as an input. However, some of the parameters like stiffness and damping are quite non-linear and complex to be represented as a constant. Therefore, real behavior of the system cannot be modeled and comparison between simulations and tests become difficult. As a solution, finite element models that resolve stiffness and damping can be integrated into the simulation steps to represent these nonlinear parameters. By doing so, simulation and test results become comparable.
3. Output voltage of the EM harvester is simulated by using ‘Voltage Induced in a Coil by a Moving Magnet’ model of COMSOL. In this model, we can assign initial motion to the moving magnet. However, interaction between moving and fixed magnets and contribution of magnetic forces to the motion cannot be simulated. As a solution, the simulator model can be improved by the addition of magnetic flux feature.

4. How the motion of moving magnet cannot be defined experimentally. What I do is observation of output voltage waveform by using oscilloscope. Usage of a laser measurement devices can let us track the motion and understand the physics more clearly. With this better understanding, further improvements can be applied.
5. Improvements on the proposed simulator for resonance frequency detection is necessary. Magnetic forces are determined via FEA; however, these values do not reflect actual values. It is better to get real magnetic force vs displacement characteristic of the systems by taking measurements from laboratory. To do so, output of the simulator will be much closer to the actual values.
6. The load of the EM energy harvester is integrated circuit to convert generated AC signal to DC signal which has 3 k $\Omega$  resistance. With the advancements on IC technology, the resistance can be reduced so that input and load resistances can be matched.
7. In this thesis, how to design an EM energy harvester is explained. Under the guidance of this work, an efficient design belonging to a specific vibration in nature can be proposed.

## REFERENCES

- [1] C.B. Williams, A. Pavic, R.S. Crouch, R.C. Woods, "Feasibility study of vibration-electric generator for bridge vibration sensors," *Society for Experimental Mechanics, Inc, 16th International Modal Analysis Conference*, vol. 2, pp. 1111-1117, 1998.
- [2] J. A. Paradiso, T. E. Stamer, "Human-generated power for mobile electronics," *Low-power electronics design*, pp. 45-1, 2004.
- [3] R. Amirtharajah, J. Collier, J. Siebert, B. Zhou, A. Chandrakasan, "DSPs for energy harvesting sensors: applications and architectures," *IEEE Pervasive Computing*, vol. 4, no. 3, pp. 72-79, 2005.
- [4] P. D. Mitcheson, E. M. Yeatman, G. K. Rao, A. S. Holmes, T. C. Green, "Energy harvesting from human and machine motion for wireless electronic devices," *Proceedings of the IEEE*, vol. 96, no. 9, pp. 1457-1486, 2008.
- [5] P. B. Koeneman, I. J. Bush-Vishniac, K. L. Wood, "Feasibility of micro power supplies for MEMS," *Journal of Microelectromechanical Systems*, vol. 6, no. 4, pp. 355-362, 1997.
- [6] P. Constantinou, P. H. Mellor, P. Wilcox, "A model of a magnetically sprung vibration generator for power harvesting applications," *Electric Machines & Drives Conference, 2007. IEMDC'07. IEEE International*, vol. 1, pp. 725-730, 2007.
- [7] J. A. Paradiso and T. Starner, , "Energy scavenging for mobile and wireless electronics," *IEEE Pervasive Output*, vol. 4, no. 1, pp. 18-27, 2005.
- [8] J. P. Thomas, M. A. Qidwai, J. C. Kellogg, "Energy scavenging for small-scale unmanned systems," *Journal of Power sources*, vol. 159, no. 2, pp. 1494-1509, 2006.
- [9] S. Roundy, P. K. Wright, J. Rabaey, "A study of low level vibrations as a power source for wireless sensor nodes," *Computer communications*, vol. 26, no. 11, pp. 1131-1144, 2003.
- [10] C. Knight, J. Davidson, S. Behrens, "Energy options for wireless sensor nodes," *IEEE Sensors and Journal*, vol. 8, no. 12, pp. 8037-8066, 2008.
- [11] S. Roundy, "Energy scavenging for wireless sensor nodes with a focus on vibration to electricity conversion," *Ph. D. Thesis in Mechanical Engineering, University of California, Berkeley*, 2003.

- [12] M. T. Penella-Lopez, M. Gasulla-Forner, *Powering autonomous sensors: an integral approach with focus on solar and RF energy harvesting*, Springer Science & Business Media, 2011.
- [13] H. Kulah, K. Najafi, "An electromagnetic micro power generator for low frequency environmental vibrations," in *Micro Electro Mechanical Systems, 2004. 17th IEEE International Conference on.(MEMS)*, 2004.
- [14] E. P. James, M. J. Tudor, S. P. Beeby, N. R. Harris, P. Glynne-Jones, J. N. Ross, N. M. White, "An investigation of self-powered systems for condition monitoring applications," *Sensors and Actuators A: Physical*, vol. 110, no. 1, pp. 171-176, 2004.
- [15] J. M. Lee, S. C. Yuen, W. J. Li, P. H. W. Leong, "Development of an AA size energy transducer with micro resonators," *Circuits and Systems, 2003. ISCAS'03. Proceedings of the 2003 International Symposium on IEEE*, vol. 4, pp. IV-IV, 2003.
- [16] T. Sterken, K. Baert, C. Van Hoof, R. Puers, G. Borghs, P. Fiorini, "Comparative modelling for vibration scavengers [MEMS energy scavengers]," *Sensors, 2004. Proceedings of IEEE*, pp. 1249-1252, 2004.
- [17] F. Peano, T. Tambosso, "Design and optimization of a MEMS electret-based capacitive energy scavenger," *Journal of Microelectromechanical Systems*, vol. 14, no. 3, pp. 429-435, 2005.
- [18] Y. Naruse, N. Matsubara, K. Mabuchi, M. Izumi, S. Suzuki, "Electrostatic micro power generation from low-frequency vibration such as human motion," *Journal of Micromechanics and Microengineering*, vol. 19, no. 9, 2009.
- [19] L. Gu, "Low-frequency piezoelectric energy harvesting prototype suitable for the MEMS implementation," *Microelectronics Journal*, vol. 42, no. 2, pp. 277-282, 2011.
- [20] T. Galchev, E. E. Aktakka, H. Kim, K. Najafi, "A piezoelectric frequency-increased power generator for scavenging low-frequency ambient vibration," *Micro Electro Mechanical Systems (MEMS), 2010 IEEE 23rd International Conference on*, pp. 1203-1206, 2010.
- [21] N. Zhang, L. Li, Z. Gui, "Degradation of piezoelectric and dielectric relaxation properties due to electric fatigue in PLZT ferroelectric capacitors," *Materials Letters*, vol. 48, no. 1, pp. 39-43, 2001.
- [22] G. Poulin, E. Sarraute, F. Costa, "Generation of electrical energy for portable devices: Comparative study of an electromagnetic and a piezoelectric system," *Sensors and Actuators A: physical*, vol. 116, no. 3, pp. 461-471, 2004.
- [23] K. Najafi, T. Galchev, E. E. Aktakka, R. L. Peterson, J. McCullagh, "Microsystems for energy harvesting," *Solid-State Sensors, Actuators and Microsystems Conference (TRANSDUCERS), 2011 16th International*, pp. 1845-1850, 2011.

- [24] S. P. Beeby, R. N. Torah, M. J. Tudor, P. Glynn-Jones, T. O'donnell, C. R. Saha, S. Roy, "A micro electromagnetic generator for vibration energy harvesting," *Journal of Micromechanics and microengineering*, vol. 17, no. 7, pp. 1257-1265, 2007.
- [25] C. Cernik, O. Radler, S. Rosenbaum, T. Ströhla, U. Wallrabe, "Effective optimization of electromagnetic energy harvesters through direct computation of the electromagnetic coupling," *Sensors and Actuators A: Physical*, vol. 167, no. 2, pp. 416-421, 2011.
- [26] I. Shahosseini, K. Najafi, "Cylindrical halbach magnet array for electromagnetic vibration energy harvesters," *Micro Electro Mechanical Systems (MEMS), 2015 28th IEEE International Conference on IEEE*, pp. 1051-1054, 2015.
- [27] A. Munaz, B. C. Lee, G. S. Chung, "A study of an electromagnetic energy harvester using multi-pole magnet," *Sensors and Actuators A: Physical*, vol. 201, pp. 134-140, 2013.
- [28] Y. Rao, S. Cheng, D. P. Arnold, "An energy harvesting system for passively generating power from human activities," *Journal of Micromechanics and Microengineering*, vol. 23, no. 11, 2013.
- [29] N. Fondevilla, C. Serre, A. Pérez-Rodríguez, M. C. Acero, E. Cabruja, H. Campanella, J. Esteve, "Electromagnetic harvester device for scavenging ambient mechanical energy with slow, variable, and randomness nature," *Power Engineering, Energy and Electrical Drives (POWERENG), 2011 International Conference on IEEE*, pp. 1-5, 2011.
- [30] E. Bonisoli, A. Canova, F. Freschi, S. Moos, M. Repetto, S. Tornincasa, "Dynamic simulation of an electromechanical energy scavenging device," *IEEE Transactions on Magnetics*, vol. 46, no. 8, pp. 2856-2859, 2010.
- [31] Z. Li, L. Zuo, G. Luhrs, L. Lin, Y. X. Qin, "Electromagnetic energy-harvesting shock absorbers: design, modeling, and road tests," *IEEE Transactions on Vehicular Technology*, vol. 62, no. 3, pp. 1065-1074, 2013.
- [32] F. U. Khan, I. Ahmad, "Vibration-based electromagnetic type energy harvester for bridge monitoring sensor application," *Emerging Technologies (ICET), 2014 International Conference on IEEE*, pp. 125-129, 2014.
- [33] M. S. Soliman, E. M. Abdel-Rahman, E. F. El-Saadany, R. R. Mansour, "A design procedure for wideband micropower generators," *Journal of Microelectromechanical Systems*, vol. 18, no. 6, pp. 1288-1299, 2009.
- [34] L. D. Liao, P. C. P. Chao, J. T. Chen, W. D. Chen, W. H. Hsu, C. W. Chiu, C. T. Lin, "A miniaturized electromagnetic generator with planar coils and its energy harvest circuit," *IEEE transactions on magnetics*, vol. 45, no. 10, pp. 4621-4627, 2009.

- [35] C. R. Saha, T. O'Donnell, H. Loder, S. Beeby, J. Tudor, "Optimization of an electromagnetic energy harvesting device," *IEEE Transactions on Magnetics*, vol. 42, no. 10, pp. 3509-3511, 2006.
- [36] R. Ramlan, M. J. Brennan, B. R. Mace, I. Kovacic, "Potential benefits of a non-linear stiffness in an energy harvesting device," *Nonlinear Dynamics*, vol. 59, no. 4, pp. 545-558, 2010.
- [37] Z. L. Xu, X. B. Shan, R. J. Song, T. Xie, "Electromechanical modeling and experimental verification of nonlinear hybrid vibration energy harvester," *Applications of Ferroelectrics, International Workshop on Acoustic Transduction Materials and Devices & Workshop on Piezoresponse Force Microscopy (ISAF/IWATMD/PFM), 2014 Joint IEEE International Symposium on the*, pp. 1-4, 2014.
- [38] B. P. Mann, N. D. Sims, "Energy harvesting from the nonlinear oscillations of magnetic levitation," *Journal of Sound and Vibration*, vol. 319, no. 1, pp. 515-530, 2009.
- [39] N. G. Stephen, "On energy harvesting from ambient vibration," *Journal of sound and vibration*, vol. 293, no. 1, pp. 409-425, 2006.
- [40] I. Shahosseini, R. L. Peterson, E. E. Aktakka, K. Najafi, "Electromagnetic generator optimization for non-resonant energy harvester," *SENSORS, 2014 IEEE*, pp. 178-181, 2014.
- [41] C. B. Williams, C. Shearwood, M. A. Harradine, P. H. Mellor, T. S. Birch, R. B. Yates, "Development of an electromagnetic micro-generator," *IEE Proceedings-Circuits, Devices and Systems*, vol. 148, no. 6, pp. 337-342, 2001.
- [42] H. Uluşan, O. Yaşar, Ö. Zorlu, H. Külah, "Optimized Electromagnetic Harvester with a Non-Magnetic Inertial Mass," *Procedia Engineering*, vol. 120, pp. 337-340, 2015.
- [43] C. R. Saha, T. O'donnell, N. Wang, P. McCloskey, "Electromagnetic generator for harvesting energy from human motion," *Sensors and Actuators A: Physical*, vol. 147, no. 1, pp. 248-253, 2008.
- [44] R. Dayal, S. Dwari, L. Parsa, "A new design for vibration-based electromagnetic energy harvesting systems using coil inductance of microgenerator," *IEEE Transactions on Industry Applications*, vol. 47, no. 2, pp. 820-830, 2011.
- [45] D. Spreemann, B. Folkmer, Y. Manoli, "Comparative study of electromagnetic coupling architectures for vibration energy harvesting devices," *Proceedings of PowerMems*, pp. 257-260, 2008.